Advanced Robust Control via Disturbance Observer: Implementations in the Motion Control Framework

August 2014

A thesis submitted in partial fulfilment of the requirements for the degree of
Doctor of Philosophy in Engineering

Keio University

Graduate School of Science and Technology
School of Integrated Design Engineering

Emre Sariyildiz

Acknowledgements

This dissertation is the summary of my researches from September 2011 to June 2014 as a member of the Ohnishi laboratory in Keio University. I should admit that this dissertation could have never been accomplished without the help of many people who have encouraged and supported me in my life. Therefore, I would like to express my acknowledgements to them for their valuable assistances, co-operations, and guidance.

First of all, I would like to express my sincere gratitude to my supervisor Professor Dr. Kouhei Ohnishi in Keio University. His valuable advices have always helped me to enlighten and solve my research challenges. During my Ph.D. researches, I have had a chance to observe a real scientist that inspired me to be a good researcher. I appreciate him very much, because he has always encouraged me to follow my own ideas that improved my self-confidence as a scientific researcher. I can't emphasize the life changing experience I have had from meeting and working with Professor Dr. Kouhei Ohnishi. He has helped me to develop my engineering skills as well as my interpersonal skills. Without his help, I could not have accomplished this dissertation.

I greatly appreciate to the members of my Ph.D. dissertation committee, Professor Dr. Toshiyuki Murakami in Keio University, Professor Dr. Hiromitsu Ohmori in Keio University, and Professor Dr. Hideo Saito in Keio University. Their comments and advices greatly helped me to improve the dissertation.

I gratefully acknowledge to all of the current and past SUM members including colleagues in Ohnishi laboratory, who assisted me and guided me with their encouraging comments. My deepest appreciation goes to Professor Dr. Toshiyuki Murakami in Keio University, Professor Dr. Hiroaki Nishi in Keio University, Associate Professor Dr. Seiichiro Katsura in Keio University, and Associate Professor Dr. Takahiro Yakoh in Keio University. The kind and warm comments and the suggestions given in the SUM meetings inspired and improved my researches. Appropriate feedback obtained from colleagues guided me in a right and new direction.

I have had many valuable help that simplified my life in Japan by Mr. Kazuki Tanida. I should admit that without his friendly help, I would not have been able to adapt to the daily-life in Japan and accomplish this dissertation easily. Also, I would like to thank Mr. Murat Ufuk Hurufuk for his valuable

supports during my research life.

I would like to thank Yoshida Scholarship Foundation (YKK), which supported me in many ways including financially support.

Last but not the least I place a deep sense of gratitude to my family members who have been constant source of inspiration during the preparation of this dissertation. My beloved father and mother Mr. Ayhan Sariyildiz and Mrs. Saniye Sariyildiz and my beloved brother and sister in law Mr. Hakan Sariyildiz and Mrs. Tulay Sariyildiz have never left me alone and always encouraged and inspired me. I cannot imagine my research life without them.

There are a lot of people, whom I may have missed out their names, helped me throughout this dissertation, and I am ever so grateful to every single individual who has participated in my research. I would like to express my sincere gratitude again to all the people who have supported me.

August, 2014

Emre Sariyildiz

Contents

List of Figures

List of Tables

Chapter 1

Introduction

In Chapter 1, the background and objective of this dissertation are presented in detail. The approaches that are used to achieve the objectives are clarified. This chapter ends by giving the chapter organization and nomenclature.

1.1 Background of This Dissertation

In the conventional analysis and design methods of control systems, it is assumed that the dynamics of plants that are desired to be controlled are known accurately [1, 2]. However, the assumption is not practical in many cases; in reality, the dynamics of plants can be identified at some level of accuracy in a limited bandwidth, so there is a discrepancy between the mathematical models and the actual dynamics of systems [3, 4]. Typical sources of the discrepancy are un-modeled high frequency dynamics, model simplification, order reduction, system parameter variations, torn-and-worn factors, and so on. If a controller is designed by considering only the identified dynamic model, i.e., nominal plant model, then the stability and performance of the system may deteriorate by the uncertain plant dynamics that are not considered in the design of the controller [3, 4]. Besides the perturbations of plant dynamics, external disturbances, such as gust disturbance on a crane or aircraft, sensor noises, etc., may degrade the performances of control systems, significantly [5, 6].

To improve the stability and performance of control systems in practice, plant uncertainties and external disturbances should be considered in the design of controllers. In the literature, it is examined under the problem of ”Robust Control” that is described in this dissertation as follows:

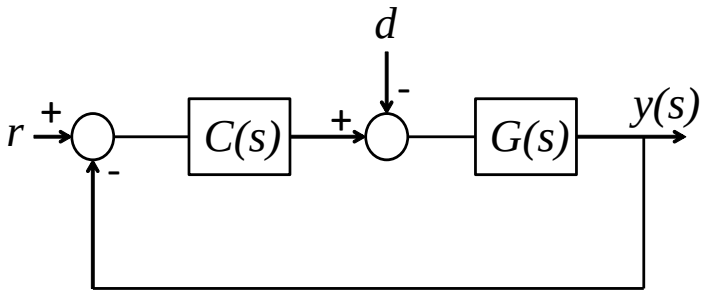

Fig. 1-1: Block diagram of a basic feedback control system.

"Designing a controller such that stability and performance goals are achieved irrespective of plant uncertainties and external disturbances."

It is a well-known fact that high gain controllers are naturally robust; parameter variations can be neglected by using sufficiently high gain control signals [7–9]. Equation (1.1) shows the transfer function of a basic feedback control system that is shown in Fig. 1-1.

$$y(s) = \frac{C(s)G(s)}{1 + C(s)G(s)} r(s) - \frac{G(s)}{1 + C(s)G(s)} d(s), \tag{1.1}$$

where $C(s)$ and $G(s)$ denote controller and plant, respectively; $r(s)$ and $d(s)$ denote reference and disturbance external inputs, respectively; and $y(s)$ denotes response. Equation (1.1) shows that as the control signal is increased, $C(s)$ becomes more dominant in the closed loop response of the system and attenuation of external disturbance is improved, i.e., the robustness of the control system is improved. However, increasing control gain has several disadvantages such as exciting high frequency dynamics or resonant frequency, increasing noise, energy consumption, and so on. Therefore, the robustness of control systems cannot be achieved by only increasing the control gain in general.

The theory of modern Robust Control began in the late of 70s and early of 80s by noticing that optimal feed-back control methods fail to recognize the importance of model uncertainty in limiting achievable control performance [10, 11]. After that, several researches have been conducted to suppress the effects of plant uncertainties and external disturbances [11–13]. The definition of the dynamic perturbations of plants is the basis of the robust analysis and design control methods. In general, robust control methods can be categorized by considering the dynamic perturbations of plants, namely real parametric uncertainties and unstructured uncertainties as shown in Fig. 1-2.

In the real parametric uncertainty based analysis and design methods, as it can be deduced from the name directly, it is assumed that the general structure of a plant's dynamics is known accurately; however,

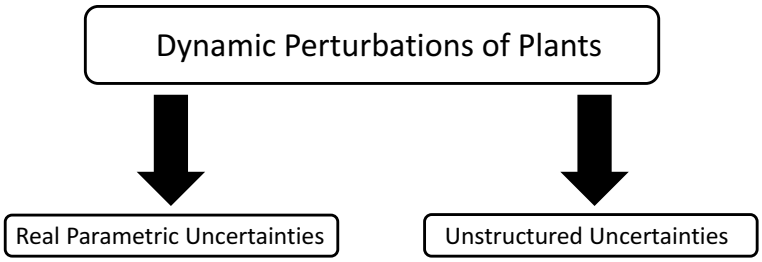

Fig. 1-2: Dynamic perturbations of plants.

the parameters of the dynamic model include uncertainties in which the upper and lower bounds of parameters can be determined [14, 15]. Equation (1.2) and eq. (1.3) show the model of a servo system by using real parametric uncertainties.

$$m\ddot{q} + c\dot{q} + kq = f(t), \tag{1.2}$$

$$(m_n + \delta_m)\ddot{q} + (c_n + \delta_c)\dot{q} + (k_n + \delta_k)q = f(t), \tag{1.3}$$

where $\bullet_n$ denotes nominal, i.e, identified, parameters; and $\delta_\bullet$ denotes parameter variations.

The dynamic perturbations in many industrial applications can be modeled by considering the real parametric uncertainties such as torn-and-worn effects on plant components, shifting operating point, and so on [15]. Conventionally, systems that include real parametric uncertainties are analyzed by gridding the uncertain parameters in admissible regions; however, it is computationally inefficient [14]. Kharitonov theorem is the basis of the modern real parametric uncertainty based robust analysis and design control methods [16, 17]. It shows that at most four polynomials should be analyzed to show the asymptotic stability of interval polynomials, so the computational complexity and load of the conventional gridding methods are eliminated. After Kharitonov theorem, several real parametric uncertainty based analysis methods were proposed in this field, e.g., Edge and Tsypkin-Polyak theorems which are used in Chapter 3 [18, 19]. The real parametric uncertainty based analysis methods have two main disadvantages. The first one is that only the real parametric uncertainties can be considered in this method; therefore, the general structure of the dynamic model should be obtained accurately, e.g., the relative degree or the order of the plant model should be identified precisely. The second one is that it is not an easy task to derive compact solutions in the robustness analysis. Therefore, in general, numerical or geometry-based control algorithms are used in the analysis and design of the robust control systems. Although useful analysis algorithms can be obtained numerically, designing a robust controller is not an easy task in general.

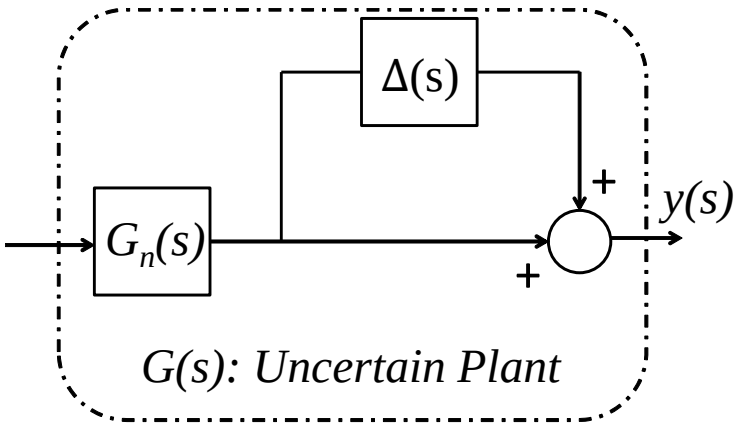

Fig. 1-3: Description of output multiplicative uncertainty.

In the unstructured uncertainty description, many perturbations, such as order reduction, parametric uncertainties, un-modeled non-linearities, etc., can be lumped into one single perturbation block [3, 4, 20]. Therefore, any kind of plant uncertainties can be easily considered by using the unstructured uncertainty based description. There are different unstructured uncertainty definition methods in the literature such as additive perturbation, inverse additive perturbation, input-output multiplicative perturbations, and so on [4]. All of the perturbation definition methods have their own advantages and disadvantages, so they are chosen by considering the robust control problem [4]. The output multiplicative uncertainty based description, which is used in Chapter 3, is shown in eq. (1.4) and Fig. 1-3.

$$G(s) = G_n(s)(1 + \Delta(s)), \tag{1.4}$$

where $\Delta(s)$ denotes the unstructured uncertainty block.

Several robust analysis and design control methods have been proposed by using the unstructured uncertainty based plant description [11–13]. Small Gain theorem is one of the most widely used robust control tools to analyze the robust stability by using the unstructured uncertainty model of an exact plant [21, 22]. The main advantage of the Small Gain theorem is that the robust stability and performance criteria can be analytically defined in a compact form for any kind of plant dynamics. However, Small Gain theorem considers only the amplitude response of Nyquist plot; therefore, it suffers by the conservatism which may degrade the performance of control systems significantly as shown in Chapter 3.

H_∞ control is another important robust analysis and design control method that can be implemented into several different robust control problems such as multi-variable control [23, 24]. Several researches have been conducted on H_∞ based robust control in the literature, and the robust control systems can

be simply designed by using the advanced H_∞ control toolbox provided by Matlab [25, 26]. The main disadvantages of H_∞ control are that it has a complicated mathematical structure which is a very serious problem for practitioners and even researchers, robust controllers that are designed by using H_∞ control methods may not be implemented easily that is a very challenging issue in practical applications, and it suffers from conservatism. The conservatism can be decreased by using Structured Singular Values, i.e., μ synthesis, introduced by J. C. Doyle [27]. However, μ synthesis based analysis and design methods have also complicated mathematical structures. To analyze and design μ synthesis based robust controllers, μ control toolbox provided by Matlab can be used [28].

There are also another conventional robust control methods in the literature such as Linear Quadratic Gaussian (LQG) optimal control problem [29]. However, complicated mathematical structures and impractical controllers are the main challenging issues of the conventional Robust Control methods in general.

Besides the conventional robust control methods, two-degrees-of-freedoms (2-DOF) controllers are widely used to achieve robust control systems in the literature. In 2-DOF control systems, against the conventional methods, a robustness controller forces uncertain/exact plant to behave as its nominal plant model and suppresses external disturbances so that the performance controllers can be easily designed by considering only the dynamics of the nominal plant model. Consequently, the robustness and performance goals of the systems are controlled independently by using two different controllers, namely the robustness and performance controllers. Several 2-DOF robust control structures have been proposed in the literature such as Generalized Internal Model Control (GIMC) and Disturbance Observer (DOb) based controllers [30–33]. Among them, DOb is one of the most popular robust control tools since the robustness can be adjusted in a desired bandwidth, intuitively. The basis of the DOb design depends on the unknown or unmeasured input observation methods which were proposed in the beginning of 70s [34, 35]. However, it has been widely used in robust motion control applications after it was proposed by K. Ohnishi in 1983 [32]. A DOb is a very important design tool to achieve robustness in sliding mode based control systems (SMC), e.g., acceleration based controller (ABC) in motion control systems [36].

1.2 Objective

There are two main objectives of this dissertation. They are stated as follows:

(1) To extend the application area of DOb beyond the motion control.

(2) To clarify the design constraints in the DOb based robust motion control systems.

Although DOb has long been a very well-known robust control tool in the literature and has a very simple control structure, its applications are mainly limited in the motion control field. One of the most important reasons of this limitation is that DOb based robust control systems have not sufficient analysis and design control methods. To extend the application area of DOb beyond the motion control, new analysis and design control methods should be proposed by considering different dynamic characteristics of uncertain/exact plant, e.g., non-minimum phase systems.

DOb has been widely used in motion control applications, such as robotics and automotive, since it was presented in the first IPEC conference [32]. However, DOb based robust motion control applications still suffer from insufficient analysis and design control methods, so its implementations highly depend on designers' own experiences. To improve the robustness, stability, and performance of DOb based motion control systems, the robust motion control structures should be re-considered, the robustness and stability should be clarified, and novel analysis and design control methods should be proposed.

1.3 Approach

In this dissertation, novel analysis and design control methods are proposed for DOb based robust control systems.

Several different uncertain/exact plant dynamics, such as plants with real parametric uncertainties and right half plane pole(s) and zero(s), are considered in the design of DOb so as to extend its application area. The design constraints of DOb are clarified by using advanced control methods such as Kharitonov and Bode integral theorems. The main advantage of the proposed methods is that they clarify the robustness characteristics of DOb practically, e.g., if an uncertain/exact plant is minimum phase and includes only real parametric uncertainties, then the robust stability margin of the control system can be improved by increasing the bandwidth of DOb. The proposed methods can be easily implemented into many different robust control problems without requiring advanced mathematical background.

Although the robustness and stability of DOb based motion control systems have been previously researched in the literature, they are re-considered in this dissertation so as to clarify the practical design constraints of DOb in the motion control applications. Against the conventional analysis methods, imperfect velocity measurement, in which a LPF is used to suppress noise of velocity measurement in practice, is considered in the proposed analysis; and a new robustness design constraint is derived. It

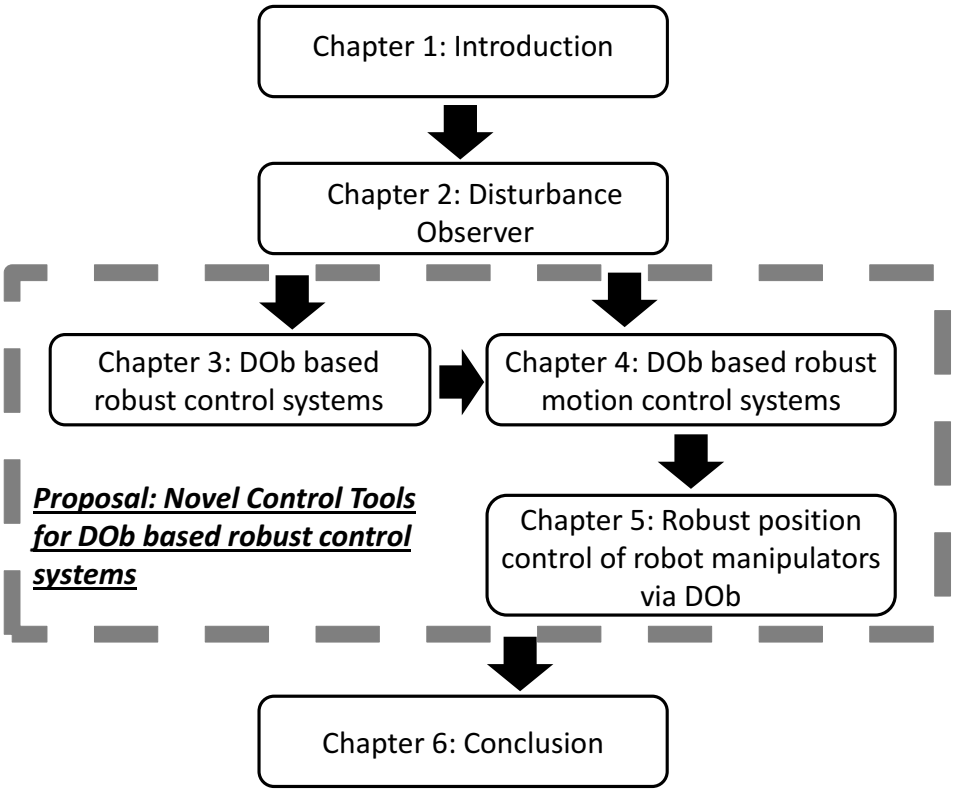

Fig. 1-4: Chapter organization.

is shown that the proposed robustness constraint directly limits the stability and performance of DOb based motion control systems. The stability of DOb based robust motion control systems, i.e., position and force control systems, are analyzed, and new practical design constraints, which improve the performance of motion control systems significantly, are proposed. The author believes that the proposed control tools are very useful not only for researchers, but also for practitioners of motion control field due to their simplicity.

1.4 Chapter Organization

Fig. 1-4 shows the chapter organization. Chapter 2 explains the general structure of DOb based robust control systems, briefly. Chapter 3 analyzes the DOb based robust control systems by considering real parametric and unstructured uncertainties. Firstly, DOb is implemented into the robust control problem of minimum phase systems that include real parametric uncertainties; and it is shown that the robustness

of the system can be achieved by increasing the bandwidth of DOb. Secondly, unstructured uncertainty is considered, and the analyses are extended to non-minimum phase and unstable plants and higher order DOb (HODOb). Several design constraints are provided for different robust control systems by using Bode and Poisson integral theorems. Chapter 4 analyzes the DOb based robust motion control systems. A new robustness design constraint is proposed by considering the practical velocity measurement that is obtained by using a low-pass-filter (LPF). It is shown that the bandwidth of DOb and nominal inertia are limited by the robustness. Novel stability analysis methods are proposed for DOb based position and force control systems. The trade-off between the robustness of DOb and stability of motion control systems is explained clearly. Robust force control systems are discussed in detail by considering practical environmental impedance estimation methods. It is shown that the robustness is crucial not only in position control systems, but also in force control systems. Chapter 5 analyzes the DOb based robust position control problem of multi-degrees-of-freedom robot manipulators by using non-linear control methods. The equivalence between the passivity and DOb based controllers are used in the analysis of the robust position control systems. A new design constraint for the nominal inertia matrix is proposed to improve the stability of the robust position control system. It is shown that the error of the robust position control system is uniformly ultimately bounded if trajectory tracking problem is considered; and the radius of the error bound can be shrunk by increasing the bandwidth of DOb and/or nominal inertia matrix. However, asymptotic stability is achieved if regulator problem is considered. Chapter 6 summarizes and concludes this dissertation.

Nomenclature

DOb	Disturbance observer
HODOb	Higher order disturbance observer
DOF	Degree-of-freedom
RFOb	Reaction force observer
RLMSE	Recursive least mean square error
ABC	Acceleration based control
LQG	Linear quadratic Gaussian
SMC	Sliding mode control
SSV	Structured Singular Values
LPF	Low pass filter
MIMO	Multi-input-multi-output
MISO	Multi-input-single-output
RHP	Right half plane
GA	Genetic algorithm
$\sup$	Supremum
e_{min}	Minimum modeling error
e_{max}	Maximum modeling error
τ	Delay time
$G(s)$	Uncertain/Exact plant model
$G_n(s)$	Nominal plant model
$\hat{G}_n(s)$	Approximate minimum-phase nominal plant model
$Q(s)$	Low-pass-filter of DOb
$C(s)$	Outer-loop performance controller
$L(s)$	Open loop transfer function
$\tilde{L}$	Minimum phase open loop transfer function
r	Reference external input
d	Disturbance external input
ξ	Noise external input
$y(s)$	System response, i.e., output
$\widehat{d^*}(s)$	Estimated disturbance
$r^{con}(s)$	Control signal
$W_P(s)$	Performance weighting function
$W_S(s)$	Stability weighting function
$T(s)$	Co-sensitivity function
$S(s)$	Sensitivity function
Δ	Uncertain block in which $\|\|\Delta\|\|_\infty < 1$
g_0	Bandwidth of DOb

z_{RHP}	Right half plane zero
p_{RHP}	Right half plane pole
w_B	Bandwidth of closed loop system
J_{mn}	Nominal inertia/mass of motor
J_m	Inertia/mass of motor
ΔJ_m	Inertia/mass variation
$K_{\tau n}$	Nominal thrust coefficient of motor
K_τ	Thrust coefficient of motor
ΔK_τ	Thrust coefficient variation
I_m	Motor current
I_m^{des}	Desired motor current
I_m^{cmp}	Compensate motor current
q_m	Angle/position of motor
$\dot{q}_m$	Velocity of motor
$\ddot{q}_m$	Acceleration of motor
$\ddot{q}_m^{des}$	Desired acceleration
$\dot{q}_m^{noise}$	Noise of velocity measurement
q_m^{ref}	Reference angle/position
$\dot{q}_m^{ref}$	Reference velocity
$\ddot{q}_m^{ref}$	Reference acceleration
g_{DOb}	Cut-off frequency of DOb
g_{RFOb}	Cut-off frequency of RFOb
g_v	Cut-off frequency of velocity measurement
τ_m^{load}	Loading torque/force
τ_m^{frc}	Friction torque/force
τ_m^{int}	Interactive torque/force
τ_m^d	Total external disturbance
τ_m^{dis}	Total disturbance
$\hat{\tau}_m^{dis}$	Estimation of τ_m^{dis}
$\hat{\tau}_m^{frc}$	Estimation of τ_m^{frc}
$\hat{\tau}_m^{int}$	Estimation of τ_m^{int}
$\hat{\tau}_m^{load}$	Estimation of τ_m^{load}
τ_{ref}^{load}	Reference torque/force
${}^{ext}\tau_m^d$	External disturbance
$T_{sen}^{DOb}(s)$	Sensitivity function of DOb based motion control system
$T_{cosen}^{DOb}(s)$	Co-sensitivity function of DOb based motion control system
$L_{DOb}(s)$	Open loop transfer function of DOb based motion control system
$T_{sen}^{PC}(s)$	Sensitivity function of the DOb based position control system
$T_{cosen}^{PC}(s)$	Co-sensitivity function of the DOb based position control system

$L_{PC}(s)$	Open loop transfer function of the DOb based position control system
w_n	Natural frequency
ξ	Damping coefficient
K_D	Derivative gain of performance controller
K_P	Proportional gain of performance controller
R	Fictitious robust control switch
C_f	Force control gain
$L_{CFC}(s)$	Open loop transfer function of the DOb based conventional explicit robust force control system
$L_{RFOB}(s)$	Open loop transfer function of the explicit robust force control system with RFOb
J_{sen}	Sensor inertia/mass
D_{sen}	Sensor damping
K_{sen}	Sensor stiffness
g_{sen}	Bandwidth of force estimation
ρ	Compliance selection constant
μ	Forgetting factor
Prj	Projection function
$\mathbf{M_n}$	Nominal inertia matrix
$\mathbf{M(q)}$	Inertia matrix
$\mathbf{\Delta M(q)}$	Inertia matrix variation
$\mathbf{C(q,\dot{q})}$	Coriolis and centrifugal matrix
$\mathbf{g(q)}$	Gravity torque/force vector
τ	Generalized torque control input vector
$\tau^{\mathbf{frc}}$	Friction torque/force vector
$\tau^{\mathbf{load}}$	Load torque/force vector
$\mathbf{q}$	Angle vector
$\mathbf{\dot{q}}$	Velocity vector
$\mathbf{\ddot{q}}$	Acceleration vector
$\mathbf{\ddot{q}^{des}}$	Desired acceleration vector
$\mathbf{e}$	Angle/position error vector
$\mathbf{\dot{e}}$	Velocity error vector
$\mathbf{e_D}$	Vector of the error dynamics
$\mathbf{\dot{e}_D}$	Derivative of the error dynamics vector
$\mathbf{q^{ref}}$	Reference angle vector
$\mathbf{\dot{q}^{ref}}$	Reference velocity vector
$\mathbf{\ddot{q}^{ref}}$	Reference acceleration vector
$\underline{\sigma}(\cdot)$	Minimum eigenvalue of $\cdot$
$\overline{\sigma}(\cdot)$	Maximum eigenvalue of $\cdot$
$\tau^{\mathbf{des}}$	Desired torque/force vector
$\hat{\tau}^{\mathbf{dis}}$	Vector of disturbance estimation

$\tau^{\mathbf{d}}$	External disturbance vector
$\tau^{\mathbf{des}}$	Desired torque input vector
$\mathbf{G_{DOb}}$	Bandwidth of DOb in a diagonal matrix form
$\mathbf{G_{LPF}(s)}$	LPF of DOb in a diagonal matrix form
$\widehat{\mathbf{G}}_{\mathbf{DOb}}$	Bandwidth of DOb and integrator in a diagonal matrix form
$\mathbf{K_D}$	Derivative gain in a diagonal matrix form
$\mathbf{K_P}$	Proportional gain in a diagonal matrix form
V	Lyapunov function candidate
$\dot{V}$	Derivative of Lyapunov function candidate

Superscript

con	Control
ref	Reference
des	Desired
dis	Total disturbance, including external disturbances and system uncertainties
d	External disturbance
frc	Friction
load	Load
int	Interactive
DOb	Disturbance observer
RFOb	Reaction force observer

Subscript

DOb	Disturbance observer
RFOb	Reaction force observer
sen	Sensitivity function
cosen	co-sensitivity function
m	motor

This dissertation is written in time domain unless otherwise stated.
"(s)" signs after variables indicate that the variables are in Laplace domain.

Chapter 2

Disturbance Observer

2.1 Introduction

In this chapter, DOb based robust control systems will be explained, briefly.

2.2 Disturbance Observer based Robust Control Systems

A DOb, which was proposed by Ohnishi et al., is a robust control tool that estimates external disturbances and system uncertainties [32, 33]. In DOb based robust control systems, the estimated disturbances, including system uncertainties, are fed-backed in a feed-back loop, namely inner-loop, so that the robustness of a system is obtained. To achieve performance goals, another feed-back loop, namely outer-loop, is designed independently by considering only nominal plant parameters, since a DOb nominalizes uncertain plant and suppresses external disturbances in the inner-loop. The control structure, in which the robustness and performance are adjusted independently, is called as two-degrees-of-freedom (2-DOF) control in the literature [37]. The main advantage of a DOb is that it suppresses external disturbances and system uncertainties without affecting the outer-loop performance controller [38]. Therefore, it has wide range of application areas, specifically in the motion control field, e.g., industrial automation, automotive, and robotics [39–42].

A Block diagram for a DOb based robust control system is shown in Fig. 2-1, in which 2-DOF robust control structure is clarified.

In this figure, $G(s)$ and $G_n(s)$ denote uncertain and nominal plant models, respectively; $Q(s)$ denotes the low-pass-filter (LPF) of DOb; $C(s)$ denotes the outer-loop performance controller; r, d, and

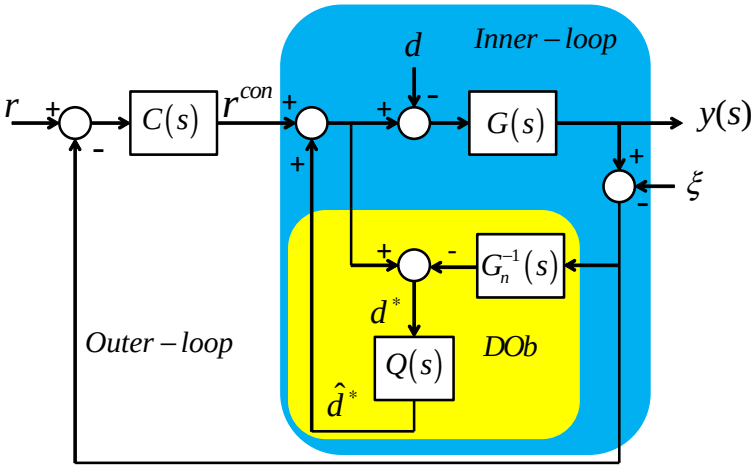

Fig. 2-1: Block diagram of a DOb based robust control system.

ξ denote reference, disturbance, and noise external inputs, respectively; d^* denotes system disturbances including external disturbances and plant uncertainties, and $\widehat{d}^*$ denotes its estimation; and r^{con} denotes outer loop control signal.

Equation (2.1), eq. (2.2), and eq. (2.3) are derived directly from Fig. 2-1 as follows:

$$r^{con} + \widehat{d}^* - G\left(s\right)^{-1} y = d, \tag{2.1}$$

$$r^{con} + \widehat{d}^* - G_n^{-1}(s)\left(y - \xi\right) = d^*, \tag{2.2}$$

$$\left(r^{con} + \widehat{d}^* - G_n^{-1}(s)\left(y - \xi\right)\right) Q\left(s\right) = \widehat{d}^*. \tag{2.3}$$

Equation (2.1) indicates external disturbances; however, eq. (2.2) indicates external disturbances as well as system uncertainties. Equation (2.3) shows that a DOb can estimate external disturbances and system uncertainties precisely if they stay within the bandwidth of $Q\left(s\right)$ and the output measurement is not influenced by noise, i.e., $\xi = 0$. Therefore,

- The higher the bandwidth of DOb is, the more the disturbance suppression improves.
- The output measurement influences the performance of DOb based robust control systems, significantly.

Equation (2.1), eq. (2.2), eq. (2.3) and Fig. 2-1 indicate that the dynamic characteristics of a DOb based robust control system depend on the dynamics of the LPF of DOb, the discrepancy between the nominal and uncertain plant dynamics, and the outer-loop performance controller. In the next chapter,

DOb based robust control systems are analyzed by considering the dynamics of plants, LPF of DOb, and outer-loop performance controller, in detail.

2.3 Summary

This chapter briefly explains DOb based 2-DOF robust control systems. There are several different 2-DOF robust control structures in the literature, such as generalized internal model control (GIMC); however, among them, DOb is one of the most popular robust control tools due to its simplicity. As it can be seen from Fig. 2-1 and eq. (2.1)-eq. (2.3), the main advantage of a DOb is that a robust control system can be intuitively designed in a limited bandwidth without requiring complicated mathematical methods. However, the stability and performance of DOb based robust control systems are influenced by the design parameters of DOb, such as the dynamics of LPF and nominal plant model, significantly. Therefore, more advanced analysis and design methods should be proposed to improve the DOb based robust control systems.

Chapter 3

Robustness of Disturbance Observer Based Control Systems

3.1 Introduction

In this chapter, the robustness of DOb based control systems will be analyzed in detail. Firstly, the conventional analysis method, which is based on the Small Gain theorem, will be discussed briefly in section 3.2 [31]. The robustness of a DOb based control system can be easily analyzed by using the conventional method; however, it has several disadvantageous, e.g., the conservatism limits the bandwidth of DOb which degrades the performance of control systems significantly, and the conventional analysis method does not provide clear insight into the robustness characteristics of DOb. To decrease the conservatism, the robustness of a DOb based control system is analyzed by using Structured Singular Values (SSV), i.e., μ-synthesis, in section 3.3 [43, 44]. Although the conservatism can be decreased by using the SSV, it cannot be removed completely due to the discontinuity problem of the real SSV. Besides, as the conventional analysis method, μ-synthesis cannot provide us a clear insight into the robustness characteristics of a DOb based control system.

To solve the aforementioned problems, two novel robustness analysis methods are proposed for the control systems based on DOb. In the first analysis method, it is assumed that a minimum-phase uncertain plant includes only real parametric uncertainties and the order of DOb is one. Kharitonov and Edge theorems are implemented into the DOb based control systems, and it is shown that the robust stability can be achieved if the bandwidth of DOb is higher than its lower limit that is defined in section 3.4. Tsypkin-Polyak theorem is also implemented into the defined problem, and it is shown that the stability

margin of the control system is improved as the bandwidth of DOb is increased [43]. The proposed method does not suffer from conservatism and gives a clear insight into the robustness characteristic of a DOb based control system; however, the applications are limited by the strict assumptions on the uncertain plant model and DOb dynamics. To analyze the robustness of more general control systems and higher order DOb (HODOb), Bode and Poisson integral theorems are implemented into the DOb based robust control systems, and the strict assumptions on the uncertain plant model and DOb are released in the second proposal. It is shown that the bandwidth of a DOb is limited by the robustness constraint if the uncertain plant includes time delay and/or right half plane zero(s). However, if the uncertain plant includes right half plane pole(s), then the bandwidth of DOb has lower bound due to the robustness constraint. Besides, the performance of a DOb can be improved by increasing its order, yet the robustness deteriorates and the bandwidth constraints of DOb become more strict. The proposed method provides a deep insight into the robustness of DOb based control systems in a wide range of application area such as non-minimum phase and unstable plants; however, it suffers from the conservatism that is explained in section 3.5 [45]. This chapter is finally concluded in section 3.6 by giving summaries.

To clarify the conservatism and design constraints of a DOb, a general second order plant model, which is shown in eq. (3.1) and eq. (3.2), is analyzed in this chapter.

$$G_n(s) = \frac{s+9}{s^2+8s+20}, \tag{3.1}$$

$$G(s) = G(s) = \frac{\beta_1 s + \beta_0}{\alpha_2 s^2 + \alpha_1 s + \alpha_0} + \Delta W_A(s), \tag{3.2}$$

where $12 \leq \alpha_0 \leq 32$; $3 \leq \alpha_1 \leq 15$; $0.2 \leq \alpha_2 \leq 8$; $6 \leq \beta_0 \leq 13$; $0.2 \leq \beta_1 \leq 3$; $W_A(s) = \frac{s+0.1}{0.5s+700}$ denotes an additive unstructured uncertainty weighting function; and $\|\Delta\|_\infty = 1$.

In the definition of the uncertain plant model dynamics, it is assumed that the plant includes high parametric uncertainties, and it is also influenced by the additive unstructured uncertainty, which is defined by $W_A(s)$, after 700 rad/s., significantly. Fig. 3-1 shows the step response of the nominal plant and pole spread of the uncertain plant models when a PID controller, in which $K_p = 10$, $K_i = 30$ and $K_d = 0.5$ are used as proportional, integral and derivative gains, is implemented in the feed-back control.

It is clear from Fig. 3-1 that the system response changes significantly by the plant perturbations. Although the PID controller provides a good performance for the nominal plant model, the stability cannot be achieved when the plant uncertainties are considered. It is a well known fact that the robustness can be improved by increasing the control gain when plant is minimum phase. However, as discussed in

Chapter 1, it has several practical disadvantages such as exciting resonant frequency.

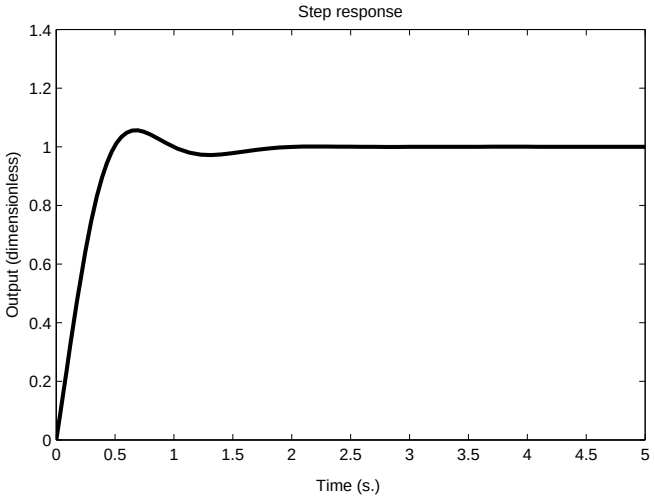

(a) Step response of the nominal plant model when the PID controller is implemented.

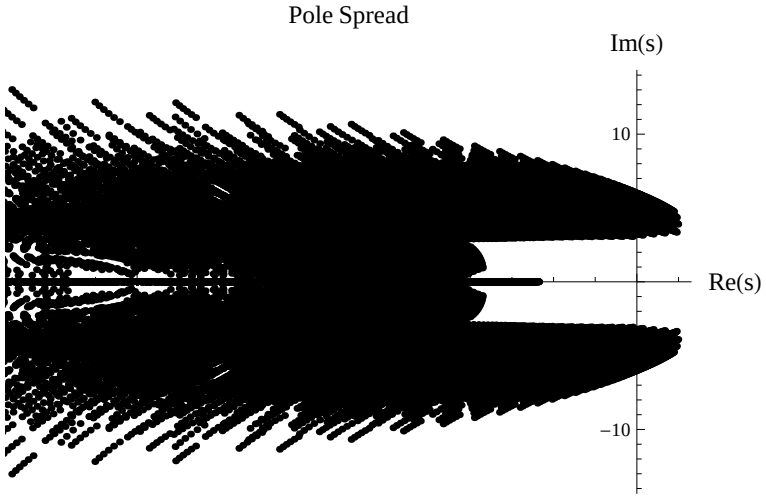

(b) Pole spread of the uncertain plant model when the PID controller is implemented.

Fig. 3-1: Step response and pole spread of the second order plant when the PID controller is implemented.

3.2 Conventional Analysis Method

Conventionally, a DOb based robust control system is analyzed by using the Small Gain theorem due to its simplicity [31, 46–48]. In the conventional analysis method, an uncertain plant is described by using an unstructured uncertainty model, so any kind of uncertainty can be easily considered in a compact form [47, 48]. For the sake of simplicity, the robustness is analyzed analytically by considering only the amplitude response of Nyquist plot [3, 4, 22]. However, the simplification causes conservatism which is the main drawback of the Small Gain theorem [49–51].

A block diagram for a DOb based robust control system is shown in Fig. 3-2 when plant is defined by using an output multiplicative unstructured uncertainty.

In this figure, $G(s)$ and $G_n(s)$ denote uncertain and nominal plant dynamics, respectively; $W_S\,(s)$ and $W_P\,(s)$ denote robust stability and performance weighting functions, respectively; $C(s)$ denotes outer-loop performance controller; $Q(s)$ denotes the LPF of DOb; r, d and ξ denote reference, disturbance and noise external inputs, respectively; $\widehat{d^*}$ denotes estimated disturbance; and $\|\Delta\|_\infty < 1$.

The robustness, i.e., the robust stability and performance, of a DOb based control system can be analyzed analytically by using the output multiplicative unstructured uncertainty and Small Gain theorem as follows:

Robust Stability:

$$\|\Delta W_S T\|_\infty < 1, \tag{3.3}$$

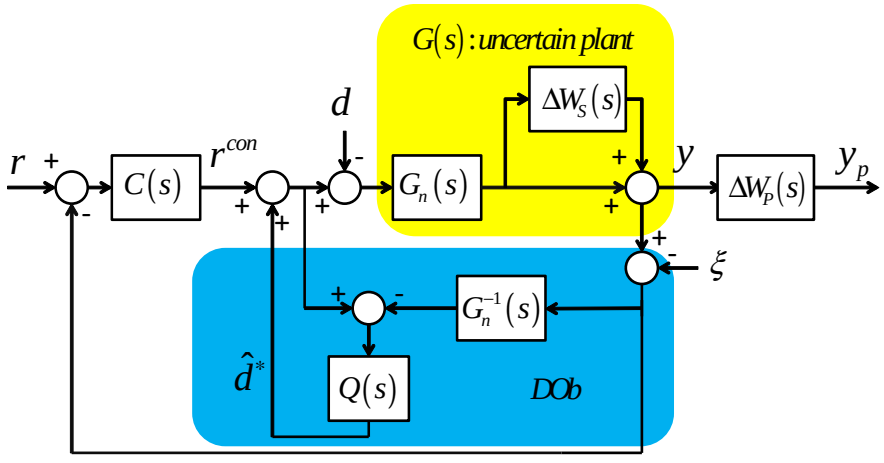

Fig. 3-2: Block diagram of a DOb based robust control system when output multiplicative unstructured uncertainty is used to define uncertain plant.

Robust Performance:

$$\|\Delta W_P S\|_\infty < 1, \tag{3.4}$$

where $S(s)$ and $T(s)$ denote the sensitivity and co-sensitivity transfer functions, respectively.

Equation (3.3) and eq. (3.4) show that the robust stability and performance of a DOb based control system can be easily analyzed by deriving the sensitivity and co-sensitivity transfer functions. However, in general, weighting function design is the most challenging issue and influences the performances of control systems and conservatism of analyses, significantly.

Sensitivity and co-sensitivity transfer functions of a DOb based robust control system are derived directly from Fig. 3-2 as follows:

Inner-loop:

$$S_i(s) = \frac{G_n(s)(1-Q(s))}{G_n(s)(1-Q(s)) + G(s)Q(s)}, \tag{3.5}$$

$$T_i(s) = \frac{G(s)Q(s)}{G_n(s)(1-Q(s)) + G(s)Q(s)}, \tag{3.6}$$

Outer-loop:

$$S_o(s) = \frac{G_n(s)(1-Q(s)) + G(s)Q(s)}{G_n(s)(1-Q(s)) + G(s)Q(s) + G(s)G_n(s)C(s)}, \tag{3.7}$$

$$T_o(s) = \frac{G(s)G_n(s)C(s)}{G_n(s)(1-Q(s)) + G(s)Q(s) + G(s)G_n(s)C(s)}, \tag{3.8}$$

where $S_\bullet(s)$ and $T_\bullet(s)$ denote inner and outer-loops' sensitivity and co-sensitivity transfer functions, respectively.

Equation (3.3) and eq. (3.6) show that the bandwidth of a DOb is directly limited by the robust stability weighting function, i.e., if the bandwidth of DOb is higher than the frequency in which the nominal plant model cannot describe the dynamics of the exact plant sufficiently, then the robust stability deteriorates. Consequently, the bandwidth of DOb, i.e, the performance of the robust control system, is limited by the identification of plant uncertainties, i.e., the dynamics of $W_S(s)$.

At low frequencies, i.e., $Q(s) \cong 1$, the sensitivity and co-sensitivity transfer functions are derived as follows:

Inner-Loop:

$$\begin{aligned} S_i(s) &= 0, \\ T_i(s) &= 1, \end{aligned} \tag{3.9}$$

Outer-Loop:

$$\begin{aligned} S_o(s) &= \frac{G(s)}{G(s) + G(s) G_n(s) C(s)}, \\ T_o(s) &= \frac{G(s) G_n(s) C(s)}{G(s) + G(s) G_n(s) C(s)}. \end{aligned} \tag{3.10}$$

It is clear from eq. (3.9) that if external disturbances have low frequencies, then a DOb provides good robustness by suppressing external disturbances in the inner loop. Although, in general, it is assumed that the robustness and performance of a DOb based control system are independently adjusted in the inner and outer-loops, respectively, eq. (3.10) shows that the performance controller, $C(s)$, changes the robustness of the outer-loop.

At high frequencies, i.e., $Q(s) \cong 0$, the sensitivity and co-sensitivity transfer functions are derived as follows:

Inner-Loop:

$$\begin{aligned} S_i(s) &= 1, \\ T_i(s) &= 0, \end{aligned} \tag{3.11}$$

Outer-Loop:

$$\begin{aligned} S_o(s) &= \frac{G_n(s)}{G_n(s) + G(s) G_n(s) C(s)}, \\ T_o(s) &= \frac{G(s) G_n(s) C(s)}{G_n(s) + G(s) G_n(s) C(s)}. \end{aligned} \tag{3.12}$$

Equation (3.11) shows that a DOb is sensitive to external disturbances at high frequencies, however noise can be suppressed precisely in the inner-loop.

The sensitivity and co-sensitivity transfer functions clearly show the asymptotic behaves of a DOb based robust control system's frequency responses. However, as shown in eq. (3.3) and eq. (3.4), the robust stability and performance are determined by the supremums' of the sensitivity and co-sensitivity transfer functions' frequency responses. Therefore, the analyses of asymptotic behaves are not sufficient to determine the robustness.

3.2.1 Simulations

In the simulations, a DOb based robust control system is designed for the uncertain plant model that is defined in eq. (3.1) and eq. (3.2). Robust stability and performance of the DOb based control system

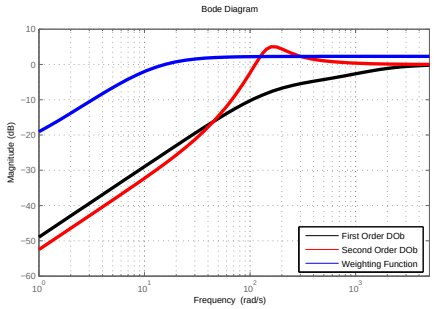

(a) Inner-loop sensitivity function.

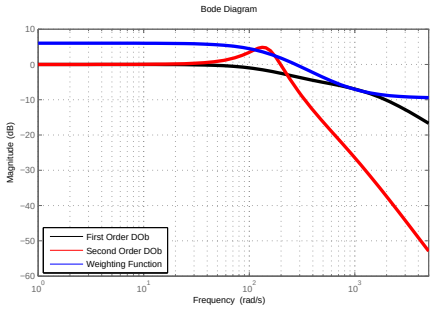

(b) Inner-loop co-sensitivity function.

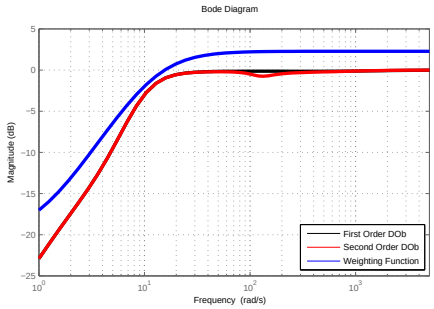

(c) Outer-loop sensitivity function.

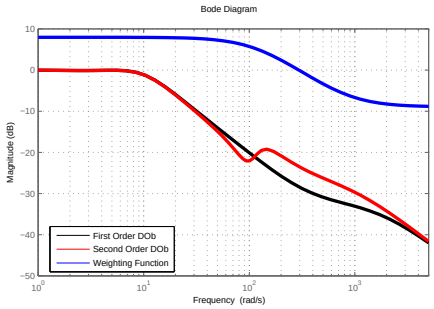

(d) Outer-loop co-sensitivity function.

Fig. 3-3: Sensitivity and Co-sensitivity function frequency responses.

are analyzed by using the Small Gain theorem so as to clarify the conventional analysis method. The uncertain plant model is obtained by using the first order approximation of the output-multiplicative unstructured uncertainty weighting function as follows:

$$G(s) = \frac{s+9}{s^2+8s+20}\left(1+\Delta\frac{2s+120}{s+600}\right). \tag{3.13}$$

The performance weighting function is chosen as $W_P(s) = \frac{0.5s+10}{s+0.5}$. The sensitivity and co-sensitivity transfer function frequency responses are shown in Fig. 3-3.

Fig. 3-3 shows the inner and outer loops' sensitivity and co-sensitivity transer functions frequency responses, i.e., the inner and outer loops' robust performance and stability, respectively. Fig. 3-3(a) and Fig. 3-3(b), respectively, indicate that the robust performance and stability of the inner-loop are related to the bandwidth of DOb significantly, and as the bandwidth of DOb is increased, the robustness of inner-loop deteriorates. In the simulations, the upper bound of the bandwidth of DOb is obtained as 200 rad/s..

to satisfy the robust stability and performance. As shown in Fig. 3-3, the bandwidth constraints become more severe as the order of DOb is increased. It is a well-known fact that although the robustness deteriorates, the performance of a DOb is improved by using a HODOb. Fig. 3-3 clearly indicates that the outer-loop performance controller changes the robustness of a DOb based control system.

3.3 Structured Singular Values (μ-synthesis)

To decrease the conservatism, structured uncertainty based analysis methods are generally used in the literature [31, 52]. Structured Singular Values (SSV), which was proposed by Doyle, is one of the most widely used structured uncertainty based robustness analysis methods [27]. It can be easily implemented into many different robust control problems, e.g., multi-input-multi-output (MIMO) control systems, by using the μ and "Robust Control" toolboxes of Matlab [26, 28]. Although the conservatism can be decreased by using the SSV, it cannot be removed completely due to the discontinuity problem of the real SSV [53].

Guvenc et al. and Sariyildiz et al. analyzed the robustness of DOb based control systems by using the SSV and obtained less conservative results than the conventional analysis method [44, 47]. Block diagram of a DOb based robust control system is shown in Fig. 3-4 when an uncertain plant is defined by using the SSV.

In this figure, $M_{\alpha_2^{-1}} = \begin{bmatrix} -\alpha_{2_\delta} & -\alpha_{2_n}^{-1} \\ -\alpha_{2_\delta} & -\alpha_{2_n}^{-1} \end{bmatrix}$, $M_{\alpha_i} = \begin{bmatrix} 0 & 1 \\ \alpha_{i_\delta}\alpha_{i_n} & \alpha_{i_n} \end{bmatrix}$ and $M_{\beta_j} = \begin{bmatrix} 0 & 1 \\ \beta_{j_\delta}\beta_{j_n} & \beta_{j_n} \end{bmatrix}$ denote the linear fractional transformations; $\alpha_i = \alpha_{i_n}\left(1 + \alpha_{i_\delta}\delta_{\alpha_i}\right)$, $\beta_j = \beta_{j_n}\left(1 + \beta_{j_\delta}\delta_{\beta_j}\right)$ denote structured parametric uncertainties in which α_{i_n} and β_{j_n} denote nominal plant parameters and $\alpha_{i_\delta}\delta_{\alpha_i}$ and $\beta_{j_\delta}\delta_{\beta_j}$ denote parametric uncertainties.

By using the SSV, the robust stability of a control system can be simply analyzed in a compact form as follows:

$$\sup\left(\mu_\Delta\left(M\right)\right) < 1, \tag{3.14}$$

where $\mu_\Delta\left(M\right) = \frac{1}{\min\{\overline{\sigma}(\Delta):\det(I-M\Delta)=0, \Delta\, is\, structured\}}$.

The robust performance can be similarly analyzed by using the SSV [26, 28]. The SSV can be implemented into DOb based robust control systems systematically by using the μ toolbox of Matlab; however, the robustness characteristics of a DOb cannot be clarified by using the μ toolbox.

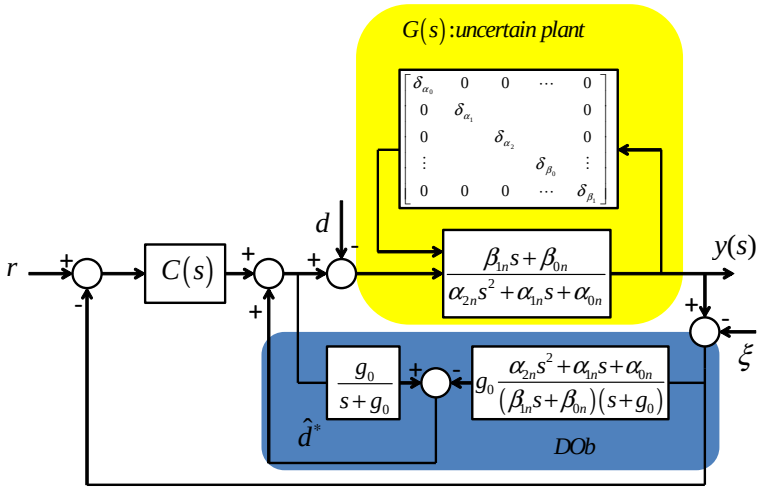

(a) SSV structure.

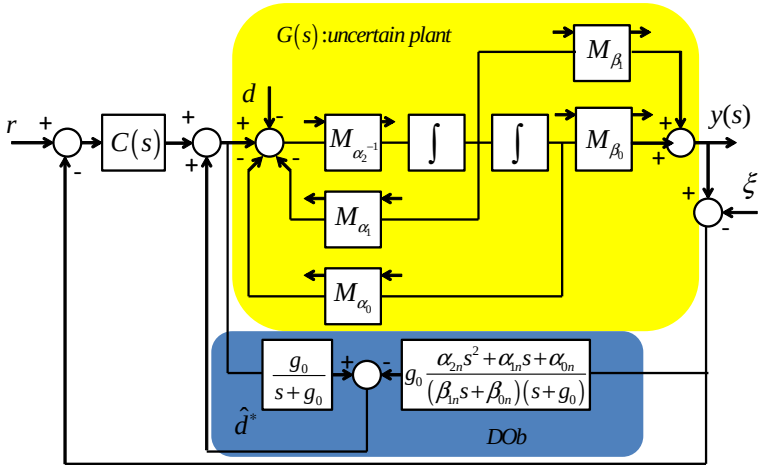

(b) Linear Fractional Transformation.

Fig. 3-4: Block diagram of a DOb based robust control system when SSV is implemented.

3.3.1 Simulations

In the simulations, DOb based robust control problem of the uncertain plant that is defined in eq. (3.1) and eq. (3.2) is re-considered by using the SSV. The robustness of the control system is analyzed by using the μ toolbox of Matlab. Fig. 3-5 and Fig. 3-6 show the robust stability and performance analysis results, respectively.

To solve the discontinuity problem, fictitious complex coefficients, which cause small conservatisms,

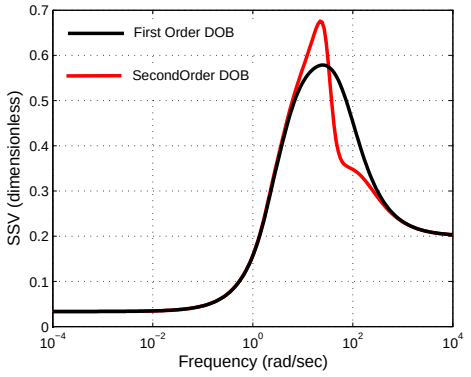

(a) Inner-loop robust stability analysis. Bandwidth of DOb is 80 rad/s.

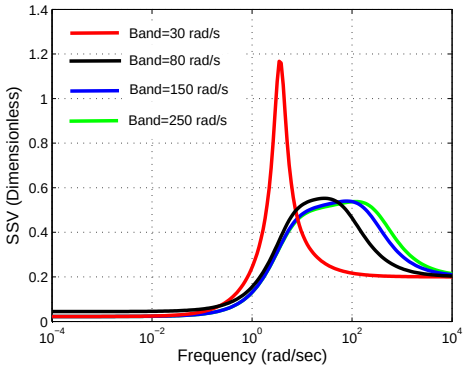

(b) Inner-loop robust stability analysis.

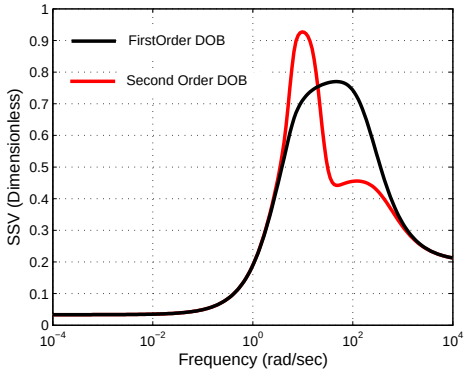

(c) Outer-loop robust stability analysis. Bandwidth of DOb is 180 rad/s.

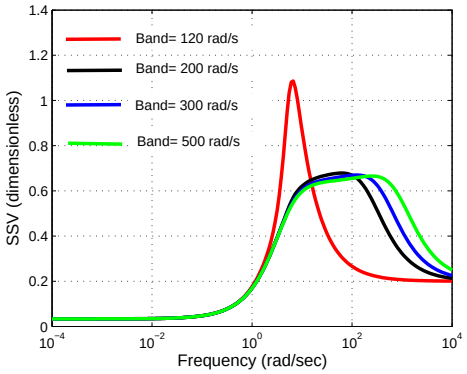

(d) Outer-loop robust stability analysis.

Fig. 3-5: Robust stability analysis by using the SSV.

are used in the definitions of the structured uncertainties.

Fig. 3-5 shows that increasing the bandwidth of DOb improves the robust stability; however, increasing the order of DOb deteriorates the robustness. The analysis shows that the robustness of the system is achieved when the bandwidth of DOb is 250 rad/s.. However, in the previous section, the conventional analysis shows that the bandwidth of DOb should be smaller than 200 rad/s. to achieve the robust stability. It is clear that the conservatism degrades the performance of DOb based control systems significantly by limiting the bandwidth of DOb.

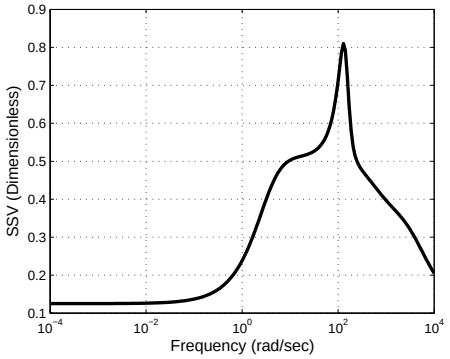

Fig. 3-6: Robust performance analysis by using the SSV.

3.4 DOb Design Constraints in the Presence of Real Parametric Uncertainty

In this section, the robustness of DOb based control systems is analyzed by using the robust control methods based on real parametric uncertainties [43]. To obtain a general result, it is assumed that the order of DOb is one and the uncertain plant is minimum phase. However, the proposed method can be similarly implemented into different plants that have real parametric uncertainties to determine the robustness. Kharitonov and Edge theorems are implemented into interval and affinely linear characteristic polynomials, respectively, and it is shown that the robustness of the control system is achieved if the bandwidth of DOb is higher than its lower bound [54–56]. Besides, Tsypkin-Polyak theorem is used, and it is shown that the robust stability margin of the DOb based control system improves as the bandwidth of DOb is increased [54–56]. Mikhailov criterion is used to show the robust stability [14]. The Mikhailov criterion, Kharitonov and Edge theorems are given without proofs as follows:

Theorem 3.1 Mikhailov Criterion: The real polynomial $p(s) = q_0 + q_1 s + \ldots + q_n s^n$ of degree n is stable if and only if the plot of $p(jw)$ with w increasing from 0 to ∞ turns strictly counterclockwise and goes through n quadrants in turn [14].

Theorem 3.2 Kharitanov Theorem: An interval polynomial $p(s) = q_0 + q_1 s + \ldots + q_n s^n$ where

$q_i^- \leq q_i \leq q_i^+$, is stable if and only if the following four Kharitanov polynomials are stable.

$$\begin{aligned} p^{--}(s) &= q_0^- + q_1^- s + q_2^+ s^2 + q_3^+ s^3 + q_4^- s^4 + q_5^- s^5 + \dots , \\ p^{-+}(s) &= q_0^- + q_1^+ s + q_2^+ s^2 + q_3^- s^3 + q_4^- s^4 + q_5^+ s^5 + \dots , \\ p^{+-}(s) &= q_0^+ + q_1^- s + q_2^- s^2 + q_3^+ s^3 + q_4^+ s^4 + q_5^- s^5 + \dots , \\ p^{++}(s) &= q_0^+ + q_1^+ s + q_2^- s^2 + q_3^- s^3 + q_4^+ s^4 + q_5^+ s^5 + \dots . \end{aligned} \tag{3.15}$$

It is sufficient to check the stability of $p^{+-}(s)$ if $p(s)$ is third order; $p^{+-}(s)$ and $p^{++}(s)$ if $p(s)$ is fourth order and $p^{+-}(s)$, $p^{++}(s)$ and $p^{-+}(s)$ if $p(s)$ is fifth order [14, 16, 17].

Theorem 3.3 Edge Theorem: An affinely linear polynomial, $p(s) = p_0(s) + \sum_{i=1}^{n} q_i p_i(s)$, in which $q_i^- \leq q_i \leq q_i^+$, is stable if and only if all edge polynomials are stable [14].

Kharitonov theorem is a very useful robust stability analysis tool when a characteristic polynomial is interval. However, the strict restriction on the characteristic polynomial limits the applications of Kharitonov theorem. Although it can be used even if a characteristic polynomial is not interval, results include conservatism. As shown in eq. (3.15), at most four polynomials should be analyzed to determine the robustness of uncertain systems when Kharitonov theorem is used. If a characteristic polynomial is affinely linear, then Edge theorem is used to obtain non-conservative robustness analysis results. However, $l \times 2^{l-1}$ number of edge polynomials should be analyzed for l number of uncertain parameters when Edge theorem is used.

Let us assume that a plant that includes real parametric uncertainties is defined as follows:

$$G(s) = \frac{\beta_{n-1} s^{n-1} + \beta_{n-2} s^{n-2} + \ldots + \beta_1 s + \beta_0}{\alpha_n s^n + \alpha_{n-1} s^{n-1} + \ldots + \alpha_1 s + \alpha_0}, \tag{3.16}$$

where $\alpha_i^- \leq \alpha_i \leq \alpha_i^+$ and $\beta_i^- \leq \beta_i \leq \beta_i^+$ denote real uncertain parameters.

If the characteristic polynomials of a DOb based robust control system, which are given in eq. (3.5) and eq. (3.7), are considered, then a new property is obtained as follows:

Property: If the uncertain parameters are only at the denominator of the plant model, i.e., β_i is known, and the relative degree of the plant model is one, then the characteristic equations of the inner and outer loop transfer functions given in eq. (3.5) and eq. (3.7) are interval polynomials. However, if the uncertain parameters are also at the numerator of the plant model and / or its relative degree is higher than one, then the characteristic equations of the inner and outer loop transfer functions are affinely linear polynomials.

Proof: The property can be proved by using a general example. Let us consider: a PID controller that

is defined by $C(s) = K_p + K_i\frac{1}{s} + K_d s$, the LPF of a DOb that is defined by $Q(s) = \frac{g_0}{s+g_0}$ in which g_0 denotes the bandwidth of DOb, and a general second order uncertain plant model that is defined by $G(s) = \frac{\beta_1 s+\beta_0}{\alpha_2 s^2+\alpha_1 s+\alpha_0}$. The characteristic equations of the inner and outer loop transfer functions are derived as follows:

Inner-Loop:

$$\nabla_i(s) = \lambda_{i0} + \lambda_{i1}s + \lambda_{i2}s^2 + \lambda_{i3}s^3 + \lambda_{i4}s^4, \tag{3.17}$$

where $\lambda_{i0} = \alpha_{0_n} g_0$, $\lambda_{i1} = \alpha_0 + \alpha_{1_n} g_0$, $\lambda_{i2} = \alpha_1 + \alpha_{2_n} g_0$, $\lambda_{i3} = \alpha_2$, and $\lambda_{i4} = 0$ if the numerator parameters of the plant are known; however, $\lambda_{i0} = \alpha_{0_n}\beta_0 g_0$, $\lambda_{i1} = \alpha_0\beta_{0_n} + \alpha_{1_n}\beta_0 g_0 + \alpha_{0_n}\beta_1 g_0$, $\lambda_{i2} = \alpha_1\beta_{0_n} + \alpha_0\beta_{1_n} + \alpha_{2_n}\beta_0 g_0 + \alpha_{1_n}\beta_1 g_0$, $\lambda_{i3} = \alpha_2\beta_{0_n} + \alpha_1\beta_{1_n} + \alpha_{2_n}\beta_1 g_0$, and $\lambda_{i4} = \alpha_2\beta_{1_n}$ if the numerator parameters of the plant are uncertain.

Outer-Loop:

$$\nabla_o(s) = \lambda_{o0} + \lambda_{o1}s + \lambda_{o2}s^2 + \lambda_{o3}s^3 + \lambda_{o4}s^4 + \lambda_{o5}s^5, \tag{3.18}$$

where $\lambda_{o0} = \beta_{0_n} g_0 K_i$, $\lambda_{o1} = \alpha_{0_n} g_0 + \beta_{0_n} K_i + \beta_{0_n} g_0 K_p + \beta_{1_n} g_0 K_i$, $\lambda_{o2} = \alpha_0 + \alpha_{1_n} g_0 + \beta_{0_n} g_0 K_d + \beta_{0_n} K_p + \beta_{1_n} K_i + \beta_{1_n} g_0 K_p$, $\lambda_{o3} = \alpha_1 + \alpha_{2_n} g_0 + \beta_{0_n} K_d + \beta_{1_n} g_0 K_d + \beta_{1_n} K_p$, $\lambda_{o4} = \alpha_2 + \beta_{1_n} K_d$, and $\lambda_{o5} = 0$ if the numerator parameters of the plant are known; however, $\lambda_{o0} = \beta_0\beta_{0_n} g_0 K_i$, $\lambda_{o1} = \alpha_{0_n}\beta_0 g_0 + \beta_0\beta_{0_n} K_i + \beta_{0_n}\beta_1 g_0 K_i + \beta_0\beta_{1_n} g_0 K_i + \beta_0\beta_{0_n} g_0 K_p$, $\lambda_{o2} = \alpha_0\beta_{0_n} + \alpha_{1_n}\beta_0 g_0 + \alpha_{0_n}\beta_1 g_0 + \beta_0\beta_{0_n} g_0 K_d + \beta_{0_n}\beta_1 K_i + \beta_0\beta_{1_n} K_i + \beta_1\beta_{1_n} g_0 K_i + \beta_0\beta_{0_n} K_p + \beta_{0_n}\beta_1 g_0 K_p + \beta_0\beta_{1_n} g_0 K_p$, $\lambda_{o3} = \alpha_1\beta_{0_n} + \alpha_0\beta_{1_n} + \alpha_{2_n}\beta_0 g_0 + \alpha_{1_n}\beta_1 g_0 + \beta_0\beta_{0_n} K_d + \beta_{0_n}\beta_1 g_0 K_d + \beta_0\beta_{1_n} g_0 K_d + \beta_1\beta_{1_n} K_i + \beta_{0_n}\beta_1 K_p + \beta_0\beta_{1_n} K_p + \beta_1\beta_{1_n} g_0 K_p$, $\lambda_{o4} = \alpha_2\beta_{0_n} + \alpha_1\beta_{1_n} + \alpha_{2_n}\beta_1 g_0 + \beta_{0_n}\beta_1 K_d + \beta_0\beta_{1_n} K_d + \beta_1\beta_{1_n} g_0 K_d + \beta_1\beta_{1_n} K_p$, and $\lambda_{o5} = \alpha_2\beta_{1_n} + \beta_1\beta_{1_n} K_d$ if the numerator parameters of the plant are uncertain. α_i and β_i denote uncertain plant parameters and α_{i_n} and β_{i_n} denote their nominal values, respectively.

The parameters of the controller and nominal plant model are known. Therefore, as it can be directly deduced from eq. (3.17) and eq. (3.18), the characteristic polynomials become interval (affinely linear) if the numerator parameters of $G(s)$ are known (uncertain). The relative degree case can be shown, similarly.

By using *Property*, the robust stability of the DOb based control systems are analyzed as follows:

Theorem 3.4 Robust Stability of DOb Based Control Systems with Real Parametric Uncertainties: The plant with real parametric uncertainties given in eq. (3.16) is robustly stable if the bandwidth of DOb, g_0, is higher than its lower bound g_{lower}.

Proof: Let us first consider the interval inner and outer loop characteristic polynomials case, in which

β_i is a known parameter. The Kharitonov polynomials of the inner and outer loop characteristic polynomials are as follows:

$$\begin{aligned}
\nabla_i^{--}(s) &= \lambda_{i0}^- + \lambda_{i1}^- s + \lambda_{i2}^+ s^2 + \lambda_{i3}^+ s^3 + \lambda_{i4}^- s^4 + \dots, \\
\nabla_i^{-+}(s) &= \lambda_{i0}^- + \lambda_{i1}^+ s + \lambda_{i2}^+ s^2 + \lambda_{i3}^- s^3 + \lambda_{i4}^- s^4 + \dots, \\
\nabla_i^{+-}(s) &= \lambda_{i0}^+ + \lambda_{i1}^- s + \lambda_{i2}^- s^2 + \lambda_{i3}^+ s^3 + \lambda_{i4}^+ s^4 + \dots, \\
\nabla_i^{++}(s) &= \lambda_{i0}^+ + \lambda_{i1}^+ s + \lambda_{i2}^- s^2 + \lambda_{i3}^- s^3 + \lambda_{i4}^+ s^4 + \dots,
\end{aligned} \tag{3.19}$$

$$\begin{aligned}
\nabla_o^{--}(s) &= \lambda_{o0}^- + \lambda_{o1}^- s + \lambda_{o2}^+ s^2 + \lambda_{o3}^+ s^3 + \lambda_{o4}^- s^4 + \dots, \\
\nabla_o^{-+}(s) &= \lambda_{o0}^- + \lambda_{o1}^+ s + \lambda_{o2}^+ s^2 + \lambda_{o3}^- s^3 + \lambda_{o4}^- s^4 + \dots, \\
\nabla_o^{+-}(s) &= \lambda_{o0}^+ + \lambda_{o1}^- s + \lambda_{o2}^- s^2 + \lambda_{o3}^+ s^3 + \lambda_{o4}^+ s^4 + \dots, \\
\nabla_o^{++}(s) &= \lambda_{o0}^+ + \lambda_{o1}^+ s + \lambda_{o2}^- s^2 + \lambda_{o3}^- s^3 + \lambda_{o4}^+ s^4 + \dots.
\end{aligned} \tag{3.20}$$

The lower bound on the bandwidth of DOb is derived by using the Mikhailov and Kharitonov theorems as follows:

Let us consider the outer loop Kharitonov polynomial of $\nabla_o^{-+}(s)$. It can be written in frequency domain by using

$$\nabla_o^{-+}(w) = \mathrm{Re}_{\nabla_o^{-+}}\left(w, g_0, \alpha_i^{\pm}\right) + jw\mathrm{Im}_{\nabla_o^{-+}}\left(w, g_0, \alpha_i^{\pm}\right), \tag{3.21}$$

where

$$\begin{aligned}
\mathrm{Re}_{\nabla_o^{-+}}\left(w, g_0, \alpha_i^{\pm}\right) &= \lambda_{o0}^- - \lambda_{o2}^+ w^2 + \lambda_{o4}^- w^4 - \dots, \\
\mathrm{Im}_{\nabla_o^{-+}}\left(w, g_0, \alpha_i^{\pm}\right) &= \lambda_{o1}^+ - \lambda_{o3}^- w^2 + \lambda_{o5}^+ w^4 - \dots.
\end{aligned} \tag{3.22}$$

If the polynomial $\nabla_o^{-+}(s)$ is stable, then the frequency response of the polynomial $\nabla_o^{-+}(jw)$ with w increasing from 0 to ∞ turns strictly counterclockwise and goes through $n+2$ quadrants in turn. If

$$\begin{aligned}
\mathrm{Re}_{\nabla_o^{-+}}\left(w, g_0, \alpha_i^{\pm}\right) &= \lambda_{o0}^- - \lambda_{o2}^+ w^2 + \lambda_{o4}^- w^4 - \dots = 0, \\
\mathrm{Im}_{\nabla_o^{-+}}\left(w, g_0, \alpha_i^{\pm}\right) &= \lambda_{o1}^+ - \lambda_{o3}^- w^2 + \lambda_{o5}^+ w^4 - \dots = 0,
\end{aligned} \tag{3.23}$$

are solved in terms of g_0 and $\alpha_i^{\pm}$, then $w_i = \psi_i\left(g_0, \alpha_i^{\pm}\right)$, in which $i = 1, 2, 3, \ldots, n+2$, is derived. Let us assume that $w_1 \leq w_2 \leq w_3 \ldots$. Consequently, the following conditions are derived to determine the stability of $\nabla_o^{-+}(s)$.

$$\begin{aligned}
\mathrm{Im}_{\nabla_o^{-+}}\left(w_1, g_0, \alpha_i^{\pm}\right) &= \mathrm{Im}_{\nabla_o^{-+}}\left(\psi_1\left(g_0, \alpha_i^{\pm}\right), g_0, \alpha_i^{\pm}\right) > 0, \\
\mathrm{Re}_{\nabla_o^{-+}}\left(w_2, g_0, \alpha_i^{\pm}\right) &= \mathrm{Re}_{\nabla_o^{-+}}\left(\psi_2\left(g_0, \alpha_i^{\pm}\right), g_0, \alpha_i^{\pm}\right) < 0, \\
\mathrm{Im}_{\nabla_o^{-+}}\left(w_3, g_0, \alpha_i^{\pm}\right) &= \mathrm{Im}_{\nabla_o^{-+}}\left(\psi_3\left(g_0, \alpha_i^{\pm}\right), g_0, \alpha_i^{\pm}\right) < 0, \\
\mathrm{Re}_{\nabla_o^{-+}}\left(w_4, g_0, \alpha_i^{\pm}\right) &= \mathrm{Re}_{\nabla_o^{-+}}\left(\psi_4\left(g_0, \alpha_i^{\pm}\right), g_0, \alpha_i^{\pm}\right) > 0.
\end{aligned} \tag{3.24}$$

The minimum value of g_0, which satisfies all inequalities in eq. (3.24), gives us the stabilizing bandwidth, $g_{\nabla_o^{-+}}$, for the polynomial of $\nabla_o^{-+}(s)$. Consequently, the lower bound on the bandwidth of DOb is derived as follows:

$$g_{lower} = \max\left(\max\left(g_{\nabla_i^{--}}, g_{\nabla_i^{-+}}, g_{\nabla_i^{+-}}, g_{\nabla_i^{++}}\right), \max\left(g_{\nabla_o^{--}}, g_{\nabla_o^{-+}}, g_{\nabla_o^{+-}}, g_{\nabla_o^{++}}\right)\right). \tag{3.25}$$

Now, let us consider the affinely linear characteristic polynomial case, in which β_i is an uncertain parameter. The Edge theorem is used to determine the lower bound on the bandwidth of DOb. $(n+m) \times 2^{n+m-1}$ number of edge polynomials should be analyzed to find the lower bound on the bandwidth of DOb. They can be defined as follows:

There are 2^{n+m} vertex polynomials,

$$\begin{aligned}
p_{v_0} &= \nabla(s, \alpha, \beta, g_0)\,|_{\alpha_n=\alpha_n^-,\ldots,\alpha_0=\alpha_0^-,\beta_m=\beta_m^-\ldots\beta_0=\beta_0^-}, \\
p_{v_1} &= \nabla(s, \alpha, \beta, g_0)\,|_{\alpha_n=\alpha_n^-,\ldots,\alpha_0=\alpha_0^-,\beta_m=\beta_m^-\ldots\beta_0=\beta_0^+}, \\
p_{v_{2^{n+m-1}}} &= \nabla(s, \alpha, \beta, g_0)\,|_{\alpha_n=\alpha_n^-,\ldots,\alpha_0=\alpha_0^+,\beta_m=\beta_m^+\ldots\beta_0=\beta_0^+}.
\end{aligned} \tag{3.26}$$

$(n+m) \times 2^{n+m-1}$ number of edge polynomials are derived by using the vertex polynomials as follows:

$$\begin{aligned}
p_{e_1} &= \kappa p_{v_1} + (1-\kappa) p_{v_2}, \\
p_{e_2} &= \kappa p_{v_1} + (1-\kappa) p_{v_3}, \\
p_{e_{2^{n+m-1}}} &= \kappa p_{v_{2^{n+m-1}}} + (1-\kappa) p_{v_1},
\end{aligned} \tag{3.27}$$

where $0 \leq \kappa \leq 1$.

The minimum value of g_0, which guarantees that all edge polynomials are stable, gives us the lower bound on the bandwidth of DOb. The Bialas theorem can be used to analyze the stability of edge polynomials [57, 58]. Also the algorithm, which is derived to find the lower bound in the interval polynomial case, can be used to find the lower bound in the affinely linear polynomial case as well. However, the constraint of $0 \leq \kappa \leq 1$ should also be considered in this case.

It should be noted here that it is very hard to find the analytical solution of the lower bound if the characteristic polynomial is affinely linear or the characteristic polynomial is interval and the number of the uncertain parameters is higher than three. For instance, the lower bound can be derived for the third order interval characteristic polynomial as follows:

$$g_0 > 0 \qquad and \qquad g_0 > \frac{\alpha_{0_n}\alpha_2^+ - \alpha_{1_n}\alpha_1^- - \alpha_{2_n}\alpha_0^-}{\alpha_{1_n}\alpha_{2_n}}. \tag{3.28}$$

However, the lower bound can be easily obtained by using numerical solution methods for both of the interval and affinely linear characteristic polynomials. To simplify the solution, Kharitonov theorem can also be applied to the affinely linear characteristic polynomials if the conservatism is acceptable. The acceptable conservatism means that the derived lower bound on the bandwidth of DOb should be smaller than its upper bound which is generally determined by practical constraints.

The numerical solutions can be extended to the polynomial coefficient case, which is more general form of the characteristic polynomials, by using the mapping theorem [14, 15]. However, only the interval and affinely linear polynomials are considered in this dissertation.

Theorem 3.4 is useful to determine whether a system is robustly stable or not; however, the degree of robust stability cannot be determined. The stability margin of a DOb based control system is determined by using *Theorem 3.6* as follows:

Let us first consider an interval polynomial $p(s) = q_0 + q_1 s + q_2 s^2 + \ldots + q_n s^n$, in which $q_i = q_i^0 + \delta_i q_i^*$, q_i^0 is nominal parameter, $q_i^* \leq 1$ is the normalized uncertain parameter, and δ_i is the coefficient of the normalized uncertain parameter. Without loose of generality, the normalized uncertain parameter is derived by using $q^* = \frac{2q - q^+ - q^-}{q^+ - q^-}$, in which q^- and q^+ denote lower and upper bounds of the uncertain parameter, respectively. Let us define new polynomials as follows:

$$p^0(w) = \text{Re}\left(p^0(jw)\right) + j\text{Im}\left(p^0(jw)\right) = U(w) + jV(w), \tag{3.29}$$

where $p^0(jw) = a_0^0 + a_1^0 s + \ldots + a_n^0 s^n$, and

$$\begin{aligned} S(w) &= \eta_0 + \eta_2 w^2 + \eta_4 w^4 + \ldots, \\ T(w) &= \eta_1 + \eta_3 w^2 + \eta_5 w^4 + \ldots, \end{aligned} \tag{3.30}$$

where $\left|a - a_i^0\right| < \gamma\eta_i$. Hence, a new function is defined as follows:

$$Z_{int} = \frac{U(w)}{S(w)} + j\frac{V(w)}{T(w)}. \tag{3.31}$$

Let us now consider an affinely linear polynomial that is $p(s) = p_0(s) + \sum_{i+1}^{l} q_i p_i(s)$, in which $|q_i| \leq 1$ is the uncertain parameter. A new function is defined as follows:

$$\begin{aligned} \tau(w) &= \max_{1\leq j\leq n} \frac{|\mathrm{Im}\left(p_0(jw)/p_k(jw)\right)|}{\sum_{i=1}^{l} |\mathrm{Im}\left(p_0(jw)/p_k(jw)\right)|} \qquad if\ w \neq w_s, \\ \tau(w) &= \frac{|p_0(jw)|}{\sum_{l}^{i=1} |p_i(jw)|}, \qquad w = w_s. \end{aligned} \tag{3.32}$$

Tsypkin-Polyak theorems for the interval and affinely linear polynomials are stated as follows:

Theorem 3.5 Tsypkin Polyak Theorem:

Interval Polynomial: An interval polynomial is robustly stable if the function $Z_{int}(w)$ holds the following conditions:

(1) It goes through n quadrants in counterclockwise direction for $w \in [0, \infty]$.

(2) It does not intersect the square centered at the origin with side length 2γ.

(3) Its boundary points, $Z_{int}(w)$ and $Z_{int}(\infty)$, have coordinates with absolute values larger than γ.

The stability margin of the interval polynomial is 2γ.

Affinely Linear Polynomial: An affinely linear polynomial is robustly stable if it holds the following conditions:

(1) $p_0(s)$ is stable.

(2) $\tau(w) > 1$, where $0 \leq w \leq \infty$.

or

(1) $p_0(s) \neq 0$ is stable.

(2) $Z_{aff}(w) = \frac{p_0(w)}{|p_0(w)|}$ goes for $0 \leq w \leq \infty$ through n quadrants and does not intersect the unit circle.

The stability margin of the affinely linear polynomial is $\min\left(\tau\left(w\right), \tau\left(w_s\right), \tau\left(0\right), \tau\left(\infty\right)\right)$.

Theorem 3.6 Stability Margin of the DOb Based Control Systems with Real Parametric Uncertainties: The stability margin of the system with the real parametric uncertainties increases as the bandwidth of DOb, g_0, increases, and the system becomes robustly stable if the bandwidth of DOb is higher than its lower bound $g_0 > g_{lower}$.

Proof: Let us consider the interval inner and outer loop characteristic polynomials case by using

$$\nabla_\bullet\left(s, g_0, q\right) = q_0 + q_1 s + \ldots + q_n s^n, \tag{3.33}$$

where $q_i = q_i^0 + \delta_i q_i^*$. The function $Z_{int}(w)$ is derived directly from eq. (3.31) as follows:

$$Z_{int}(w, g_0) = \frac{U\left(w, g_0\right)}{S\left(w\right)} + j\frac{V\left(w, g_0\right)}{T\left(w\right)}. \tag{3.34}$$

The second condition of *Theorem 3.5* is re-written as follows:

$$\frac{U\left(w, g_0\right)}{S\left(w\right)} > \gamma \qquad and \qquad \frac{V\left(w, g_0\right)}{T\left(w\right)} > \gamma. \tag{3.35}$$

Equation (3.35) gives us the robust stability radius of the DOb based control system. It directly shows that as the bandwidth of DOb increases, the robust stability margin of the system also increases since the characteristic polynomials of a DOb based control system are as follows:

$$\begin{aligned} \nabla_i\left(s\right) &= D\left(s\right) N_{n(s)} s + D_n\left(s\right) N\left(s\right) g_0, \\ \nabla_o\left(s\right) &= D\left(s\right) N_{n(s)} s + D_n\left(s\right) N\left(s\right) g_0 + N\left(s\right) N_n\left(s\right) C\left(s\right), \end{aligned} \tag{3.36}$$

where $N\left(s\right), D\left(s\right), N_{n(s)}$ and $D_{n(s)}$ denote the uncertain and nominal numerator and denominator polynomials, respectively. It should be noted here that the conditions 1 and 3 should also be checked to determine the robust stability.

Let us now consider the affinely linear characteristics polynomial case. The characteristic polynomial is rewritten as follows:

$$p_0(s) + \sum_{i=1}^{l} q_i p_i(s), \tag{3.37}$$

where $|q_i| \leq 1$. The function $\tau(w)$ is re-written by using eq. (3.38) as follows:

$$\begin{aligned} \tau(w, g_0) &= \max_{1 \leq j \leq n} \frac{|Im(p_0(jw, g_0)/p_k(jw, g_0))|}{\sum_{i=1}^{l} |Im(p_0(jw, g_0)/p_k(jw, g_0))|}, \qquad if\ w \neq w_s, \\ \tau(w, g_0) &= \frac{|p_0(jw, g_0)|}{\sum_{l}^{i=1} |p_i(jw, g_0)|}, \qquad w = w_s. \end{aligned} \tag{3.38}$$

The second condition of *Theorem 3.5* gives the robust stability radius of a DOb based control system. If the characteristic polynomials of the inner and outer loops, which are given in eq. (3.36), are considered, then it can be easily seen that as the bandwidth of DOb is increased the function $\tau(w, g_0)$ increases as well. Therefore, the stability margin of the system is improved as the bandwidth of DOb is increased. The stability margin of the system is derived as follows:

$$\begin{aligned} &\min(\tau(w), \tau(w_s), \tau(0), \tau(\infty)) \qquad or, \\ &Z_{aff}(w) = \tfrac{p_0(w)}{|p_0(w)|}. \end{aligned} \tag{3.39}$$

3.4.1 Simulations

Let us consider the uncertain plant model that is given in eq. (3.1) and eq. (3.2). The non-conservative robust stability analysis result can be obtained by using *Theorem 3.4*. If it is applied to the uncertain plant model, then the lower bound on the bandwidth of DOb are derived as 16 rad/s. and 25 rad/s. in the inner and outer loops, respectively. Consequently, the lower bound is derived as 25 rad/s. to obtain the robust stability. The Mikhailov plots of the inner and outer loop characteristic polynomials are shown in Fig. 3-7(a) and Fig. 3-7(b), respectively. If *Teorem 3.4* is used for the affinely linear characteristic polynomials by considering the Kharitonov and Edge theorems, then the lower bounds on the bandwidth of DOb are derived as 925 rad/s. and 166 rad/s., respectively. Since the former is higher than 700 rad/s., the conservative result of the theorem cannot be used in this system. The Mikhailov plots of the inner and outer loop characteristic polynomials are shown in Fig. 3-7(c) and Fig. 3-7(d), respectively.

The stability margin analysis is obtained by using *Theorem 3.6*. Fig. 3-8(a) and Fig. 3-8(b) show the frequency responses of the functions $Z_{int}(w)$ and $Z_{aff}(w)$ when the characteristic polynomials

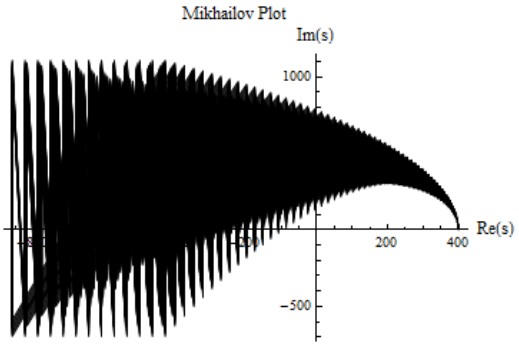

(a) Inner-loop interval characteristic polynomial.

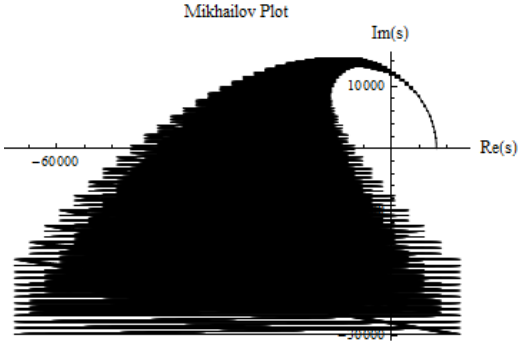

(b) Outer-loop interval characteristic polynomial.

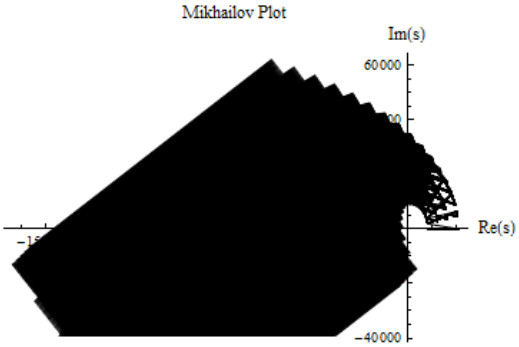

(c) Inner-loop affinely linear characteristic polynomial.

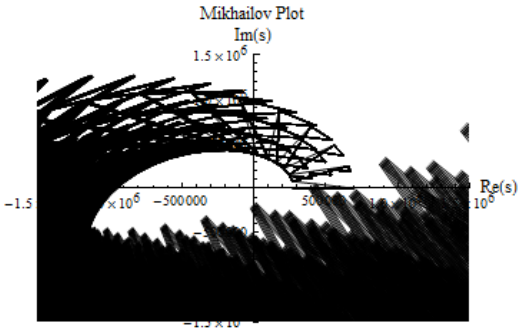

(d) Outer-loop affinely linear characteristic polynomial.

Fig. 3-7: Mikhailov plots of the inner and outer loop characteristic polynomials.

are interval and affinely linear, respectively. The unit square/circle indicates the limit of the robust stability, and the system becomes robustly stable if the curve of $Z_{int}(w)$ / $Z_{aff}(w)$ stays out of the unit square/circle. The minimum distance between the curve of $Z_{int}(w)$ / $Z_{aff}(w)$ and the unit square/circle determines the robust stability margin. The red, black, blue, green and cyan curves of $Z_{int}(w)$ / $Z_{aff}(w)$ are sketched when the bandwidth of DOb, g_0,is 15 rad/s., 25 rad/s., 30 rad/s., 40 rad/s., and 60 rad/s. in Fig. 3-8(a) and 130 rad/s., 166 rad/s., 180 rad/s., 200 rad/s., and 300 rad/s. in Fig. 3-8(b). As it can be directly seen from the figures, as the bandwidth of DOb is increased, the stability margin of the system is increased as well.

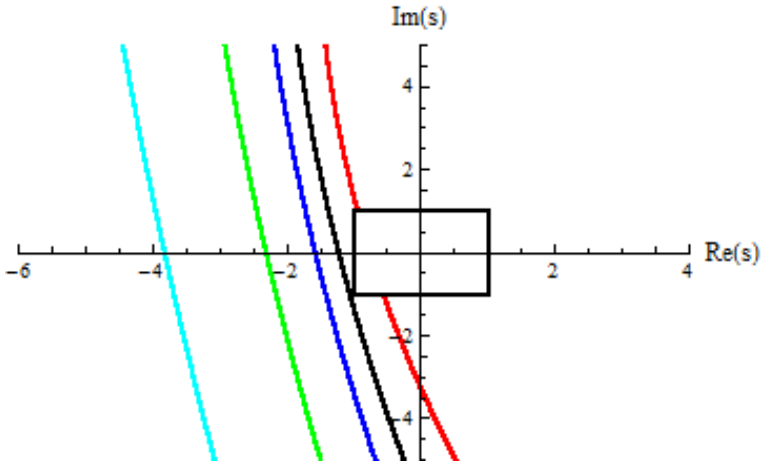

(a) Frequency response of $Z_{int}(w)$.

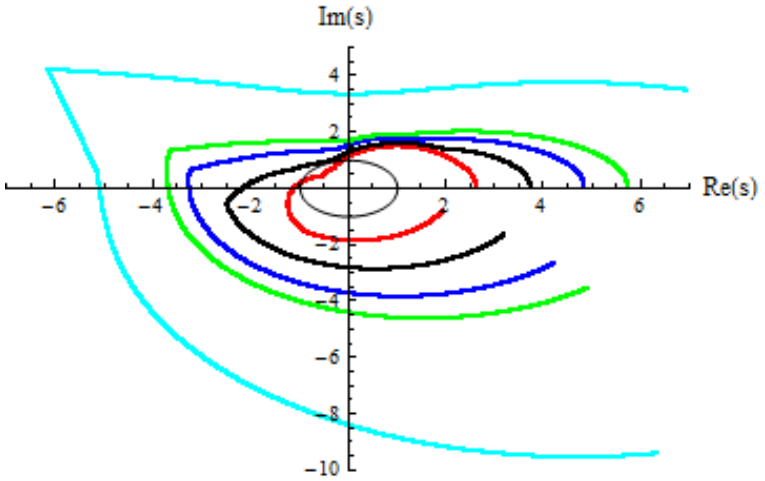

(b) Frequency response of $Z_{aff}(w)$.

Fig. 3-8: Stability margin analysis of interval and affinely linear characteristic polynomials.

3.5 DOb Design Constraints in the Presence of Unstructured Uncertainty

In this section, design constraints of DOb based robust control systems are derived analytically by using unstructured uncertainty based analysis methods [45]. Bode integral formula is utilized so that the robustness constraints are derived for minimum phase and time delay systems [45, 59–61]; and Poisson integral formula is utilized to derive the robustness constraints of systems with right half plane

(RHP) zero(s) and pole(s) [45, 61, 62]. It is shown that RHP zero(s) and/or time-delay of a plant limit the bandwidth of DOb; however, RHP pole(s) of a plant put(s) a lower bound on the bandwidth of DOb to obtain a good robustness. Besides that increasing the order of DOb improves the performance of the system by using the bandwidth of DOb more efficiently; however, the bandwidth constraints become more severe, and the robustness of the system deteriorates. If a DOb is implemented to a non-minimum phase system, then internal stability problem occurs since inverse of nominal plant model is required in the design of a DOb. The internal stability problem is solved by using an approximate minimum phase model of the uncertain non-minimum phase plant. A new performance controller is proposed to improve the DOb based robust control systems when plants have RHP pole(s). Against the real parametric uncertainty based analysis, the proposed method includes conservatism. Therefore, it is not suitable to design a controller. However, the proposed tools provide clear insight into the robustness characteristics of a DOb based control system.

To analyze the robustness of a DOb based control system, uncertain plant model is defined by using the output multiplicative unstructured uncertainty as follows:

$$G(s) = G_n(s)\left(1 + \Delta W(s)\right)\exp\left(-\tau s\right), \tag{3.40}$$

where $G(s)$ and $G_n(s)$ denote uncertain and nominal plant models, respectively; $W(s)$ denotes multiplicative unstructured uncertainty weighting function; and τ denotes delay time. First order approximation of the output multiplicative unstructured uncertainty weighting function is used as follows:

$$W(s) = \frac{w_T^{-1}s + e_{min}}{w_T^{-1}e_{max}s + 1}, \tag{3.41}$$

where e_{min} and e_{max} denote minimum and maximum modeling errors, respectively; and w_T denotes the frequency, in which the nominal plant model starts to be a bad indicator for the uncertain plant [4]. It is assumed that $e_{max}^{-1} < \Delta < 1$ instead of $\Delta < 1$ not to add a RHP zero due to uncertainty. The n^{th} order LPF of DOb is defined as follows:

$$Q(s) = \frac{g_0}{s^n + g_{n-1}s^{n-1} + \ldots + g_1 s + g_0}, \tag{3.42}$$

The inner-loop's open loop, sensitivity and co-sensitivity transfer functions are derived by using eq. (3.40) and Fig. 3-2 as follows:

$$\begin{aligned} L_i(s) &= \frac{Q(s)}{1-Q(s)}\left(1+\Delta W(s)\right)\exp\left(-\tau s\right), \\ S_i(s) &= \frac{1-Q(s)}{1-Q(s)+Q(s)\left(1+\Delta W(s)\right)\exp\left(-\tau s\right)}, \\ T_i(s) &= \frac{Q(s)\left(1+\Delta W(s)\right)\exp\left(-\tau s\right)}{1-Q(s)+Q(s)\left(1+\Delta W(s)\right)\exp\left(-\tau s\right)}. \end{aligned} \tag{3.43}$$

Let us first consider minimum phase plants.

Lemma1: Let us consider the plant model given in eq. (3.40) and assume that the uncertain plant is minimum phase and the order of DOb is one. Then, it can be shown that the inner-loop is strictly robust if $\Delta > 0$ and its robustness can be guaranteed for a wide range of DOb's bandwidth if $\Delta < 0$. However, if a HODOb is used instead of DOb and/or the plant includes time delay, then the robustness of inner-loop cannot be guaranteed for a wide range of DOb's bandwidth even if $\Delta > 0$, and the bandwidth of DOb becomes limited.

Proof: The open loop-transfer function of the inner-loop given in eq. (3.43) can be re-written when a first order DOb is used in the robust control problem of minimum phase plants as follows:

$$L_i(s) = g_0\left(1+\Delta e_{max}\right)\frac{s+w_T e_{max}\left(\frac{1+\Delta e_{min}}{1+\Delta e_{max}}\right)}{s\left(s+w_T e_{max}\right)}. \tag{3.44}$$

Equation (3.44) shows that the strict robustness can be achieved when $\Delta > 0$ since the Nyquist plot of the inner-loop gets into the unit circle that is shown in Fig. 3-9 if $e_{min} > e_{max}$ which contradicts with the error assumption. Although the Nyquist plot gets inside the unit circle when $\Delta < 0$ robust stability can be achieved for a wide range of DOb' bandwidth.

If a HODOb is used instead of a DOb, then the robustness cannot be achieved for a wide range of DOb's bandwidth even if $\Delta > 0$. It can be easily shown by using a HODOb in eq. (3.43). In this case, the robustness of a system can be guaranteed for a limited bandwidth of HODOb. Besides, as shown in Fig. 3-9, the robustness cannot be guaranteed for a wide range of DOb's bandwidth if a plant includes time delay. Hence, the proof of *Lemma 1* is completed.

Although *Lemma1* gives us a basic insight into the robustness of DOb, further analysis is required for HODOb based robust control systems. HODOb can be analyzed by using the Horowitz integral formula that is given in eq. (3.45).

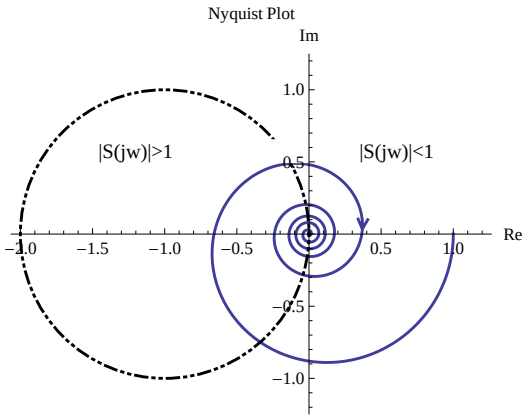

Fig. 3-9: Nyquist plot.

$$\int_0^\infty \left(\log\left(\left|S_i\left(jw\right)\right|\right) - \log\left(\left|S_i\left(j\infty\right)\right|\right)\right) dw = -\frac{\pi}{2}\mathrm{Re}s_{s=\infty}\left(\log\left(S_i\left(s\right)\right)\right). \tag{3.45}$$

The relative degree of $L_i(s)$ is higher than one when a HODOb is used. Therefore, if a HODOb is considered, then the Horowitz integral formula is simplified as the Bode integral formula by using

$$\int_0^\infty \log\left(\left|S_i\left(jw\right)\right|\right) dw = 0. \tag{3.46}$$

The peak of the sensitivity function, which is defined by $\sup\left(|S_i(jw)|\right)$, determines the robustness of control systems. However, eq. (3.46) is not suitable to determine the robustness of HODOb based control systems due to the infinite integral range. From mathematical point of view, eq. (3.46) can be balanced with a small peak in a wide frequency range. However, in general, control systems cannot exhibit this response due to uncertainties, digital control implementations, and so on. *Lemma2* limits the integral of eq. (3.46) as follows:

Lemma2: Let us assume that $L_i(s)$ satisfies

$$\left|L_i\left(s\right)\right| \leq \frac{M}{w^{k+1}} = \delta \leq \frac{1}{2}, \quad \forall w \geq w_\gamma, \tag{3.47}$$

where $M \geq \lim_{s\to\infty} \sup\left|s^{k+1}L_i(s)\right|$ and $k+1$ is the order of DOb. Then $S_i(s)$ satisfies

$$\left|\int_{w_\beta}^\infty \log\left(S_i\left(jw\right)\right) dw\right| \leq 3\frac{\delta}{2k}w_\gamma. \tag{3.48}$$

Proof: Equation (3.47) holds if a HODOb is used. Let us consider the relation by using [63, 64]

$$if\ L_i(s) \leq \frac{1}{2},\ then\ |\log\left(1+L_i(s)\right)| \leq \frac{3}{2}|L_i(s)| \leq \frac{3}{2}\delta. \tag{3.49}$$

If eq. (3.47) is put into eq. (3.49), then

$$\begin{aligned}\left|\int_{w_\gamma}^{\infty}\log\left(|S_i\left(jw\right)|\right)dw\right| &\leq \int_{w_\gamma}^{\infty}|\log\left(S_i(jw)\right)|\,dw \\ = \int_{w_\gamma}^{\infty}|\log\left(1+L_i(jw)\right)|\,dw &\leq \frac{3}{2}\int_{w_\gamma}^{\infty}\frac{M}{w^{k+1}}dw = \frac{3\delta}{2k}w_\gamma,\end{aligned} \tag{3.50}$$

The robustness constraints of a HODOb is derived by determining the performance and robustness requirements, a priori. Then, the sensitivity function frequency response is shaped by using the performance and robustness requirements. *Theorem 3.7* clarifies the bandwidth constraints of a HODOb as follows:

Theorem 3.7: Let us assume that a minimum phase plant is defined by using eq. (3.40). Let us also assume that $S_i(s)$ satisfies $|S_i(jw)| \leq \alpha < 1,\ \forall w \leq w_\beta < w_\gamma$. If a DOb is used, then the system has a good robustness in a wide frequency range, yet its performance is limited by the dynamic characteristics of the first order DOb. However, if a HODOb is used, then the low-pass-filter of HODOb should satisfy the following inequalities to obtain a good robustness and predefined performance criterion.

$$\begin{aligned}&|Q\left(jw\right)| \geq \tfrac{1-\alpha}{1+\alpha|\Delta W(jw)|},\ \forall w < \psi w_\gamma, \\ &\tfrac{|1-Q(j\psi w_\gamma)|}{|1+\Delta QW(j\psi w_\gamma)|} \geq \alpha,\end{aligned} \tag{3.51}$$

where $\psi = \frac{\sup_{w\in[w_\beta,w_\gamma]}\log(|S_i(jw)|)+\frac{3\delta}{2k}}{\sup_{w\in[w_\beta,w_\gamma]}\log(|S_i(jw)|)+\log(\alpha^{-1})}$ in which $|L_i\left(jw\right)| \leq \delta \leq \frac{1}{2},\ \forall w \geq w_\gamma$.

Poof: Lemma 1 proves the robustness of a DOb. Therefore, HODOb can be considered, directly. Let us re-write eq. (3.46) as follows:

$$\int_0^{w_\beta}\log(|S_i(jw)|)dw + \int_{w_\beta}^{w_\gamma}\log(|S_i(jw)|)dw + \int_{w_\beta}^{\infty}\log(|S_i(jw)|)dw = 0. \tag{3.52}$$

If the sensitivity constraints given in *Theorem 3.7* and *Lemma 2* are applied into eq. (3.52), then

$$\log(\alpha)\int_0^{w_\beta}dw + \sup_{w\in[w_\beta,w_\gamma]}\log(|S_i(jw)|)\int_{w_\beta}^{w_\gamma}dw + \frac{3\delta}{2k}w_\gamma \geq 0. \tag{3.53}$$

Equation (3.53) can also be written as follows:

$$\sup_{w\in[w_\beta,w_\gamma]} \log(|S_i(jw)|) \geq \log(\alpha^{-1})\frac{w_\beta}{w_\gamma - w_\beta} - \frac{3\delta}{2k}\frac{w_\gamma}{w_\gamma - w_\beta}, \tag{3.54}$$

$$\frac{w_\beta}{w_\gamma} \leq \psi = \psi = \frac{\sup_{w\in[w_\beta,w_\gamma]} \log\left(|S_i(jw)|\right) + \frac{3\delta}{2k}}{\sup_{w\in[w_\beta,w_\gamma]} \log\left(|S_i(jw)|\right) + \log\left(\alpha^{-1}\right)}. \tag{3.55}$$

If the sensitivity constraint given in *Theorem 3.7* is applied, then

$$\frac{|1 - Q\left(j\psi w_\gamma\right)|}{|1 + \Delta QW\left(j\psi w_\gamma\right)|} \leq \alpha,\ \forall w \leq w_\beta \leq w_\gamma. \tag{3.56}$$

If eq. (3.55) is applied into eq. (3.56), then eq. (3.51) is derived. Hence, the proof of *Theorem 3.7* is completed.

The frequencies w_β and w_γ get closer each other as the order of DOb is increased. Therefore, as shown in eq. (3.54), the peak of the sensitivity function increases as the order of DOb is increased.

Equation (3.56) shows that as the bandwidth of DOb is increased, α^{-1} and w_β increase as well. Therefore, as shown in eq. (3.54), the peak of the sensitivity function increases as the bandwidth of DOb is increased.

Theorem 3.7 provides a new design tool to obtain a good robustness and predefined performance criterion that are determined by α and w_β. However, it includes conservatism due to the sectionally constant sensitivity function bound that is defined by $|S_i(jw)| \leq \alpha < 1, \forall w \leq w_\beta \leq w_\gamma$. It can be lessened by using more realistic sensitivity function bounds [63, 64].

Let us now consider the design constraints when uncertain plant includes time delay. *Lemma 3* is used to bound the integral range of eq. (3.46) as follows:

Lemma 3: Let us assume that $L_i(s)$ includes time delay and satisfies

$$|L_i\left(s\right)| = \left|\tilde{L}_i\left(s\right)\exp\left(-\tau s\right)\right| \leq \frac{M}{R^k}\exp\left(-R\tau\cos\left(\theta\right)\right) \leq \delta\left(\frac{R}{|s|}\right)^k,\ \forall |s| \in S\left(R\right), \tag{3.57}$$

where $S\left(R\right) = \{s : Re\left(s\right) \geq 0\ and\ |s| \geq R\}$; $M \geq \lim_{s\to\infty}\sup\left|s^k L\left(s\right)\right|$; k is the order of DOb; and $s = R\exp(j\theta)$. Then S_i satisfies:

$$\left|\int_R^\infty \log\left(|S_i\left(jw\right)|\right) dw\right| \leq \frac{3\pi}{4\tau}\delta. \tag{3.58}$$

Proof: Similar to *Lemma 2*.

Hence, the bandwidth constraints of a DOb are derived by using *Theorem 3.8* as follows:

Theorem 3.8: Let us assume that a plant is defined by using eq. (3.40) where $G_n(s)$ is a minimum phase nominal plant model. Let us also assume that $S_i(s)$ satisfies $|S_i(s)| \leq \alpha < 1, \forall w \leq w_\beta$. Then the LPF of a DOb should satisfy the following inequalities to obtain a good robustness and predefined performance criterion.

$$\begin{aligned} &\tfrac{|Q(jw)|}{|1-Q(jw)|} \geq \tfrac{1-\alpha}{\alpha|1+\Delta W(jw)|}, \forall w \leq \psi R, \\ &\tfrac{|1-Q(j\psi R)|}{|1-Q(j\psi R)+Q(j\psi R)(1+\Delta W(j\psi R))\exp(-j\tau\psi R)|} \geq \alpha. \end{aligned} \tag{3.59}$$

If the order of DOb is one, then

$$\begin{aligned} &g_0 \geq \tfrac{(1-\alpha)w}{\alpha|1+\Delta W(jw)|}, \forall w \leq \psi R, \\ &\tfrac{\psi R}{|j\psi R+g_0(1+\Delta W(j\psi R))\exp(-j\psi\tau R)|} \geq \alpha, \end{aligned} \tag{3.60}$$

where $\psi = \frac{\sup_{w\in[w_\beta,R]}\log(|S_i(jw)|)+\frac{3\pi}{4\tau R}\delta}{\sup_{w\in[w_\beta,R]}\log(|S_i(jw)|)+\log(\alpha^{-1})}$ in which $|L_i(s)| \leq \delta\left(\frac{R}{|s|}\right)^k, \forall |s| \in S(R)$.

Proof: Similar to *Theorem 3.7*. *Lemma 3* is used instead of *Lemma 2*.

Equation (3.59) and eq. (3.60) provide new design tools for DOb based robust control systems when uncertain plant includes time-delay. They directly show that the bandwidth of a DOb is limited due to time delay. However, the proposed design tool also includes conservatism due to the sectionally constant sensitivity function bound.

To lessen the peak of $|S_i(jw)|$, the smallest value of R that satisfies *Theorem 3.8* should be chosen.

$$\sup_{s\in S(R)}(L_i(s)) = \max\left\{\sup_{w\geq R}(|L_i(jw)|), \sup_{0\leq\theta\leq\frac{\pi}{2}}(|L_i(R\exp(j\theta))|)\right\}. \tag{3.61}$$

Equation (3.61) shows that *Theorem 3.8* holds even if $\sup_{s\in S(R)}(L_i(s)) \geq \delta$, which can be used to lessen the peak of $|S_i(jw)|$. Consequently, the peak of the sensitivity function can be lessened if the following inequalities hold.

$$\frac{w_T e_{min}}{w^2+(w_T e_{min})^2}-\frac{w_T e_{max}}{w^2+(w_T e_{max})^2}>\tau,\ 1^{st}orderDOb$$
$$\frac{w_T e_{min}}{w^2+(w_T e_{min})^2}-\frac{w_T e_{max}}{w^2+(w_T e_{max})^2}>\tau+\frac{g_1}{s+g_1},\ 2^{nd}orderDOb,$$
$$\frac{w_T e_{min}}{w^2+(w_T e_{min})^2}-\frac{w_T e_{max}}{w^2+(w_T e_{max})^2}>\tau+\frac{g_1 g_2+g_2 w^2}{g_2^2 w^2+(g_1-w^2)^2},\ 3^{rd}orderDOb. \quad (3.62)$$

As it is expected from *Theorem 3.7*, eq. (3.62) shows that as the order of DOb is increased, the peak of $|S_i(jw)|$ also increases.

Finally, let us consider uncertain plants with right half plane pole(s) and zero(s). Right half plane zero(s) and pole(s) cause undershoot and overshoot in the step response of the closed loop systems, respectively. To achieve good performance, bandwidths of control systems are limited as follows [63, 64]:

$$w_B \leq \frac{2.1991 z_{RHP}}{\log\left(1-\frac{0.9}{y_{undershoot}}\right)}, \quad (3.63)$$
$$w_B \geq \frac{2.1991 p_{RHP}}{\log\left(10\left(y_{overshoot}-0.9\right)\right)}, \quad (3.64)$$

where w_B denote the bandwidth of closed loop system; z_{RHP} and p_{RHP} denote right half plane zero and pole, respectively; $y_{undershoot}$ and $y_{overshoot}$ denote the infimum and supremum of the step response, respectively. To derive the design constraints of a DOb, Poisson integral formula is used. It can be stated as follows:

Theorem 3.9. Poisson Integral Formulas: Assume that an open loop transfer function $L(s)$ has a right half plane zero/pole at $z_{RHP}=\sigma_z+jw_z/p_{RHP}=\sigma_p+jw_p$. Let $S(s)/T(s)$ be the sensitivity/co-sensitivity transfer function defined by $\frac{1}{1+L(s)}/\frac{L(s)}{1+L(s)}$. Then, it can be shown that the sensitivity/co-sensitivity transfer function satisfies:

$$\int_{-\infty}^{\infty}\log\left(\left|S\left(jw\right)\right|\right)\frac{\sigma_z}{\sigma_z^2+\left(w_z-w\right)^2}dw=\pi\log\left(B_S^{-1}\left(z_{RHP}\right)\right), \quad (3.65)$$
$$\int_{-\infty}^{\infty}\log\left(\left|T\left(jw\right)\right|\right)\frac{\sigma_p}{\sigma_p^2+\left(w_p-w\right)^2}dw=\pi\log\left(B_T^{-1}\left(p_{RHP}\right)\right), \quad (3.66)$$

where $L(s)=\tilde{L}(s)B_S^{-1}B_T(s)$; $\tilde{L}(s)$ is a minimum phase transfer function; $\prod_{i=1}^{k}\left(\left(p_i-s\right)/\left(\overline{p}_i+s\right)\right)$;

and $\prod_{i=1}^{l}\left(\left(z_i - s\right)/\left(\overline{z}_i + s\right)\right)$ are Blaschke products [63, 64]. It is clear from eq. (3.65) and eq. (3.66) that Poisson integrals' ranges are bounded by $W_{pi}\left(w\right) = \frac{\sigma_x}{\sigma_x^2 + \left(w_x - w\right)^2}$.

Let us first consider plant with RHP zero(s). To solve the internal stability problem, approximate nominal plant model should be used in the design of DOb. It can be defined as follows:

$$G\left(s\right) = G_n\left(s\right)\left(1 + \Delta W\left(s\right)\right) = \hat{G}_n\left(s\right) r_{err}\left(s\right)\left(1 + \Delta W\left(s\right)\right), \tag{3.67}$$

where $\hat{G}_n\left(s\right)$ denotes the approximate nominal plant model that has stable inverse; and $r_{err}\left(s\right) = G_n\left(s\right)\hat{G}_n^{-1}\left(s\right)$ [65]. Then, the open loop transfer functions of inner and outer loops are derived as follows:

$$L_i\left(s\right) = \frac{r_{err}\left(s\right)\left(1 + \Delta W\left(s\right)\right)Q\left(s\right)}{1 - Q\left(s\right)}, \tag{3.68}$$

$$L_o\left(s\right) = \frac{C\left(s\right)G\left(s\right)}{1 - Q\left(s\right) + r_{err}\left(s\right)\left(1 + \Delta W\left(s\right)\right)Q\left(s\right)}. \tag{3.69}$$

The design constraints of a DOb based robust control system are derived by using *Theorem 3.10* as follows:

Theorem 3.10: Let us assume that a plant, which has a right half plane zero at z_{RHP}, is defined by using eq. (3.40) when $\tau = 0$ and $S_i(s)$ and $T_i(s)$ are the sensitivity and co-sensitivity transfer functions of the inner-loop, respectively. Let us also assume that the frequency responses of the sensitivity and co-sensitivity functions satisfy $|S_i(jw)| \leq \alpha_\beta, \forall w \leq w_\beta$ and $|T_i(jw)| \leq \alpha_\gamma, \forall w \geq w_\gamma$. Then, the LPF of a DOb should satisfy the following constraints to obtain a good robustness and predefined performance criteria.

$$\begin{aligned}
&\frac{\left|Q\left(jw\right)\right|}{\left|1 - Q\left(jw\right)\right|} \geq \frac{1 - \alpha_\beta}{\alpha_\beta\left|r_{err}\left(jw\right)\left(1 + \Delta W\left(jw\right)\right)\right|}, \forall w < z_{RHP}\psi_1, \\
&\frac{\left|1 - Q\left(jz_{RHP}\psi_1\right)\right|}{\left|1 - Q\left(jz_{RHP}\psi_1\right) + r_{err}Q\left(jz_{RHP}\psi_1\right)\left(1 + \Delta W\left(jz_{RHP}\psi_1\right)\right)\right|} \geq \alpha_\beta,
\end{aligned} \tag{3.70}$$

$$\begin{aligned}
&\frac{\left|r_{err}Q\left(jw\right)\left(1 + \Delta W\left(jw\right)\right)\right|}{\left|1 - Q\left(jw\right)\right|} \leq \frac{\alpha_\gamma}{1 - \alpha_\gamma}, \forall w > z_{RHP}\psi_2, \\
&\frac{\left|r_{err}Q\left(jz_{RHP}\psi_2\right)\left(1 + \Delta W\left(jz_{RHP}\psi_2\right)\right)\right|}{\left|1 - Q\left(jz_{RHP}\psi_2\right) + r_{err}Q\left(jz_{RHP}\psi_2\right)\left(1 + \Delta W\left(jz_{RHP}\psi_2\right)\right)\right|} \geq \alpha_\gamma,
\end{aligned} \tag{3.71}$$

where $\psi_1 = \tan(\frac{\log(1+\alpha_\gamma)(\pi - 2\vartheta(w_\gamma)) + 2\log\left(\max_{w_\beta \leq w \leq w_\gamma}\left(|S_i(jw)|\right)\right)\vartheta(w_\gamma)}{2\left(\log\left(\max_{w_\beta \leq w \leq w_\gamma}\left(|S_i(jw)|\right)\right) + \log\left(\alpha_\beta^{-1}\right)\right)}$

$$-\frac{\pi\log\left(\left|B_S^{-1}(z_{RHP})\right|\right)}{2\left(\log\left(\max_{w_\beta\le w\le w_\gamma}(|S_i(jw)|)\right)+\log\left(\alpha_\beta^{-1}\right)\right)}),$$

$$\psi_2=\tan(\frac{\log\left((1+\alpha_\gamma)^{-1}\right)\pi+2\left(\log\left(\max_{w_\beta\le w\le w_\gamma}(|S_i(jw)|)\right)+\log\left(\alpha_\beta^{-1}\right)\right)\vartheta(w_\beta)}{2\left(\log\left(\max_{w_\beta\le w\le w_\gamma}(|S_i(jw)|)\right)+\log\left((1+\alpha_\gamma)^{-1}\right)\right)}$$

$$+\frac{\pi\log\left(\left|B_S^{-1}(z_{RHP})\right|\right)}{2\left(\log\left(\max_{w_\beta\le w\le w_\gamma}(|S_i(jw)|)\right)+\log\left(\alpha_\beta^{-1}\right)\right)}),$$

and $\vartheta\left(w_\bullet\right)=\int_0^{w_\bullet}W_p dw=\int_0^{w_\bullet}\frac{z_{RHP}}{z_{RHP}^2+w^2}dw=\arctan\left(\frac{w_\bullet}{z_{RHP}}\right)$.

Proof: If $|T_i(jw)|\le\alpha_\gamma,\forall w\ge w_\gamma$, then $|S_i(jw)|\le 1+\alpha_\gamma,\forall w\ge w_\gamma$. If the sensitivity constraints are applied into eq. (3.65), then

$$\log\left(1+\alpha_\gamma\right)\left(\int_{-\infty}^{-w_\gamma}W_p\left(w\right)dw+\int_{w_\gamma}^{\infty}W_p\left(w\right)dw\right)+\log\left(\alpha_\beta\right)\int_{-w_\beta}^{w_\beta}W_p\left(w\right)dw$$
$$+\log\left(\max_{w_\beta\le w\le w_\gamma}\left(|S_i(jw)|\right)\right)\left(\int_{-w_\gamma}^{-w_\beta}W_p dw+\int_{w_\beta}^{w_\gamma}W_p dw\right)\ge\pi\log\left(B_S^{-1}(z_{RHP})\right). \quad (3.72)$$

It can be re-written as follows:

$$\log\left(\max_{w_\beta\le w\le w_\gamma}\left(|S_i(jw)|\right)\right)\ge\log\left(\alpha_\beta^{-1}\right)\frac{2\vartheta(w_\beta)}{2\left(\vartheta(w_\gamma)-\vartheta(w_\beta)\right))}$$
$$+\log\left(\left(1+\alpha_\gamma\right)^{-1}\right)\frac{\pi-2\vartheta(w_\gamma)}{2\left(\vartheta(w_\gamma)-\vartheta(w_\beta)\right))}+\left|B_S^{-1}\left(z_{RHP}\right)\right|\frac{\pi}{2\left(\vartheta(w_\gamma)-\vartheta(w_\beta)\right))}, \quad (3.73)$$

$$\vartheta\left(w_\beta\right)\le\frac{\log\left(1+\alpha_\gamma\right)\left(\pi-2\vartheta\left(w_\gamma\right)\right)+2\log\left(\max_{w_\beta\le w\le w_\gamma}\left(|S_i(jw)|\right)\right)\vartheta\left(w_\gamma\right)}{2\left(\log\left(\max_{w_\beta\le w\le w_\gamma}\left(|S_i(jw)|\right)\right)+log\left(\alpha_\beta^{-1}\right)\right)}$$
$$-\frac{\pi\log\left(\left|B_S^{-1}(z_{RHP})\right|\right)}{2\left(\log\left(\max_{w_\beta\le w\le w_\gamma}\left(|S_i(jw)|\right)\right)+log\left(\alpha_\beta^{-1}\right)\right)}, \quad (3.74)$$

$$\vartheta\left(w_\gamma\right)\ge\frac{\log\left(\left(1+\alpha_\gamma\right)^{-1}\right)\pi+2\left(\log\left(\alpha_\beta^{-1}\right)+\log\left(\max_{w_\beta\le w\le w_\gamma}\left(|S_i(jw)|\right)\right)\right)\vartheta(w_\beta))}{2\left(\log\left(\max_{w_\beta\le w\le w_\gamma}\left(|S_i(jw)|\right)\right)+\log\left(\left(1+\alpha_\gamma\right)^{-1}\right)\right)}$$
$$+\frac{\pi\log\left(\left|B_S^{-1}(z_{RHP})\right|\right)}{2\left(\log\left(\max_{w_\beta\le w\le w_\gamma}\left(|S_i(jw)|\right)\right)+\log\left(\alpha_\beta^{-1}\right)\right)}, \quad (3.75)$$

where eq. (3.74) and eq. (3.75) are the functions of ψ_1 and ψ_2 given in *Theorem 3.10*. If the sensitivity and co-sensitivity transfer functions are derived by using eq. (3.68), and the constraints given in *Theorem 3.10* are applied, then

$$\left| \frac{1 - Q(s)}{1 - Q(s) + r_{err}(s)\,(1 + \Delta W(s))\,Q(s)} \right| \leq \alpha_\beta, \forall w \leq w_\beta, \tag{3.76}$$

$$\left| \frac{r_{err}(s)\,(1 + \Delta W(s))\,Q(s)}{1 - Q(s) + r_{err}(s)\,(1 + \Delta W(s))\,Q(s)} \right| \leq \alpha_\gamma, \forall w \geq w_\gamma. \tag{3.77}$$

If eq. (3.74) and eq. (3.75) are applied into eq. (3.76) and eq. (3.77), then eq. (3.71) and eq. (3.72) are derived. Hence, the proof of *Theorem 3.10* is completed.

Equation (3.71) and eq. (3.72) are new design constraints for a DOb based robust control system when an uncertain plant includes RHP zero(s). They show that the bandwidth of a DOb is limited by the RHP zero(s). However, *Theorem 3.10* also suffers from the conservatism due to the unrealistic bounds of sensitivity and co-sensitivity transfer functions. In *Theorem 3.10*, the performance of robust control system is controlled by shaping the co-sensitivity transfer function at high frequencies.

The minimum phase approximation of a non-minimum phase system is derived by using Genetic Algorithm (GA) as follows:

Let us assume that a non-minimum phase system is defined by using

$$G(s) = \frac{N(s)}{D(s)}, \tag{3.78}$$

where $N(s)$ and $D(s)$ denote numerator and denominator, respectively. Let us also assume that the order of $N(s)$ and $D(s)$ are n and $d \leq n$, in which $l \leq n$ is the number of right half plane zeros. An error polynomial is defined as follows:

$$e(s) = N(s)A(s) - B(s), \tag{3.79}$$

where $A(s)$ and $B(s)$ are polynomials that have left half plane zeros. Let us assume that the order of $A(s)$ and $B(s)$ are m and $m + n$, respectively. If $e(s)$ is minimized, then $N(s)$ is defined by using a non-casual minimum phase transfer function by using

$$N(s) = \frac{B(s)}{A(s)}. \tag{3.80}$$

The optimization problem of $e(s)$ is defined by using a quadratic integral performance index as follows:

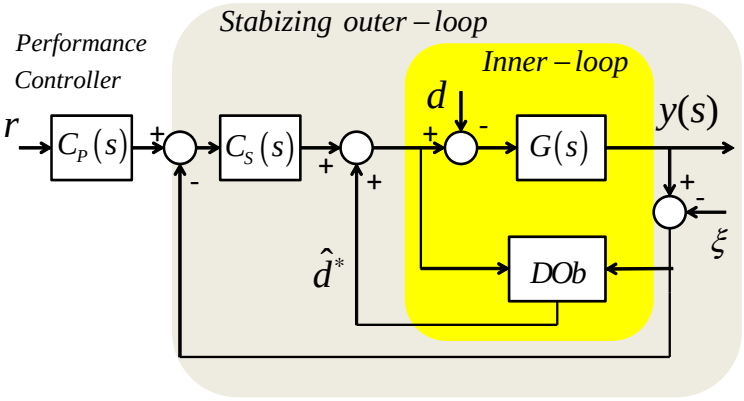

Fig. 3-10: Block diagram of a DOb based robust control system when uncertain plant is unstable.

$$\min : \int_0^{\min(Re(z_{RHP}))} \left\{ \lambda_{amp}(w)|e(jw)|^2 + \lambda_{phase}(w)(\arg(e(jw)))^2 \right\} dw,$$
$$s.t. : \left\{ \begin{array}{c} A(s), B(s) \; and \; s + gr_{err}(s) \; are \; Hurwitz \; polynomials \\ -\pi \leq \arg\left(e\left(jw\right)\right) \leq \pi \end{array} \right\}, \tag{3.81}$$

where $\lambda_{amp}(w)$ and $\lambda_{phase}(w)$ are weighting functions of magnitude and phase errors. The minimization range is bounded by $0 \leq w \leq \min(Re(z_{RHP}))$, since *Theorem 3.10* shows that the bandwidth of DOb is limited by $(Re(z_{RHP}))$.

However, it is very hard to solve the defined optimization problem analytically. Although some analytical results are proposed in the literature, they can't satisfy the optimality in the desired frequency range [66]. Minimizing the optimization problem is not a straight forward task due to the nature of the performance index and constraints. An efficient search algorithm is needed to determine the coefficients of the polynomials of $A(s)$ and $B(s)$. Genetic Algorithm (GA), which is a particular class of evolutionary algorithms, is chosen as a search algorithm. GA avoids the local minima and finds the global minimum of the optimization problem using techniques inspired by natural evolution like mutation, selection, and crossover [67, 68].

Against the conventional design of DOb based robust control systems, if a DOb is applied into the robust control problem of an unstable plant, then the outer-loop controller should be designed to satisfy the stability instead of performance. The inner-loop is always unstable when the uncertain plant has RHP pole(s). A new performance controller is proposed to improve the performance of robust control system as shown in Fig. 3-10. Design constraints of a DOb is derived by using *Theorem 3.11* as follows:

Theorem 3.11: Let us assume that a plant which has a RHP pole at p_{RHP} is defined by using eq. (3.40) when $\tau = 0$. Let us also assume that the nominal plant can be stabilized by using the stabilizing outer loop controller $C_S(s)$, and the co-sensitivity transfer function of the outer loop, $T_o(s)$, satisfies $|T_o(s)| \leq \alpha, \forall w \geq w_\alpha$. Then, the LPF of DOb should satisfy the following constraint to obtain a good robustness and predefined performance criterion.

$$|1 + \Delta Q(jw)W(jw))| \geq \frac{1-\alpha}{\alpha} |C_S(jw))G(jw)|, \forall w \geq p_{RHP}\psi, \tag{3.82}$$

where $\psi = \tan\left(\frac{\pi\left(log\left(\alpha^{-1}\right)+\log\left(\left|B_T^{-1}(p_{RHP})\right|\right)\right)}{2\left(\log(\alpha^{-1})+\log\left(\|T_o\|_\infty\right)\right)}\right)$.

Proof: Similar to *Theorem 3.10*.

Equation (3.82) provides a new design tool for DOb based robust control systems when the uncertain plant includes RHP pole(s). It shows that the bandwidth of DOb has a lower bound to obtain good robustness when the plant is unstable. *Theorem 3.11* also suffers from the conservatism.

3.5.1 Simulations

In the simulations, four case studies are carried out to show the validity of the proposed design constraints of DOb. Let us first consider a minimum phase plant by using

$$G_n(s) = \frac{s+5}{s^2+5s+6},\ G(s) = G_n(s)\left(1 + \Delta W_S(s)\right), \tag{3.83}$$

where $W_S(s) = \frac{5s+100}{s+500}$; and $-0.2 < \Delta < 1$. To achieve the robust stability in the inner-loop, the bandwidth of DOb should be smaller than 100 rad/s.. Fig. 3-11 shows that as the order of DOb is increased, the bandwidth of DOb is used more efficiently and noise suppression is improved. However, as shown in *Theorem 3.7*, the robustness deteriorates and the bandwidth constraints of DOb become more severe. The robustness and performance of a DOb based control system are improved as follows:

The design parameters k,α and $\sup_{w\in[w_\beta,w_\gamma]} \log\left(|S_i(jw)|\right)$ should be determined by considering the robustness and performance requirements. The order of DOb determines δ that is directly related to the slope of $L_i(s)$. Let us assume that a second order DOb is used and the design parameters are set as $\alpha = 0.1$ and $\sup_{w\in[w_\beta,w_\gamma]} \log\left(|S_i(jw)|\right) = \sqrt{2}$. Then $\delta = 0.4$ satisfies for $\forall w \geq 100$ rad/s.. Hence, the performance and robustness constraints are derived from *Theorem 3.7* as follows:

$$w_\beta = 46 \text{ rad/s. } and\ Bandwidth < 100 \text{ rad/s.}, \tag{3.84}$$

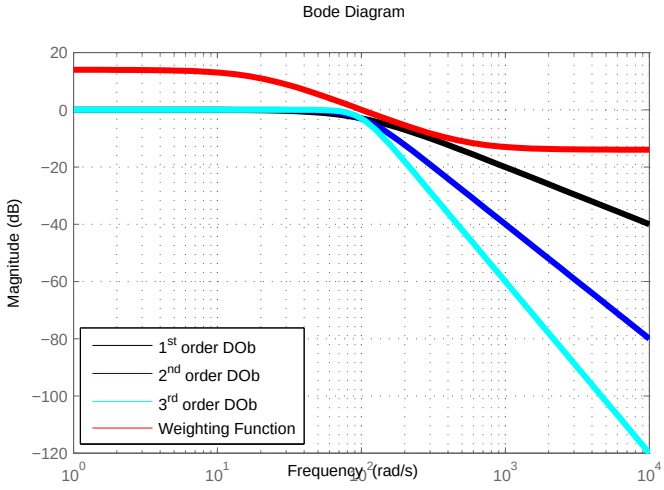

(a) Co-sensitivity function frequency responses.

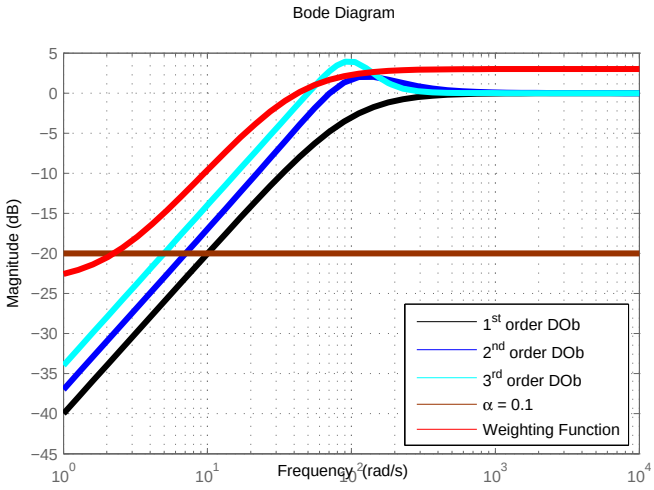

(b) Sensitivity function frequency responses.

Fig. 3-11: Frequency responses of the inner-loop sensitivity and co-sensitivity transfer functions when the bandwidth of DOb is 100 rad/s..

Fig. 3-12 shows the frequency responses of the inner-loop sensitivity and co-sensitivity transfer functions when a second order DOb is designed by using different bandwidth values. The performance and robustness constraints, which are different from eq. (3.84) due to conservatism, are obtained directly from Fig. 3-12 as follows:

$$w_\beta = 15\,\text{rad/s}.\ and\ Bandwidth < 65\,\text{rad/s}.. \tag{3.85}$$

The weighting function of the sensitivity transfer function is $W_P(s) = \frac{0.707s+30}{s+2}$.

Let us now consider the DOb constraints when uncertain plant includes time delay. The uncertain plant model is described as follows:

$$G_n(s) = \frac{s+10}{s^2+5s+10}\ and\ G(s) = G_n(s)\left(1+\Delta W_S(s)\right)\exp(-0.01s), \tag{3.86}$$

where $W_S(s) = \frac{3s+240}{s+600}$. The bandwidth constraint of DOb is derived by using *Theorem 3.8* as follows:

The design parameters α and $\sup_{w\in[w_\beta,w_\gamma]}\log\left(|S_i(jw)|\right)$ should be determined by considering the robustness and performance requirements. Besides, δ and R, which depend on the order of DOb, should be determined. Let us assume that the order of DOb is one and the design parameters are set as $\sup_{w\in[w_\beta,w_\gamma]}\log\left(|S_i(jw)|\right) = \sqrt{2}$ and $\alpha = 0.1$. If δ is chosen as 0.1, then $R \approx B_w\delta^{-1} = 10B_w$, in which B_w denotes the bandwidth of DOb. If *Theorem 3.8* is used, then it is drived that $\sup_{w\in[w_\beta,w_\gamma]}\log\left(|S_i(jw)|\right) = \sqrt{2}$ satisfies for a wide range of bandwidth. If a second order DOb is used, then $\sup_{w\in[w_\beta,w_\gamma]}\log\left(|S_i(jw)|\right) = \sqrt{2}$ satisfies for $B_w \leq 500\,\text{rad/s}.$. Fig. 3-13 shows the frequency responses of the inner-loop's sensitivity and co-sensitivity transfer functions. The bandwidth constraint is derived as $B_w \leq 70\,\text{rad/s}.$ from Fig. 3-13. The difference between the bandwidth constraints is due to the conservatism of *Theorem 3.8*. The weighting function of the sensitivity transfer function is $W_P(s) = \frac{0.707s+30}{s+2}$.

Let us now consider the design constraints of DOb for plants with right half plane zero(s). The model of the plant is as follows:

$$G_n(s) = \frac{-s+50}{s^2+25s+40}\ and\ G(s) = G_n(s)\left(1+\Delta W_S(s)\right), \tag{3.87}$$

where $W_S(s) = \frac{3.75s+450}{s+1500}$ and $\hat{G}_s = \frac{s^2+200s+20}{(4s+0.4)(s^2+25s+40)}$ [65]. The bandwidth constraint of DOb is derived by using *Theorem 3.10* as follows:

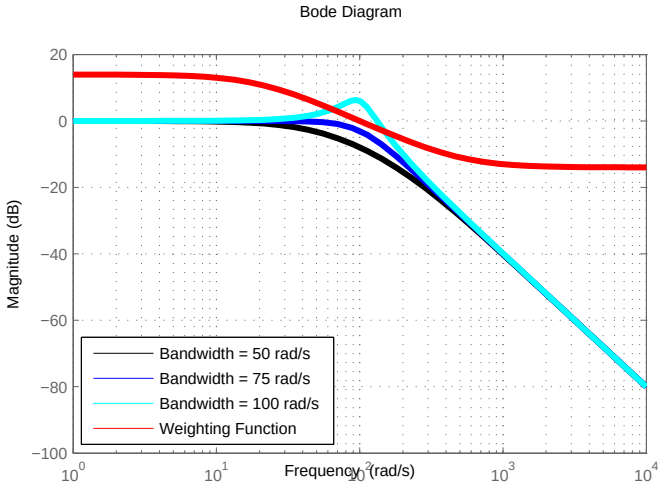

(a) Co-sensitivity function frequency responses.

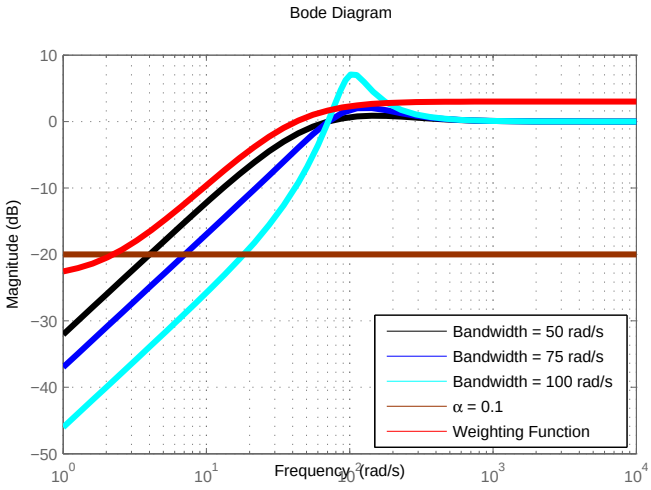

(b) Sensitivity function frequency responses.

Fig. 3-12: Frequency responses of the inner-loop sensitivity and co-sensitivity transfer functions when a 2^{nd} order DOb is used.

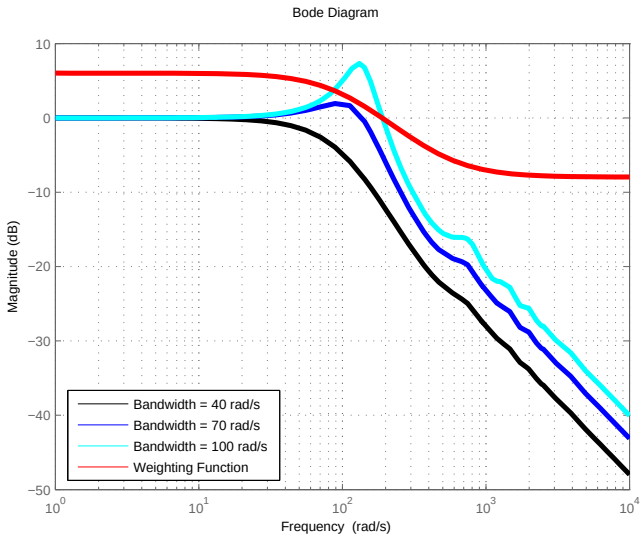

(a) Co-sensitivity function frequency responses.

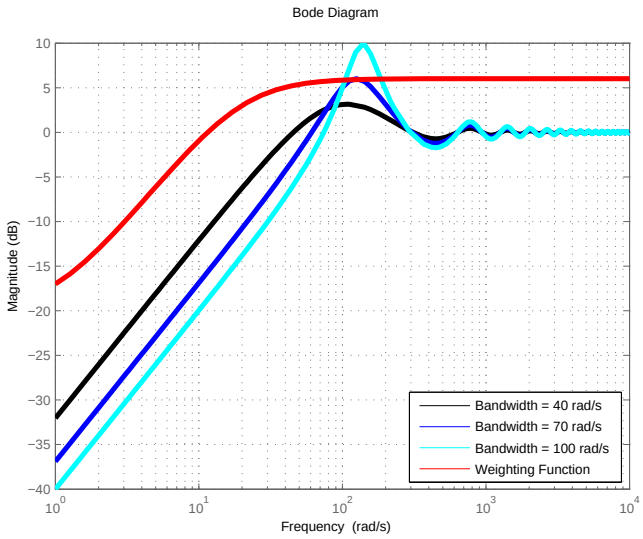

(b) Sensitivity function frequency responses.

Fig. 3-13: Frequency responses of the inner-loop sensitivity and co-sensitivity transfer functions when a 1^{st} order DOb is used and uncertain plant includes time delay.

It is assumed that $\alpha_\beta = 0.5$, $\alpha_\gamma = 0.2$,$\|S_i\|_\infty = 2$ and $w_\gamma = 2B_w$. If *Theorem 3.10* is applied by using the defined performance and robustness constraints, then

$$6 \leq B_w \leq 55, \; and \; w_\beta \leq 35 \, \text{rad/s.}, \tag{3.88}$$

are derived. Fig. 3-14 shows the frequency responses of the inner-loop sensitivity and co-sensitivity transfer functions when a first order DOb is used. The performance and bandwidth constraints, which are different from eq. (3.88) due to conservatism, are obtained directly from Fig. 3-14 as follows:

$$12 \leq B_w \leq 24, \; and \; w_\beta \leq 15 \, \text{rad/s.}. \tag{3.89}$$

The weighting function of the sensitivity transfer function is $W_P(s) = 0.5\frac{s+16}{s+2}$.

Finally, let us consider the design constraints when uncertain plant has a RHP pole. The uncertain plant model is defined as follows:

$$G_n(s) = \frac{1}{s(s-5)} \; and \; G(s) = G_n(s)\left(1 + \Delta W_S(s)\right), \tag{3.90}$$

where $W_S(s) = \frac{7.5s+600}{s+1500}$. Because a DOb is implemented in the inner-loop, the outer loop controller, in which $C_S(s) = 12s+20$, is designed to satisfy the stability by considering only the nominal plant model. The frequency responses of the outer-loop sensitivity and co-sensitivity transfer functions are shown in Fig. 3-15 when a second order DOb is used. It clearly shows that the robustness of the system improves as the bandwidth of DOb is increased. The lower bound on the bandwidth of DOb can be derived by using *Theorem 3.11* similarly; however, it also includes conservatism.

Fig. 3-16(a) shows the performance improvement of the controller, $C_P(s)$, which is designed as $C_P(s) = \frac{s+10}{4s+10}$. Fig. 3-16(b) shows the step responses for different external disturbances. As it can be seen from the figure, DOb cannot estimate high frequency disturbances precisely, so the robustness of the system deteriorates. There is a trade-off between the robustness and noise response to determine the bandwidth of a DOb.

Simulation results show that the proposed method suffers by the conservatism, significantly. The source of the conservatism is shown in Fig. 3-17. In this figure, the gray areas are determined by the sectionally constant sensitivity bounds, and the black areas denote the errors which cannot be considered in the robustness analysis. It clearly shows that there is a significant difference between the areas, which are bounded by the real sensitivity function and its approximate bound.

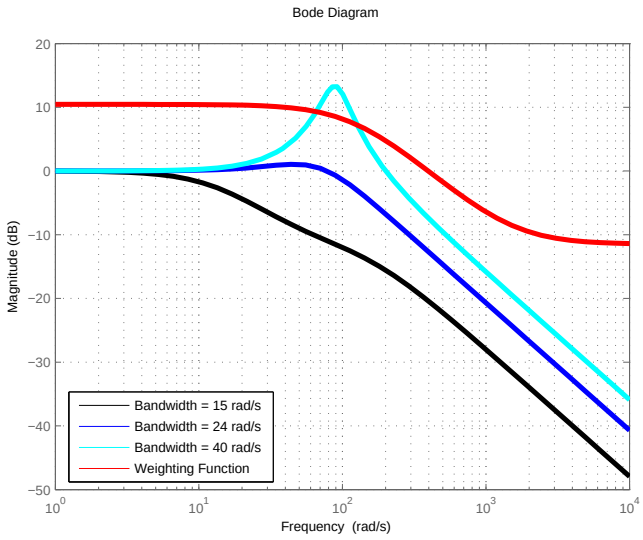

(a) Co-sensitivity function frequency responses.

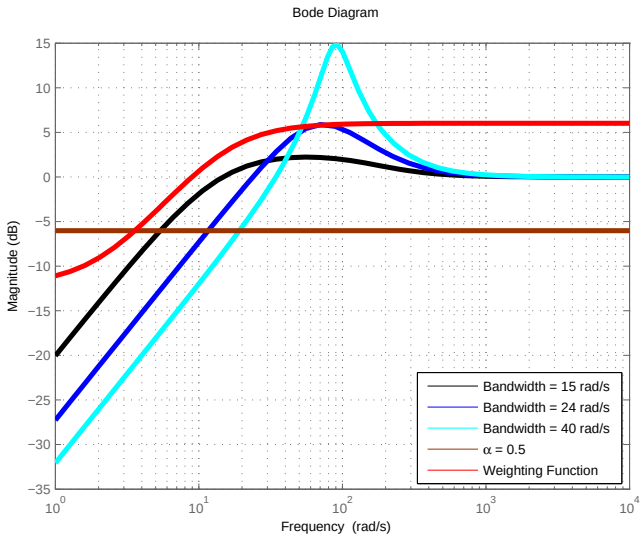

(b) Sensitivity function frequency responses.

Fig. 3-14: Frequency responses of the inner-loop sensitivity and co-sensitivity transfer functions when a 1^{st} order DOb is used and uncertain plant has a RHP zero.

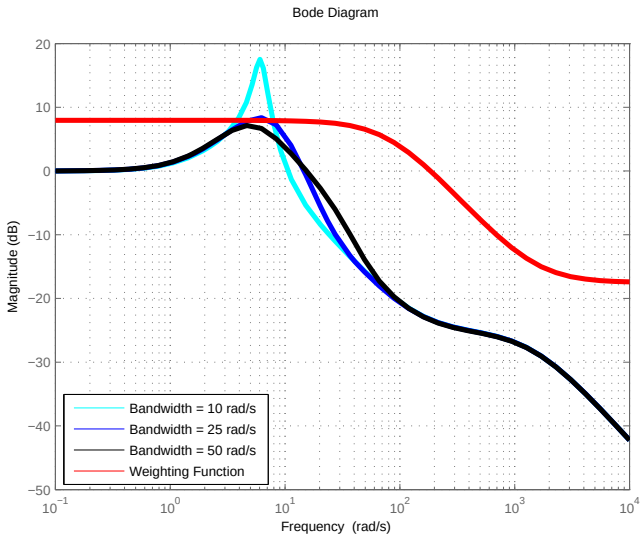

(a) Co-sensitivity function frequency responses.

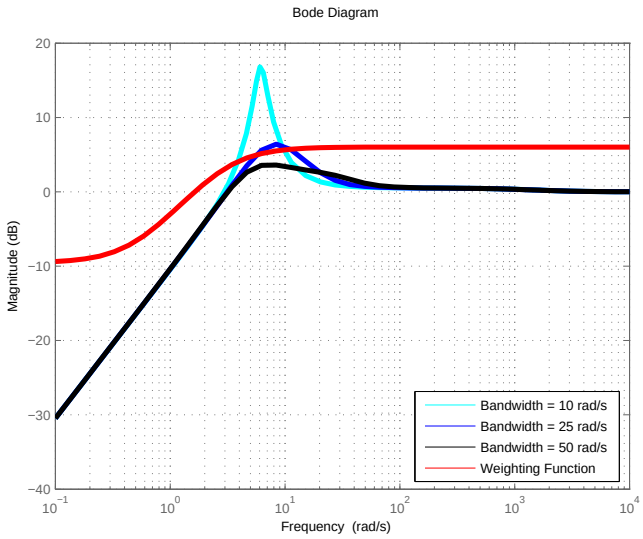

(b) Sensitivity function frequency responses.

Fig. 3-15: Frequency responses of the inner-loop sensitivity and co-sensitivity transfer functions when a 2^{nd} order DOb is used and uncertain plant has a right half plane pole.

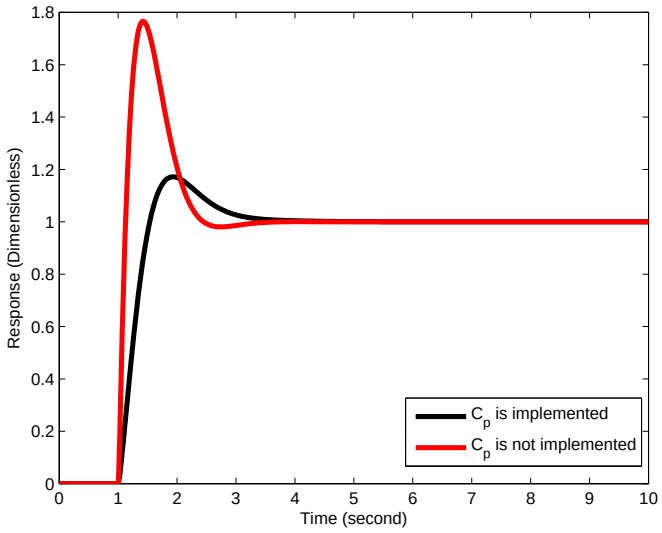

(a) Performance controller.

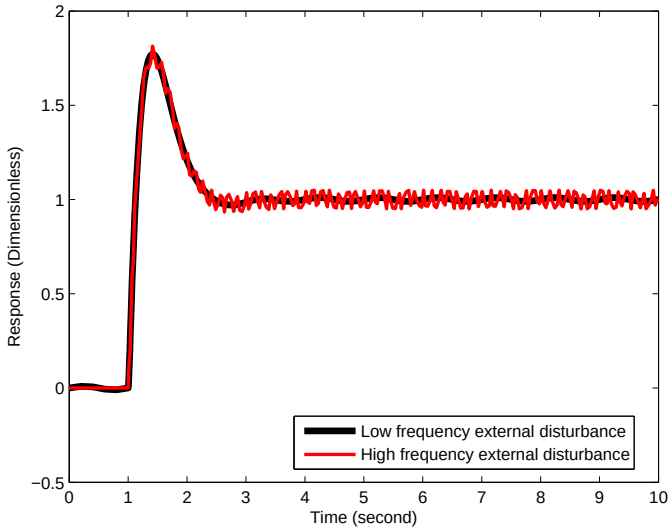

(b) External disturbance response.

Fig. 3-16: Step responses of the uncertain plant when a DOb is implemented.

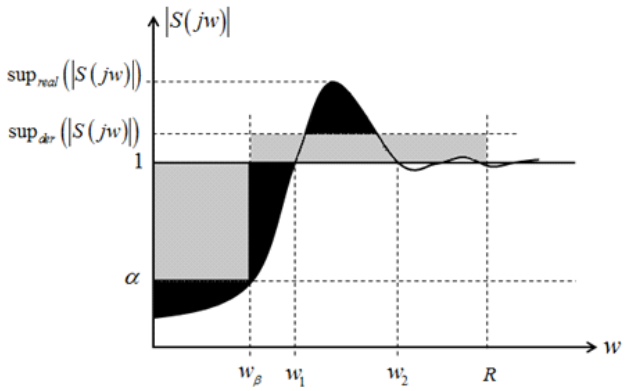

Fig. 3-17: General frequency response of a sensitivity function.

Let us again consider the plant with time-delay case, which has the most severe conservative results, to obtain more accurate bandwidth constraint by decreasing the conservatism. If the nominal plant model with time delay is considered, then the sensitivity function frequency response is derived as follows:

$$|S_i(jw)|^2 = \frac{w^2}{w^2 - 2g_0 w \sin(w\tau) + g_0^2}, \tag{3.91}$$

where g_0 is the bandwidth of the first order DOb; and τ is time delay. The frequencies of w_1 and w_2 given in Fig. 3-17 are derived approximately as follows:

$$\begin{aligned} w_1 &= \frac{\sqrt{3\tau - 1.73205\sqrt{\tau^2(3 - g\tau)}}}{\tau^3}, \\ w_2 &= \frac{\sqrt{3\tau + 1.73205\sqrt{\tau^2(3 - g\tau)}}}{\tau^3}. \end{aligned} \tag{3.92}$$

The conservatism can be decreased by using w_1 and w_2 instead of R. If the sectionally constant sensitivity bound is used with w_1 and w_2, then the bandwidth constraint of DOb, which is obtained as 70 rad/s. from sensitivity function frequency responses, is derived as 95 rad/s.. Hence, the conservatism can be lessened by considering more realistic sensitivity bounds.

3.6 Summary

In this chapter, the robustness of DOb based control systems is analyzed by using different robust control methods, in detail. Firstly, the conventional analysis method, which depends on the Small Gain theorem, is explained briefly. The robustness of a DOb based control system can be easily analyzed by using the conventional analysis method. However, it limits the bandwidth due to conservatism and does not provide a clear insight into the robustness characteristics of a DOb. The conservatism can be lessened by using the SSV in the presence of structured uncertainties. However, the conservatism cannot be removed due to the discontinuity problem of the real SSV. Although the SSV can be easily implemented to DOb based control systems by using the toolboxes of Matlab, the robustness characteristics of a DOb cannot be clarified. A new analysis method is proposed for DOb based control systems by using the real parametric uncertainty based robust control methods. To clarify the robustness characteristics of DOb, it is assumed that a minimum phase plant that has real parametric uncertainties is controlled by using a first order DOb. It is shown that the robust stability of the DOb based control system is achieved if the bandwidth of DOb is higher than its lower bound and the stability margin is improved as the bandwidth of DOb is increased. The main disadvantage of the proposed method is the strict restrictions on the dynamics of the plant and DOb. To derive the general design constraints of a DOb based control system, a new unstructured uncertainty based analysis method is proposed. Bode and Poisson integral theorems are utilized so that the design constraints of DOb are derived analytically for a wide range of application area. The proposed method also includes conservatism. However, it is not a severe problem, since it clarifies the robustness characteristics of DOb based control systems, qualitatively. Besides, the conservatism can be lessened by using more realistic sensitivity function bounds, yet it increases the computational complexity. I believe that the proposed method is very useful to understand the robustness characteristics of a DOb based control systems.

Chapter 4

Disturbance Observer Based Robust Motion Control Systems

4.1 Introduction

In this chapter, the stability, performance, and robustness of DOb based motion control systems, i.e., position and force control systems, will be analyzed in detail [69, 70]. Three decades before, DOb was proposed by Ohnishi et al. to improve the performance of motion control systems in the first IPEC conference [32]. After that it has been widely used in several motion control applications, such as robotics, industrial automation, automaotive, etc., due to its simplicity and efficiency [40, 71–78]. DOb estimates external disturbances and plant uncertainties, such as gravity, friction, inertia variations, etc., in motion control systems. It provides the robustness of motion control systems in the inner-loop as shown in the previous chapters. Since a DOb suppresses disturbances in the inner-loop, high performance acceleration based controllers (ABC) can be designed in the outer loop [36, 70, 79, 80]. In ABC, performance goals, e.g., position, force, or admittance control goals, are defined uniformly in the acceleration domain [36, 80, 81].

Although several applications of DOb based motion control systems have long been realized in the literature successfully, DOb suffers from insufficient analysis and design control methods [70, 82]. The low pass filter (LPF) of DOb, nominal inertia, and torque coefficient are the fundamental design parameters of a DOb based robust motion control system. It is a well known fact that the higher the bandwidth of DOb is, the better the disturbance suppression improves. However, so far, the relation between the bandwidth of DOb and nominal inertia and torque coefficient has not been considered in detail. In section

4.2, the design constraints of DOb and nominal plant parameters are derived analytically by considering the practical constraints of DOb based motion control systems. It is shown that the bandwidth of a DOb and nominal inertia have upper bounds to improve the robustness of DOb due to imperfect velocity estimation in practice. Besides that a DOb can be designed as a phase lead-lag compensator by adjusting the nominal inertia and torque coefficient. The stability of a DOb based motion control system can be improved by increasing / decreasing the nominal inertia / torque coefficient [70]. However, as shown in Chapter 3, nominal plant parameters are bounded by the robustness constraints in practice. Therefore, there is a trade-off between the stability and robustness, in which it is adjusted by nominal plant parameters, in the design of a DOb based motion control system. In section 4.3, DOb based robust position control systems are analyzed. It is shown that the stability of the DOb based robust position control systems is improved as the nominal inertia is increased in the design of DOb. The robustness of position control systems is clarified by deriving the sensitivity function. It is shown that the robustness of the position control systems is improved by the outer-loop performance controller. In section 4.4, DOb based explicit robust force control systems are analyzed. It is shown that there is a strict relationship between the stability and robustness in the explicit force control systems. The performance and stability are improved if the robustness of an explicit force control system is achieved. The robustness of a DOb based explicit force control system is clarified by proposing new sensitivity functions. Implicit and explicit contact force estimation methods are considered by using a force sensor and a reaction force observer (RFOb), respectively. It is shown that the explicit force control systems are improved intrinsically by using the explicit force estimation method, i.e., RFOb. Dynamic model of a force sensor is obtained by using two mass resonant system, and novel stability and robustness analysis methods are proposed. In general, an RFOb based robust force control system is considered as a feed-forward control structure, so only performance analysis has been performed so far. However, it is not true, and an RFOb has a feed-back control structure. Therefore, not only the performance but also the stability of an RFOb based robust force control system changes significantly by the design parameters of a DOb and an RFOb. A novel stability analysis method is proposed for RFOb based robust force control systems and practical design constraints are derived. By using the proposed analysis methods, a novel adaptive RFOb design method is proposed in section 4.5. The chapter ends with summaries given in section 4.6.

4.2 Disturbance Observer Based Robust Motion Control Systems

A block diagram of a DOb based robust motion control system is shown in Fig. 4-1. In this figure, the following apply:

J_{mn} and J_m	nominal and uncertain inertias/masses, respectively;
$K_{\tau n}$ and K_τ	nominal and uncertain torque/force coefficients, respectively;
I_m, I_m^{des} and I_m^{cmp}	total, desired and compensate motor currents, respectively;
q_m,$\dot{q}_m$,and $\ddot{q}_m$	angle/position, velocity and acceleration, respectively;
$\ddot{q}_m^{des}$	desired acceleration;
$\dot{q}_m^{noise}$	noise of velocity measurement;
g_{DOb}	cut-off frequency of DOb;
τ_m^{load}	loading torque/force;
τ_m^{frc}	friction torque/force;
τ_m^{int}	interactive torque/force such as Coriolis;
$\tau_m^d = \tau_m^{load} + \tau_m^{frc} + \tau_m^{int}$	total external disturbance;
τ_m^{dis} and $\hat{\tau}_m^{dis}$	total disturbance and its estimation, respectively;

Henceforth, torque and force are used interchangeably in this chapter. A DOb estimates external disturbances and plant uncertainties, such as gravity, friction, inertia variation, etc., in the inner-loop. The robustness of motion control system is achieved by feeding-back the estimated disturbances, $\hat{\tau}_m^{dis}$, as

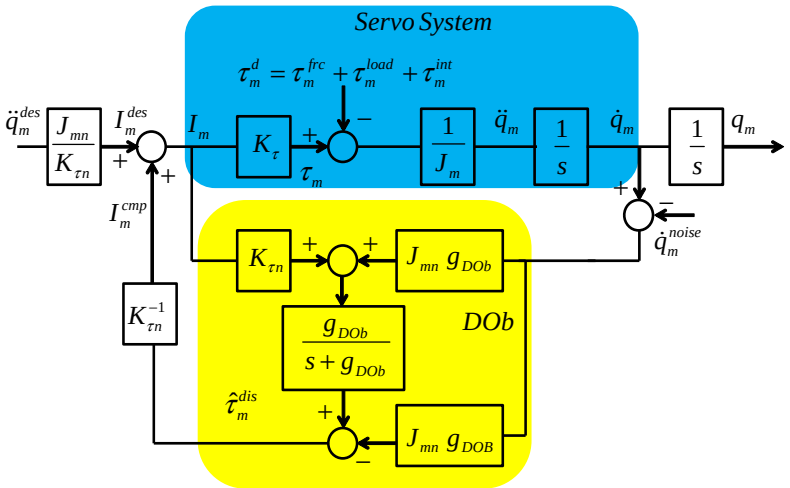

Fig. 4-1: Block diagram of a DOb based robust motion control system.

shown in Fig. 4-1. Dynamic equations of a DOb based motion control system are derived directly from Fig. 4-1 as follows:

$$K_{\tau n} I_m - J_{mn} \ddot{q}_m = \tau_m^{dis} = \tau_m^d + \Delta J_m \ddot{q}_m - \Delta K_\tau I_m, \tag{4.1}$$

$$\hat{\tau}_m^{dis} = \frac{g_{DOb}}{s+g_{DOb}} \tau_m^{dis}, \tag{4.2}$$

where $\Delta J_m = J_m - J_{mn}$; and $\Delta K_\tau = K_\tau - K_{\tau n}$ denote inertia and torque coefficient variations, respectively. Equation (4.2) shows that a disturbance can be estimated / suppressed accurately if it stays within the bandwidth of DOb. A DOb based robust motion control system has a multi input single output (MISO) control structure. Its transfer function is derived from Fig. 4-1 as follows:

$$\ddot{q}_m = \alpha \frac{s + g_{DOb}}{s + \alpha g_{DOb}} \ddot{q}_m^{des} - \frac{1}{J_m} T_{sen}^{DOb}(s)\, \tau_m^d - T_{cosen}^{DOb}(s)\, s\dot{q}_m^{noise}, \tag{4.3}$$

where $T_{sen}^{DOb}(s) = \frac{1}{1+L_{DOb}(s)}$ and $T_{cosen}^{DOb}(s) = \frac{L_{DOb}(s)}{1+L_{DOb}(s)}$ are the sensitivity and co-sensitivity transfer functions, respectively, in which $L_{DOb}(s) = \alpha \frac{g_{DOb}}{s}$; and $\alpha = \frac{J_{mn} K_\tau}{J_m K_{\tau n}}$.

Although Fig. 4-1 is used in the conventional analysis of DOb based motion control systems, in reality, it is impractical. It is a well known fact that a DOb requires precise velocity measurement. Equation (4.3) shows that the derivative of the noise of velocity measurement, q_m^{noise}, gets transferred into the output by T_{cosen}^{DOb}. Therefore, in general, velocity is estimated by using a LPF, and precise velocity measurement is achieved in a predetermined bandwidth. Practical block diagram of a DOb based motion control system is shown in Fig. 4-2.

In Fig. 4-2, g_v denotes the cut-off frequency of velocity measurement. Transfer function of a practical DOb based motion control system is derived similarly as follows:

$$\ddot{q}_m = \alpha \frac{(s + g_v)(s + g_{DOb})}{s^2 + g_v s + \alpha g_v g_{DOb}} \ddot{q}_m^{des} - \frac{1}{J_m} T_{sen}^{DOb}(s)\, \tau_m^d - T_{cosen}^{DOb}(s)\, s\dot{q}_m^{noise}, \tag{4.4}$$

where $T_{sen}^{DOb}(s) = \frac{1}{1+L_{DOb}(s)}$ and $T_{cosen}^{DOb}(s) = \frac{L_{DOb}(s)}{1+L_{DOb}(s)}$ are sensitivity and co-sensitivity transfer functions, respectively, in which $L_{DOb}(s) = \alpha \frac{g_v g_{DOb}}{s(s+g_v)}$.

Equation (4.3) and eq. (4.4) show that a DOb can be designed as a phase-lead lag compensator that is adjusted by α. If $\alpha > 1$, then a DOb works as a phase lead compensator. The stability and performance of the motion control systems are improved by increasing phase lead, i.e., α; however, the upper bound of α has not been derived yet.

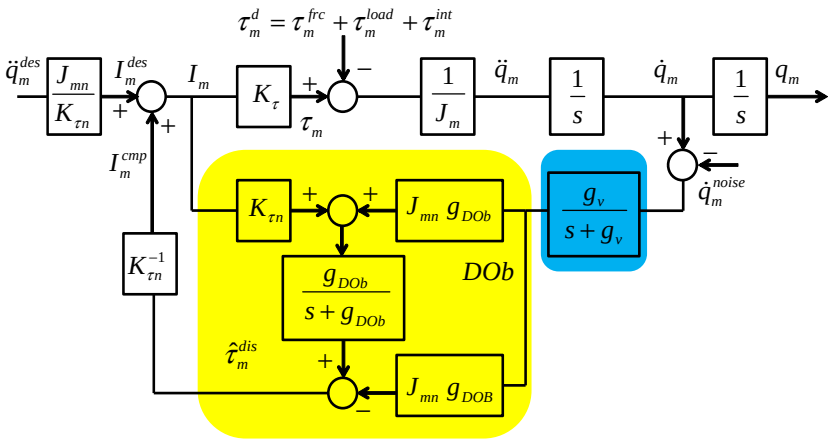

Fig. 4-2: Block diagram of a DOb based robust motion control system when a low pass filer is used in velocity measurement.

Although the structures of eq. (4.3) and eq. (4.4) are quite similar, the robustness of a DOb based motion control system changes significantly when velocity is estimated by using a LPF. The sensitivity and co-sensitivity transfer functions, i.e., disturbance and noise responses, of a DOb based motion control system are shown in eq. (4.3) and eq. (4.4). The relative degree of $L_{DOb}(s)$ is one and two when g_v is infinite and finite, respectively. In Chapter 3, Bode integral theorem shows that if the relative degree of $L_{DOb}(s)$ is higher than one, then T_{sen}^{DOb} cannot be shaped freely; the peak of T_{sen}^{DOb} at high frequencies increases as the sensitivity reduction at low frequencies is increased. Therefore, as shown in eq. (4.4), α and g_{DOb} cannot be increased freely due to the robustness constraint. A simple robustness constraint can be derived analytically as follows:

Let us consider the characteristic polynomial of T_{sen}^{DOb} / T_{cosen}^{DOb} and apply $g_v = \kappa g_{DOb}$. Then, the characteristic polynomial of the robust motion control system is as follows:

$$P_{ch}(s) = s^2 + \kappa g_{DOb} s + \alpha \kappa g_{DOb}^2. \tag{4.5}$$

The natural frequency and damping coefficient of eq. (4.5) are derived as follows:

$$w_n = \sqrt{\alpha\kappa}\, g_{DOb} \; and \; \xi = 0.5\sqrt{\alpha^{-1}\kappa}. \tag{4.6}$$

To improve the robustness of a DOb, i.e., to suppress the peak of T_{sen}^{DOb}/T_{cosen}^{DOb}, if it is assumed that $\xi \geq 0.707$, then

$$\alpha g_{DOb} \leq \frac{g_v}{2}. \tag{4.7}$$

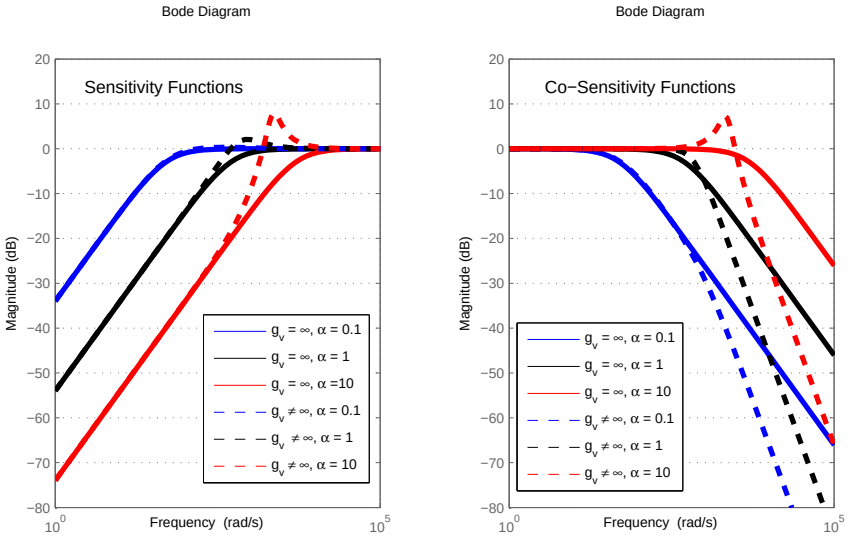

Fig. 4-3: Frequency responses of the inner-loop sensitivity and co-sensitivity transfer functions.

Equation (4.7) is a new practical design constraint for the DOb based robust motion control systems. It shows that α and g_{DOb} are limited by the robustness constraint of DOb when imperfect velocity measurement is considered. The robustness of a DOb can be improved by increasing the lower constraint of ξ; however, the upper bound of α and g_{DOb} become more severe, i.e, the stability and performance deteriorate. Consequently, there is a trade-off between the robustness, stability, and performance in DOb based motion control systems.

The robustness constraint of a DOb based motion control system is shown in Fig. 4-3. It is clear from the figure that not only the stability, but also the robustness improves as α and g_{DOb} are increased when perfect velocity measurement is achieved, i.e., g_v is infinite. However, imperfect velocity measurement changes the sensitivity and co-sensitivity transfer function frequency responses at high frequencies, i.e., the robustness of the DOb based motion control systems, significantly. It is clear from the analysis that not only the performance, but also the stability and robustness of a DOb based motion control system can be improved by using perfect velocity measurement though it is not practical.

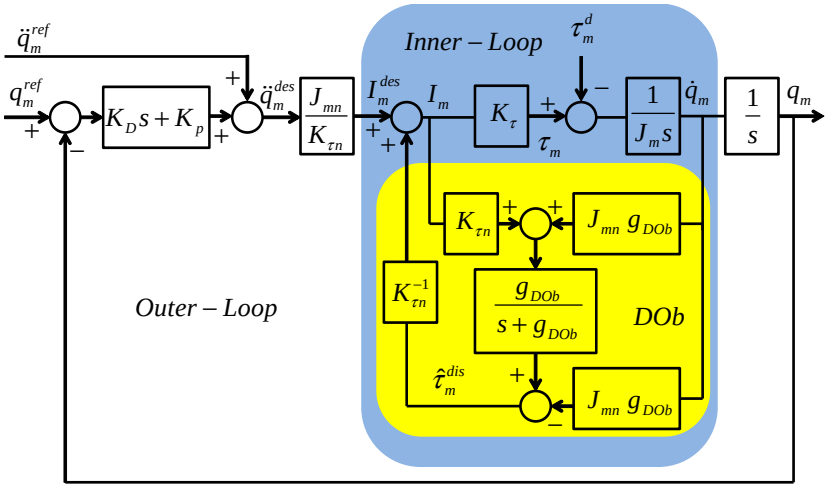

Fig. 4-4: Block diagram of a DOb based robust position control system.

4.3 Disturbance Observer Based Robust Position Control Systems

A block diagram of a DOb based robust position control system is shown in Fig. 4-4. In this figure, q_m^{ref} and $\ddot{q}_m^{ref}$ denote angle/position and acceleration reference inputs, respectively; and K_D and K_P denote derivative and proportional gains of the outer-loop acceleration controller, respectively. The other parameters are same as defined earlier. In the robust position control, a DOb provides robustness in the inner-loop and performance goals are achieved by using an ABC controller in the outer-loop.

The transfer functions between $\ddot{q}_m^{ref}$ and $\ddot{q}_m$ are derived from Fig. 4-4 as follows:

$$\frac{\ddot{q}_m}{\ddot{q}_m^{ref}} = \frac{\alpha(s+g_{DOb})(s^2+K_Ds+K_P)}{s^2(s+\alpha g_{DOb})+\alpha(s+\ \alpha g_{DOb})(K_Ds+K_P)}, \tag{4.8}$$

when g_v is infinite; and

$$\frac{\ddot{q}_m}{\ddot{q}_m^{ref}} = \frac{\alpha(s+g_v)(s+g_{DOb})(s^2+K_Ds+K_P)}{s^2(s^2+g_vs+\alpha g_v g_{DOb})+\alpha(a+g_v)(s+\alpha g_{DOb})(K_Ds+K_P)}, \tag{4.9}$$

when g_v is finite.

Let us consider eq. (4.8). If the stability analysis of the position control system is performed, for instance Routh-Hurwitzh theorem can be used, then

$$\alpha^{-1} < 1 + g_{DOb}\frac{K_D}{K_P} + \frac{K_D}{g_{DOb}} + \frac{K_D^2}{K_P}, \tag{4.10}$$

is derived as the stability criterion [1, 83]. Equation (4.10) shows that the stability of the robust position

control system is improved by increasing α and g_{DOb}. However, as shown in eq. (4.7), αg_{DOb} cannot be increased freely due to the robustness constraint in practice.

Although, in general, it is assumed that the robustness and performance of a DOb based motion control system are adjusted in the inner and outer loops, independently, it is not true. The robustness of a DOb based position control system depends on the DOb as well as the outer loop performance controller. It can be clarified by deriving the sensitivity and co-sensitivity transfer functions of a DOb based robust position control system as follows:

$$T_{sen}^{PC} = \frac{1}{1 + L_{PC}(s)}, \tag{4.11}$$

$$T_{cosen}^{PC} = \frac{L_{PC}(s)}{1 + L_{PC}(s)}, \tag{4.12}$$

where

$$L_{PC}(s) = \alpha \frac{g_{DOb}s^2 + (s + g_{DOb})(K_D s + K_P)}{s^3}, \tag{4.13}$$

when g_v is infinite; and

$$L_{PC}(s) = \alpha \frac{g_v g_{DOb}s^2 + (s + g_v)(s + g_{DOb})(K_D s + K_P)}{s^3(s + g_b)}, \tag{4.14}$$

when g_v is finite.

As it is expected, eq. (4.11) and eq. (4.12) show that the robustness of the position control system is improved by the outer loop PD controller. Although the robustness of the position control system can be improved by increasing the outer loop control gain when $\alpha g_{DOb} > 0.5 g_v$, the robustness of inner-loop becomes sensitive to disturbances at high frequencies such as noise. Besides, increasing outer-loop controller gain has several disadvantages and limitations such as energy consumption, vibration due to attracting high frequency dynamics, saturation, and so on.

4.3.1 Simulations and Experiment

In this section, simulation and experimental results are given for DOb based robust position control systems. Table 4.1 shows the parameters of the simulations.

Let us start by considering the robustness of a DOb based position control system. Fig. 4-5 shows the inner and outer loops' co-sensitivity function frequency responses, i.e., T_{cosen}^{DOb} and T_{cosen}^{PC}, when a PD controller is implemented to achieve position control goals. As shown in Fig. 4-5(a), the frequency

Table 4.1: Simulation parameters of the robust position control system.

Variables	Definition of variables	Value
J_{mn}	Nominal mass	0.10 kg
$K_{\tau n}$	Nominal torque coefficient	5.0 N/A
K_P	Position feedback gain	900
K_D	Velocity feedback gain	200

Table 4.2: Experiment parameters of the robust position control system.

Variables	Definition of variables	Value
J_{mn}	Nominal mass	0.62 kg
$K_{\tau n}$	Nominal torque coefficient	33.0 N/A
K_P	Position feedback gain	1200
K_D	Velocity feedback gain	90
g_v	Cut-off frequency of velocity measurement	1000 rad/s.
g_{DOb}	Cut-off frequency of DOb	250 rad/s.

responses of T_{cosen}^{DOb} change significantly at high frequencies as α and/or g_{DOb} are increased when g_v is finite. Against the ideal velocity measurement case, αg_{DOb} cannot be increased freely due to the robustness constraint when practical velocity measurement is considered. However, the outer-loop position controller improves the robustness of the position control system as shown in Fig. 4-5(b). Although the robustness of the outer-loop is improved by the performance controller, a DOb becomes more sensitive at high frequencies in the inner-loop as αg_{DOb} is increased.

Let us now consider the stability of a DOb based robust position control system. The root-locus of the robust position control system, which is shown in Fig. 4-6, is plotted with respect to α when g_v is 500 rad/s.. It shows that the stability of the robust position control system improves as α is increased. However, it is limited by the robustness constraint of a DOb, so there is a trade-off between the stability of the position control system and the robustness of a DOb.

A linear DC motor, which is shown in Fig. 4-7, is used to show the validity of the analysis in the experiments. Specifications of the experimental setup is shown in Table 4.2.

Fig. 4-8 shows the position control response of the linear DC motor when a DOb is implemented. In the experiment, a sinusoidal reference input is applied between 1 and 10 seconds, and the position control responses are observed by changing the nominal inertia in the design of a DOb. Initially α is set as $\alpha > 1$ and the stability of the robust position control system is improved. Even if the robustness constraint of

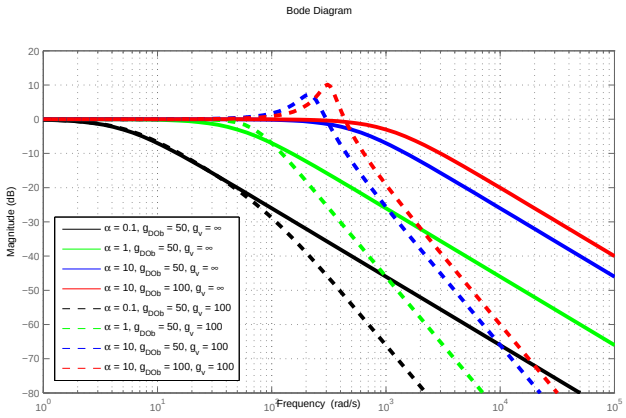

(a) Inner-loop co-sensitivity function frequency responses.

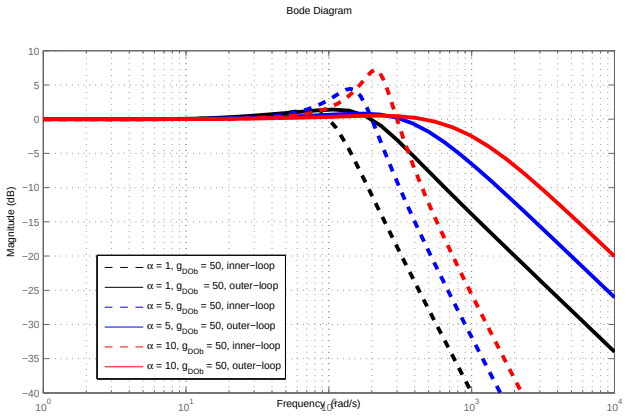

(b) Inner and outer loops co-sensitivity function frequency responses.

Fig. 4-5: Inner and outer loops' co-sensitivity functions frequency responses.

DOb is not satisfied, the outer loop controller improves the robustness of the position control system. As α is decreased, the stability of the position control system deteriorates, and the position control response starts to oscillate as shown in Fig. 4-8.

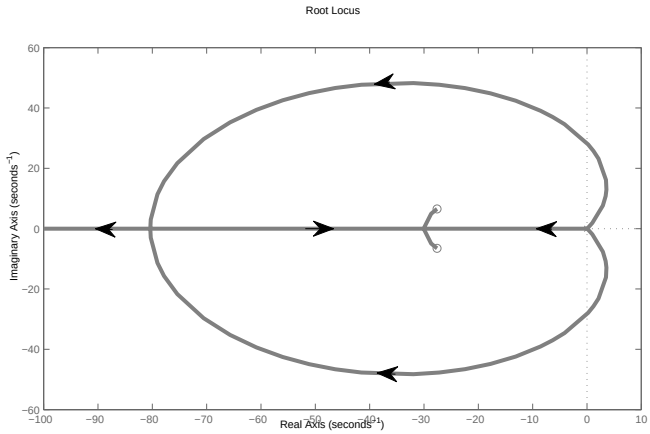

Fig. 4-6: Root locus of the robust position control system with respect to α.

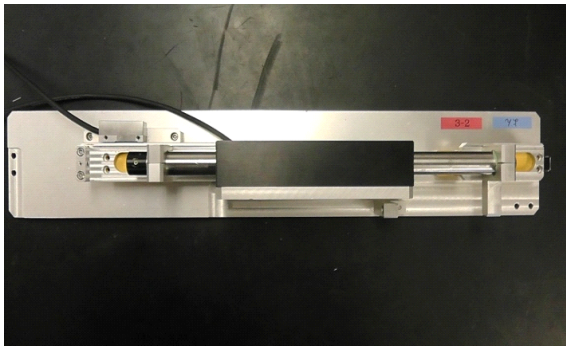

Fig. 4-7: Linear DC motor.

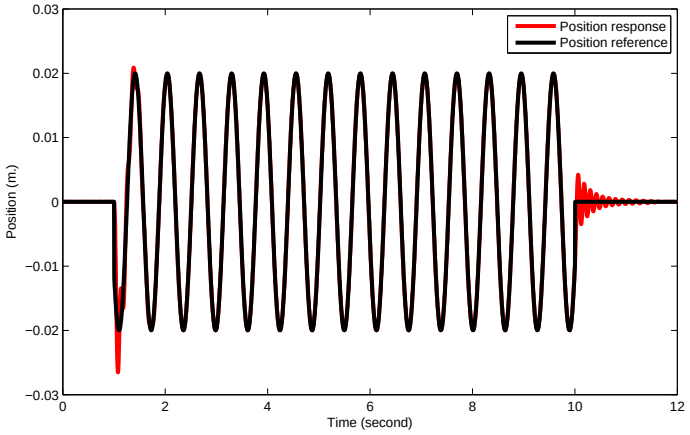

Fig. 4-8: Robust position control response of the linear DC motor when DOb is used.

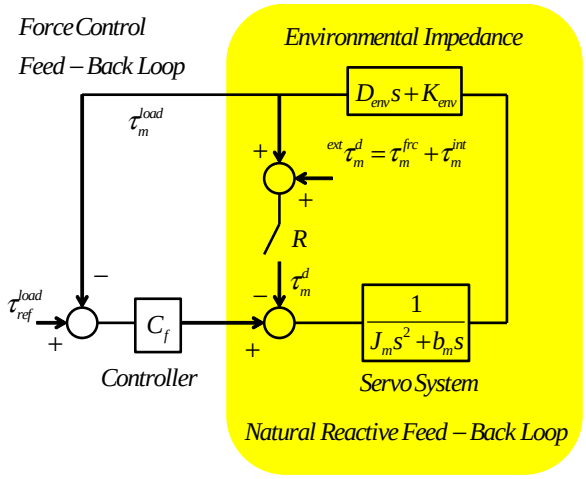

Fig. 4-9: Block diagram of a conventional explicit force control system.

4.4 Disturbance Observer Based Robust Force Control Systems

In this section, DOb based explicit robust force control systems are analyzed in detail. The stability of contact motion and low performance are the main challenging issues of explicit force control systems [84–86]. This section shows that not only the performance, but also the stability of an explicit force control system is improved by using robust force control methods [87].

Force control goals can be achieved asymptotically by using an open loop controller if external disturbances, such as gravity and friction, are ignored. However, in practice, an explicit force control system becomes very sensitive to external disturbances and environmental impedance variations when open loop controllers are used [36]. Conventionally, external disturbances are canceled by using model based control methods such as feed-back linearization, and environmental impedance variations are controlled by using a force control feed-back loop [88]. However, it is a well-known fact that modeling errors of external disturbances degrade the performance of an explicit force control system. Besides, environmental impedance variations cannot be controlled directly in a force control feed-back loop due to the natural reactive feed-back loop that is shown in Fig. 4-9. It can be explained as follows:

Natural frequency and damping coefficient of an explicit force control system are derived from Fig. 4-9 as follows:

$$w_n = \sqrt{(1+C_f)\,\frac{K_{env}}{J_m}}\ and\ \xi = \frac{b_m + (1+C_f)\,D_{env}}{2\sqrt{J_m\,(1+C_f)\,K_{env}}}, \tag{4.15}$$

when R is on; and

$$w_n = \sqrt{C_f \frac{K_{env}}{J_m}} \; and \; \xi = \frac{b_m + C_f D_{env}}{2\sqrt{J_m C_f K_{env}}}, \tag{4.16}$$

when R is off.

In Fig. 4-9, R denotes a fictitious robust control switch. External disturbances and the natural reactive feed-back loop are canceled, i.e., the robustness of the explicit force control system is achieved, when R is off. Equation (4.15) and eq. (4.16) show that an explicit force control system is more sensitive to environmental impedance variations when it is influenced by the natural reactive feed-back loop. As the stiffness of environmental impedance, K_{env}, increases, the stability deteriorates even if a low force control gain is used. However, as shown in eq. (4.16), environmental stiffness can be controlled directly when the natural reactive feed-back loop is canceled. Therefore, the fictitious robust control switch, R, should be realized. It is obvious that a DOb works as the fictitious robust control switch. However, the robustness of an explicit force control system is limited by the dynamic characteristics of DOb such as bandwidth limitations. Therefore, the dynamics of DOb should be considered in the analysis of the DOb based explicit robust force control systems.

Block diagram of a DOb based explicit robust force control system is shown in Fig. 4-10. In this figure, C_f denotes force control gain; and D_{env} and K_{env} denote environmental damping and stiffness coefficients, respectively. The other parameters are same as defined earlier.

Without any approximation, Fig. 4-10 can be simplified as shown in Fig. 4-11. In this figure, $\alpha =$

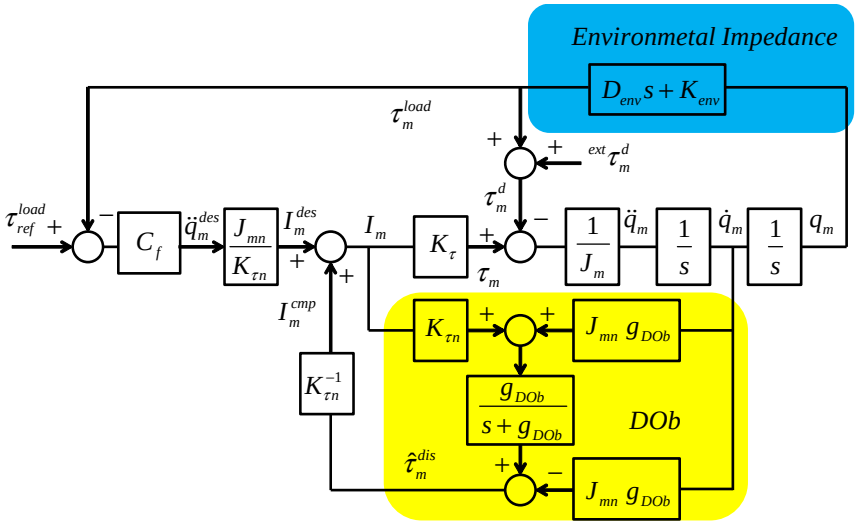

Fig. 4-10: Block diagram of a conventional DOb based explicit robust force control system.

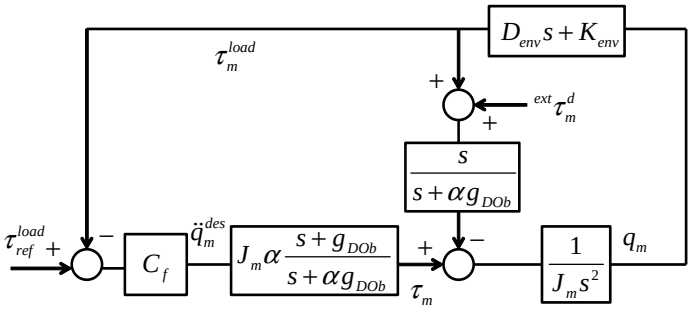

Fig. 4-11: Simplified block diagram of a conventional DOb based explicit robust force control system.

$\frac{J_{mn}K_\tau}{J_m K_{\tau n}}$. It is clear from Fig. 4-11 that a DOb works as a phase lead-lag compensator that is adjusted by α in the explicit robust force control systems; and the stability is improved by increasing phase lead, i.e., α. Besides, not only the stability, but also the disturbance suppression at low frequencies is improved by increasing α, since external disturbances and the reactive feed-back loop is suppressed in a wider frequency range as α is increased. However, as shown in the previous sections, α cannot be increased freely due to the robustness constraints of DOb. The transfer function between τ_{ref}^{load} and τ_m^{load} is directly derived from Fig. 4-11 as follows:

$$\frac{\tau_m^{load}}{\tau_{ref}^{load}} = \frac{L_{CF}(s)}{1 + L_{CF}(s)}, \tag{4.17}$$

where $L_{CFC}(s) = \frac{(s+g_{DOb})(D_{env}s+K_{env})}{s\{J_m s^2+(J_m\alpha g_{DOb}+D_{env})s+K_{env}\}}$ is the open loop transfer function of the conventional DOb based explicit robust force control system.

Equation (4.17) shows that the steady state error of the explicit robust force control system is removed by a DOb, since the open loop transfer function has a pole at the origin. The relative degree of L_{CFC} is one so the asymptotes of the root loci are at angle of π rad.. The transient response of the explicit robust force control system changes by the environmental impedance, control gain, nominal and uncertain motor parameters, and the bandwidth of DOb. As the bandwidth of DOb is increased, the robustness is improved but the stability deteriorates due to phase lag increment. Although, in practice, it is not a severe problem when environmental stiffness is high, the stability may deteriorate by increasing the bandwidth of DOb when a robot contacts with a soft environment. Therefore, the robustness of a DOb based explicit force control system should be adjusted by considering the stability of the explicit robust force control system.

The transfer functions between $^{ext}\tau_m^d$ and τ_m^{load} are derived from Fig. 4-9 and Fig. 4-11 as follows:

$$\frac{\tau_m^{load}}{{}^{ext}\tau_m^d} = -\frac{D_{env}s_+ K_{env}}{J_m s^2 + (1+C_f) D_{env} s + (1+C_f) K_{env}}, \tag{4.18}$$

when the conventional explicit force control system is considered; and

$$\frac{\tau_m^{load}}{{}^{ext}\tau_m^d} = -\frac{s\left(D_{env}s_+ K_{env}\right)}{J_m s^2 \left(s+\alpha g_{DOb}\right) + \left\{C_f J_m \alpha \left(s+g_{DOb}\right) + s\right\}\left(D_{env}s + K_{env}\right)}, \tag{4.19}$$

when the DOb based explicit robust force control system is considered.

Equation (4.18) shows that as the force control gain, C_f, is increased, the robustness of the conventional explicit force control system is improved, i.e., suppression of external disturbances is improved. However, it is a well known fact that force control gain cannot be increased freely due to the stability constraint. Therefore, the robustness of the conventional explicit force control system is limited by the stability. Equation (4.19) shows that external disturbances can be suppressed precisely at low and high frequencies when a DOb is used. However, the dynamics of the explicit robust force control system become more dominant in the intermediate frequencies. Therefore, the robustness of the explicit force control system may deteriorate in the intermediate frequency range.

Although Fig. 4-11 provides us a basic insight into the DOb based explicit robust force control systems, it is impractical due to the assumption which is that environmental impedance is known, a priori. In real explicit force control implementations, environmental impedance is generally unknown; therefore, the estimation of environmental impedance is crucial in the explicit force control systems. However, the environmental impedance estimation methods change the robustness, stability, and performance of the explicit force control systems, drastically. In this section, implicit and explicit environmental impedance estimation methods are considered by using a force sensor and an RFOb.

Let us start by considering the implicit environmental impedance estimation method, i.e.,force sensor. Force sensors are widely used to detect contact forces in conventional force control applications. A force sensor detects contact forces implicitly by estimating the strain of a strain gauge. The estimated strain is transformed into stress by using Young's modulus so as to detect contact forces. The compliance of an explicit force control system changes by a force sensor if the stiffness of the strain gauge is low. Since the stability of an explicit force control system deteriorates by the low stiffness of strain gauge, highly stiff force sensors are generally used in force control applications. However, stiff force sensors suffer from noise, because contact forces are detected by estimating infinitesimal strains. Compliance and noise are the main disadvantages of a force sensor. Besides that force sensors have several practical

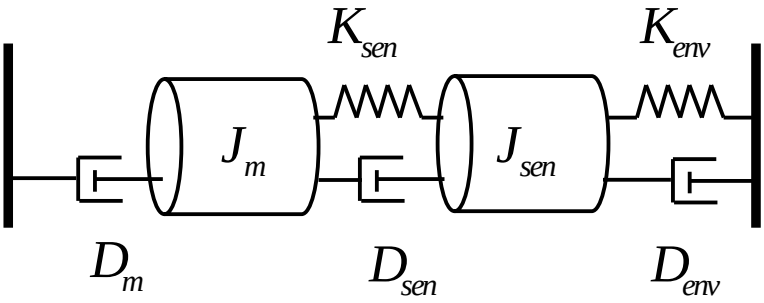

(a) Two mass resonant system model of a force sensor.

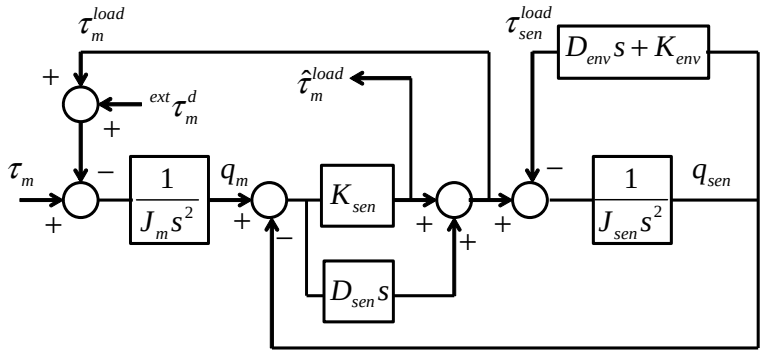

(b) Block diagram of a force sensor.

Fig. 4-12: Model and block diagram of a force sensor.

disadvantages, e.g., they require amplifiers which increase costs, mounting force sensors on robotic systems may cause some difficulties, connection between force sensor and amplifier increases design complexity, force sensors can estimate environmental impedance if they are in contact, and so on.

A two mass resonant system, which is shown in Fig. 4-12(a), is used to obtain the lumped parameter model of a force sensor. Fig. 4-12(b) shows the block diagram of a two mass resonant system model. In this figure, J_{sen}, D_{sen} and K_{sen} denote the inertia, damping and stiffness of a force sensor, respectively; D_m and D_{env} denote damping of motor and environment, respectively; K_{env} denotes stiffness of environment; and $\widehat{\tau}_m^{load}$ denotes estimated contact force. The other parameters are same as defined earlier.

Without any approximation, a simplified block diagram of the explicit robust force control system is obtained as shown in Fig. 4-13 when environmental impedance is estimated by using a force sensor. In

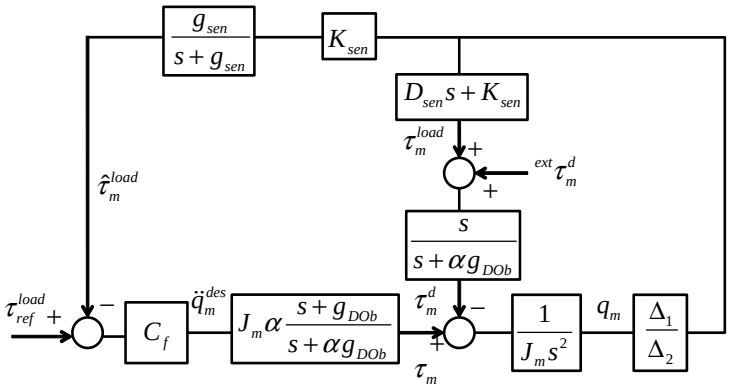

Fig. 4-13: Simplified block diagram of a DOb based explicit robust force control system when force sensor is used to estimate environmental impedance.

this figure, $\Delta_1(s) = J_{sen}s^2 + D_{env}s + K_{env}$; $\Delta_2(s) = J_{sen}s^2 + (D_{sen} + D_{env})s + K_{sen} + K_{env}$; and g_{sen} denotes the bandwidth of force estimation.

It is clear from Fig. 4-11 and Fig. 4-13 that the compliance of the explicit robust force control system changes by the dynamics of force sensor. The stability and performance of the explicit robust force control system deteriorate as the stiffness of force sensor is decreased. Therefore, in general, stiff force sensors are used in force control applications. To suppress the noise of a stiff force sensor, contact forces are detected by using a LPF as shown in Fig. 4-13. However, the LPF degrades the performance by limiting the force control bandwidth, g_{sen}, and stability by increasing phase lag.

The stability and robustness can be analyzed similarly by deriving the transfer functions of the explicit robust force control system. However, the dynamics of force sensor and LPF, which degrade the stability and performance, should be considered.

Let us now consider the explicit environmental impedance estimation method, i.e., RFOb. Block diagram of an RFOb based robust force control system is shown in Fig. 4-14. In this figure, ΔJ_m and ΔK_τ denote inertia and torque coefficient variations, respectively. A DOb estimates external disturbances and system uncertainties in the inner-loop. The robustness of the force control system is achieved by feeding back the estimated disturbances. However, system uncertainties should be identified a priori to design an RFOb in the outer-loop. Although the structures of a DOb and an RFOb are quite similar, only the latter is a model based control method which is the most challenging issue in its design. In general, an RFOb is considered as a feed-forward control structure to simplify the analysis. However, it is not true. The design parameters of a DOb and an RFOb change not only the performance, but also the stability

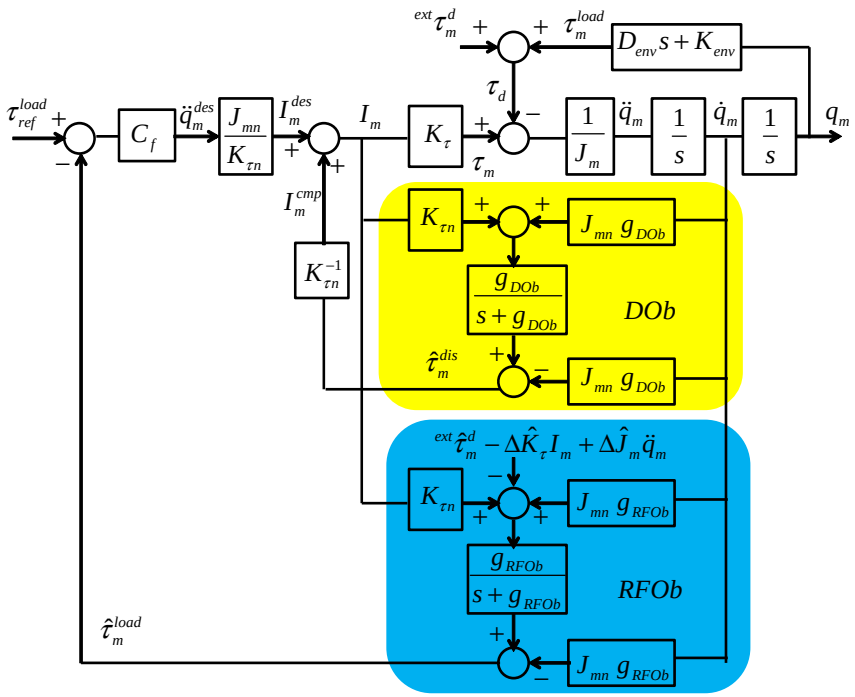

Fig. 4-14: Block diagram of a DOb based explicit robust force control system when RFOb is used to estimate environmental impedance.

of the explicit robust force control system, significantly. The stability of the explicit robust force control system is analyzed as follows:

Let us define the environmental contact by using a lumped spring-damper model as follows:

$$\tau_m^{load} = D_{env}(\dot{q}_m - \dot{q}_{env}) + K_{env}(q_m - q_{env}), \tag{4.20}$$

where D_{env} and K_{env} denote the environmental damping and stiffness, respectively; and q_{env} and $\dot{q}_{env}$ denote the position and velocity of environment at equilibrium, respectively. The dynamic equation of an RFOb based robust force control system is derived from Fig. 4-14 as follows:

$$\left(\widehat{K}_\tau I_m - \widehat{J}_m\ddot{q}_m - \hat{\tau}_m^{frc} - \hat{\tau}_m^{int}\right)\frac{g_{RFOb}}{s + g_{RFOb}} = \hat{\tau}_m^{load}, \tag{4.21}$$

where $\hat{\tau}_m^{frc}$ and $\hat{\tau}_m^{int}$ denote identified friction and interactive disturbances, respectively; and $\widehat{J}_m = J_{mn} + \Delta\widehat{J}_m$ and $\widehat{K}_\tau = K_{\tau n} + \Delta\widehat{K}_\tau$ denote identified inertia and torque coefficient, respectively.

The transfer function between τ_{ref}^{load} and $\hat{\tau}_m^{load}$ is derived by using eq. (4.1), eq. (4.2), eq. (4.21), and Fig. 4-14 as follows:

$$\frac{\hat{\tau}_m^{load}}{\tau_{ref}^{load}} = \frac{L_{RFOb}(s)}{1 + L_{RFOb}(s)}, \tag{4.22}$$

where

$$L_{RFOb}(s) = C_f \frac{g_{RFOb}\frac{J_{mn}}{K_{\tau n}}\left(s + g_{DOb}\right)\varphi\left(s\right)}{s\left\{J_m s\left(s + \alpha g_{DOb}\right) + \left(D_{env}s + K_{env}\right)\right\}\left(s + g_{RFOb}\right)}, \tag{4.23}$$

is the open loop transfer function of an RFOb based explicit robust force control system; $\varphi(s) = J_m\widehat{K}_\tau s(s + \alpha g_{DOb}) + \widehat{K}_\tau(D_{env}s + K_{env}) - \widehat{J}_m K_\tau s(s + \beta g_{DOb})$; $\alpha = \frac{J_{mn}K_\tau}{J_m K_{\tau n}}$ and $\beta = \frac{J_{mn}\widehat{K}_\tau}{\widehat{J}_m K_{\tau n}}$. The other parameters are same as defined earlier. If an RFOb is designed by using perfect identification of inertia and torque coefficient, i.e., $\alpha = \beta$, then

$$L_{RFOb}(s) = C_f \frac{g_{RFOb}J_m\alpha\left(s + g_{DOb}\right)\left(D_{env}s + K_{env}\right)}{s\left\{J_m s\left(s + \alpha g_{DOb}\right) + \left(D_{env}s + K_{env}\right)\right\}\left(s + g_{RFOb}\right)}. \tag{4.24}$$

In general, the bandwidths of a DOb and an RFOb are set to the same value. If it is applied into eq. (4.24), then

$$L_{RFOb}\left(s\right) = C_f \frac{gJ_m\alpha(D_{env}s + K_{env})}{s\left\{J_m s\left(s + \alpha g\right) + \left(D_{env}s + K_{env}\right)\right\}}. \tag{4.25}$$

Equation (4.23), eq. (4.24), and eq. (4.25) show that each of the open loop transfer function has a pole at the origin, so the steady state error is removed by a DOb in the explicit robust force control systems.

Let us first consider eq. (4.25), in which it is assumed that perfect system identification is achieved and the bandwidth of DOb and RFOb are set to the same value. The relative degree of the open loop transfer function is two, so the root loci of the robust force control system have asymptotes, at $\pm\frac{\pi}{2}$ rad.. The stability of the robust force control system deteriorates as the environmental stiffness, K_{env}, increases, since the zero of the open loop transfer function, which is at $\frac{K_{env}}{D_{env}}$, moves away from the origin and phase lag increases.

Let us now consider eq. (4.24), in which it is assumed that perfect system identification is achieved and the bandwidths of DOb and RFOb are set to the different values. The relative degree of the open loop transfer function is two, so the asymptotic behaves of the root loci do not change. However, a phase lead-lag compensator, which can be used to improve the stability and performance, is obtained by setting the bandwidths to the different values. If the bandwidth of RFOb is higher than DOb's one, then a phase lead compensator is obtained; however, if the bandwidth of DOb is higher than RFOb's one, then a phase lag compensator is obtained. It is shown clearly by re-writing eq. (4.24) as follows:

$$L_{RFOb}(s) = C_f C_{com}(s) \frac{g_{RFOb} J_m \alpha (D_{env} s + K_{env})}{s\left\{J_m s\left(s + \alpha g_{DOb}\right) + (D_{env} s + K_{env})\right\}}, \tag{4.26}$$

where $C_{com}(s) = \frac{s+g_{DOb}}{s+g_{RFOb}}$ is the phase lead-lag compensator that is adjusted by the bandwidths of DOb and RFOb.

Finally, let us consider eq. (4.23), in which imperfect identification of inertia and torque coefficient are considered. The relative degree of the open loop transfer function is one, so the root loci of the robust force control system have asymptotes at π rad.. Equation (4.23) and eq. (4.24) show that asymptotic behaves of the root loci improves when $\alpha \neq \beta$, i.e., inertia and torque coefficient are not identified precisely in the design of an RFOb. However, the stability of the robust force control system changes drastically by the imperfect identification. It can be explained as follows:

Let us consider the numerator of eq. (4.23) by using

$$C_f g_{RFOb} \frac{J_{mn}}{K_{\tau n}} \left(s + g_{DOb}\right) \varphi(s), \tag{4.27}$$

where $\varphi(s) = \left(J_m \widehat{K}_\tau - \widehat{J}_m K_\tau\right) s^2 + \widehat{K}_\tau D_{env} s + \widehat{K}_\tau K_{env}$.

As shown in eq. (4.27), the open loop transfer function has a right half plane zero if $J_m \widehat{K}_\tau < \widehat{J}_m K_\tau$, i.e., $\beta < \alpha$. Therefore, not only the performance, but also the stability of the robust force control system deteriorates significantly by the imperfect identification of inertia and torque coefficient.

The performance of an RFOb changes significantly by the imperfect identification of torque coefficient. However, in general, the error of inertia identification can be neglected due to the low accelerations in force control. In practice, although torque coefficient identification can be achieved precisely, identification of inertia may not be a simple task, e.g., the inertia of a multi-body system is quite complex and non-linear. Therefore, a new design constraint, which improve the performance and stability, is proposed for the RFOb based robust force control systems as follows:

$$\widehat{J}_m \leq J_m \qquad and \qquad \widehat{K}_\tau = K_\tau, or \tag{4.28}$$

$$\beta \geq \alpha \qquad and \qquad \widehat{K}_\tau = K_\tau. \tag{4.29}$$

If it is assumed that $\widehat{K}_\tau = K_\tau$, $\widehat{J}_m = J_m$, and $g_{DOb} = g_{RFOb} = g$, then the transfer functions of $\frac{\hat{\tau}_m^{load}}{ext\tau_m^d}$ and $\frac{\tau_m^{load}}{ext\tau_m^d}$ are derived from Fig. 4-14 as follows:

$$\frac{\hat{\tau}_m^{load}}{^{ext}\tau_m^d} = \frac{g}{s+g}\frac{J_m s^2(s+\alpha g)(1-\psi) - s(D_{env}s + K_{env})\psi}{J_m s^3 + (J_m \alpha g + D_{env})s^2 + (K_{env} + J_m \alpha g C_f D_{env})s + J_m \alpha g C_f K_{env}}, \tag{4.30}$$

$$\frac{\tau_m^{load}}{^{ext}\tau_m^d} = \frac{J_m \alpha g C_f(D_{env}s + K_{env})(1-\psi) - s(D_{env}s + K_{env})\psi}{J_m s^3 + (J_m \alpha g + D_{env})s^2 + (K_{env} + J_m \alpha g C_f D_{env})s + J_m \alpha g C_f K_{env}}, \tag{4.31}$$

where $^{ext}\hat{\tau}_m^d = ^{ext}\tau_m^d\psi$ denotes the identified external disturbances. Equation (4.30) and eq. (4.31) show that an RFOb cannot detect contact forces precisely when it suffers from imperfect identification of external disturbances, i.e., $\psi \neq 1$.

If external disturbances are identified precisely, i.e., $\psi = 1$, then eq. (4.31) is re-written as follows:

$$\frac{\tau_m^{load}}{^{ext}\tau_m^d} = -\frac{s(D_{env}s + K_{env})}{J_m s^3 + (J_m \alpha g + D_{env})s^2 + (K_{env} + J_m \alpha g C_f D_{env})s + J_m \alpha g C_f K_{env}}. \tag{4.32}$$

Equation (4.32) is quite similar to eq. (4.18). It shows that external disturbances can be suppressed precisely at low and high frequencies. However, the robustness may deteriorate in the intermediate frequency range even if $\psi = 1$.

4.4.1 Simulations and Experiment

In this section, simulation and experimental results are given for explicit robust force control systems. The stability and robustness of a DOb based explicit force control system are considered in the simulation. The parameters of the simulations are shown in Table 4.3.

The stability analyses are conducted by using the root-loci of the robust force control systems that are shown in Fig. 4-15, Fig. 4-16 and Fig. 4-17. Fig. 4-15 shows the root-loci with respect to g_{DOb} when α has different values and environmental impedance is known, a priori. It indicates that the stability of

Table 4.3: Simulation parameters of the explicit force control system.

Variables	Definition of variables	Value
J_{mn}	Nominal mass	0.10 kg
$K_{\tau n}$	Nominal torque coefficient	0.25 N/A
D_{sen}	Force sensor damping	0.02 Ns/mm
K_{sen}	Force sensor stiffness	100 N/mm
D_{env}	Damping of environmental impedance	0.01 Ns/mm

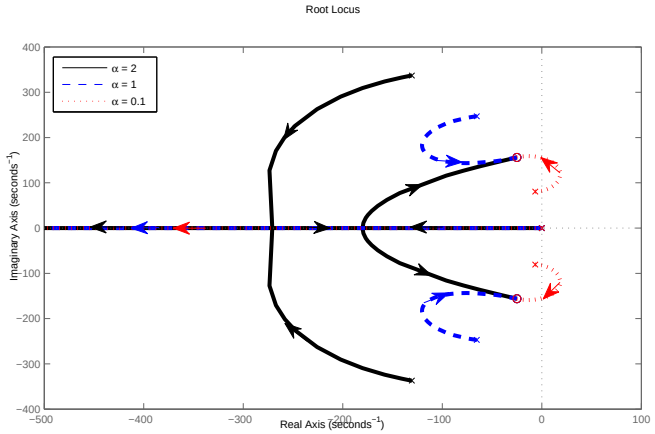

Fig. 4-15: Root loci with respect to g_{DOb} when environmental impedance is known a priori.

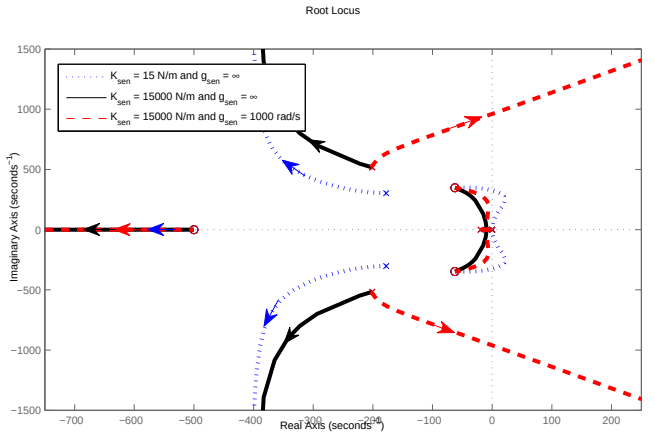

Fig. 4-16: Root loci with respect to C_f when a force sensor is used.

the robust force control system can be improved by increasing α. However, against α, increasing g_{DOb} may improve or degrade the stability of the robust force control system. If there is no a constraint on the bandwidth of DOb, then a good stability can be achieved by increasing g_{DOb}. However, in reality, it is limited by practical constraints such as noise and sampling time. Therefore, as shown in the figure, the stability deteriorates if the closed-loop poles cannot get close to the zeros when g_{DOb} is increased. In this case, decreasing the robustness, i.e., using lower g_{DOb}, can improve the stability. The stability constraint on g_{DOb} becomes more dominant as the environmental stiffness decreases. Fig. 4-16 shows the root-loci with respect to C_f when a force sensor is used. It indicates that the stability of the robust

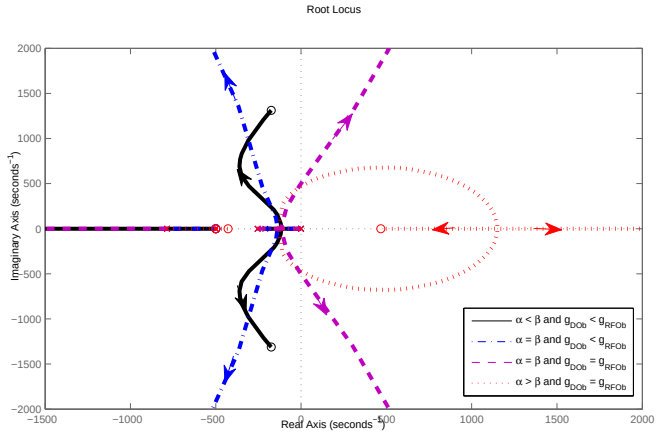

Fig. 4-17: Root loci with respect to C_f when an RFOb is used.

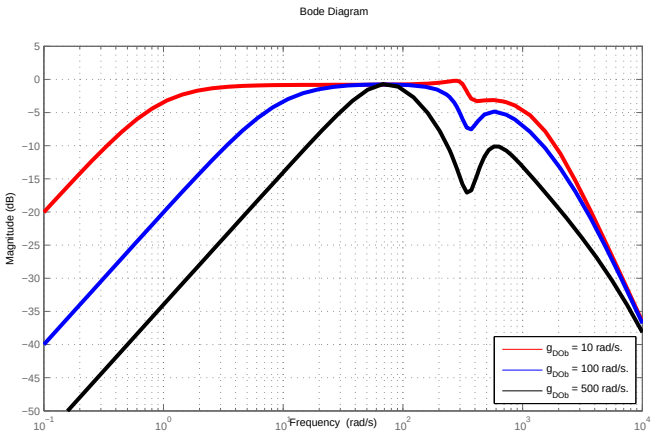

Fig. 4-18: Disturbance suppression when environmental impedance is known a priori.

force control system deteriorates if the stiffness of a force sensor is decreased and/or a LPF is used to suppress the noise of force estimation. Fig. 4-17 shows the root-loci with respect to C_f when an RFOb is used. It indicates that the stability of the robust force control system changes drastically by the design parameters of a DOb and an RFOb. The stability of the robust force control system is improved by using $\widehat{J}_m \leq J_m$, i.e., $\alpha \leq \beta$ and $g_{RFOb} \geq g_{DOb}$.

The robustness analyses of the explicit force control systems are conducted by using the frequency responses of the transfer functions between ${}^{ext}\tau_m^d$ and τ_m^{load} in Fig. 4-18, Fig. 4-19, and Fig. 4-20. Fig. 4-18 indicates that a good robustness can be achieved at low and high frequencies; however, the robustness

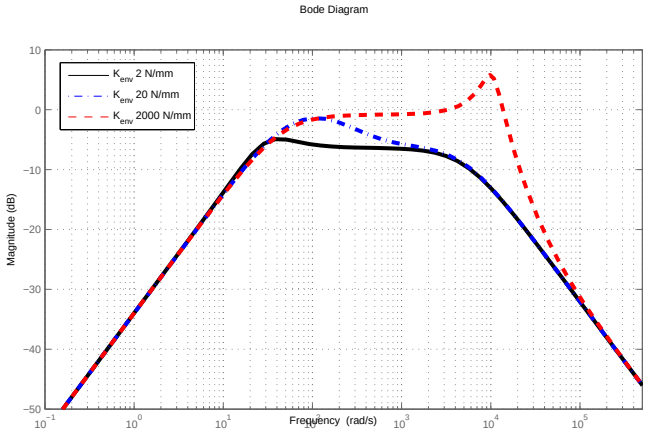

Fig. 4-19: Disturbance suppression when a force sensor is used to detect environmental impedance.

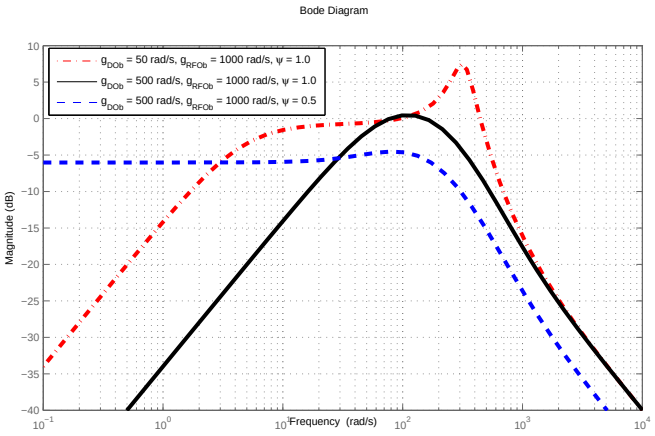

Fig. 4-20: Disturbance suppression when an RFOb is used to detect environmental impedance.

changes with respect to the dynamics of the plant, environmental impedance, and the robustness and performance controllers in the intermediate frequencies. As shown in Fig. 4-18, an external disturbance may not be suppressed even if it stays within the bandwidth of DOb, g_{DOb} . As the stiffness of environmental impedance increases, the robustness of a DOb based explicit force control system deteriorates. Fig. 4-19 and Fig. 4-20 show the robustness analyses when a force sensor and an RFOb are used to detect contact force, respectively. As the bandwidth of DOb is increased, the robustness of the explicit force control system is improved. However, it is more sensitive to external disturbances when an RFOb is used to detect environmental impedance. The performance of the explicit force control system is influenced by

Table 4.4: Experiment parameters of the explicit force control system.

Variables	Definition of variables	Value
J_{mn}	Nominal mass	0.62 kg
$K_{\tau n}$	Nominal torque coefficient	33 N/A
g_{RFOb}	Cut-off frequency of RFOb	1000 rad/s.
C_f	Force control gain	1
K_{sen}	Stiffness of force sensor	1500 N/mm

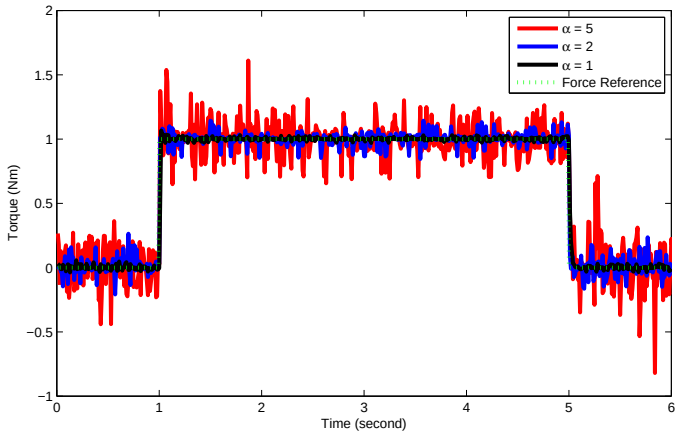

Fig. 4-21: Robustness / Noise suppression of the DC motor .

external disturbances even at low frequencies when $\psi \neq 1$.

A linear DC-motor, which is shown in Fig. 4-7, is used in the experiments. The specifications of the experimental setup are shown in Table 4.4. Sampling time is 1 ms, and KYOWA LUR-A-50NSA1 force sensor is used to estimate contact forces.

Let us start by considering the robustness constraint of a DOb. Fig. 4-21 shows the force control responses of the DC motor when α has different values and $g_{DOb} = 200$ rad/s.. It is clear from the figure that as α is increased a DOb becomes more sensitive to noise, since the robustness deteriorates. To improve the robustness of DOb, α and g_{DOb} should be tuned by considering the robustness constraint given in eq. (4.7).

Fig. 4-22 shows force control responses when contact forces are detected by using the force sensor. A step force control command is applied at 1 s., and a fictitious external disturbance, which is $\sin(wt)$, is applied between 5 and 13 s. The frequency of the external disturbance, i.e., w, is: 1 rad/s. between 5 and 7 s., 10 rad/s. between 7 and 9 s., 100 rad/s. between 9 and 11 s., and 500 rad/s. between 11 and 13 s.. Fig. 4-

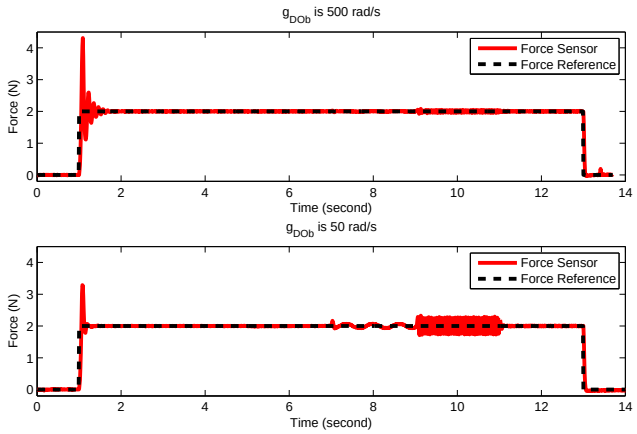

(a) Soft environment (sponge).

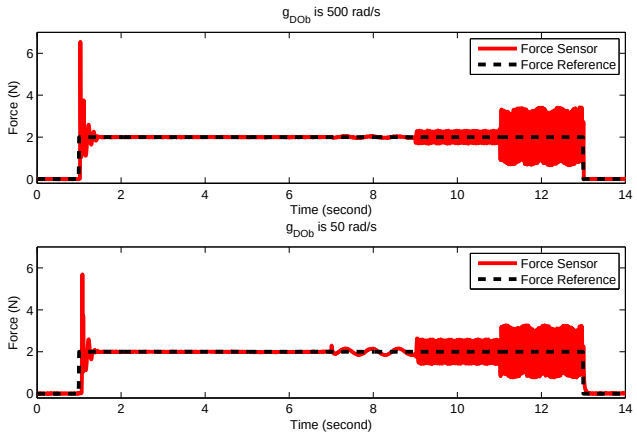

(b) Hard environment (aluminum).

Fig. 4-22: Step responses of the robust force control system when the force sensor is used to detect contact forces.

22(b) indicates that the explicit force control system becomes more sensitive to the external disturbance as the stiffness of environmental impedance increases. The external disturbance is suppressed precisely at low frequencies; however, the force control system is influenced by the fictitious external disturbance, $sin(wt)$, as w is increased. Fig. 4-22(a) shows that although the fictitious external disturbance is out of the bandwidth of DOb, the explicit force control system can suppress it when environmental stiffness is low. The stability of the explicit robust force control system is improved by decreasing g_{DOb}; however,

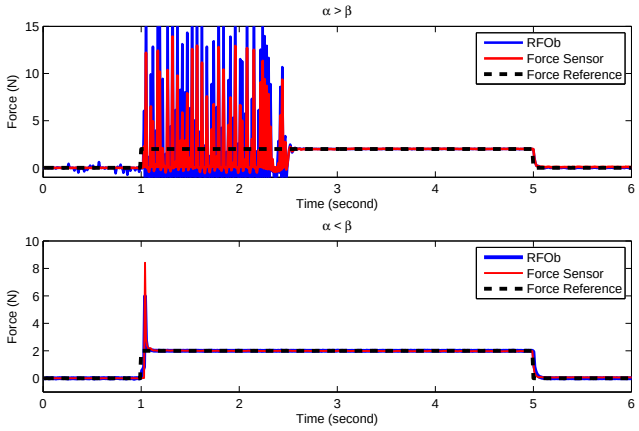

(a) Soft environment (sponge).

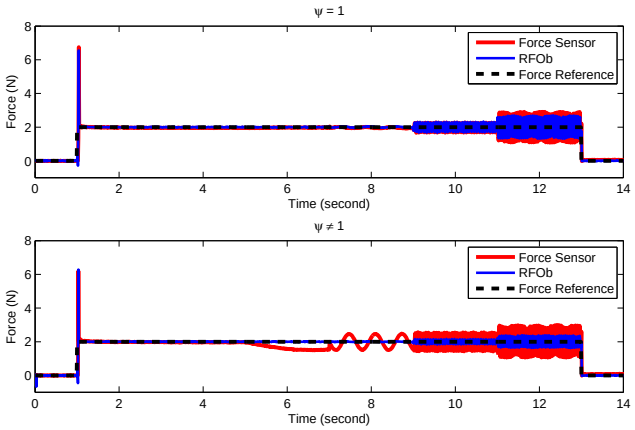

(b) Hard environment (aluminum).

Fig. 4-23: Step responses of the robust force control system when RFOb is used to detect contact forces.

the robustness deteriorates. The stability improvement is more dominant when environmental stiffness is low.

Fig. 4-23 shows force control responses when contact forces are detected by using an RFOb. Force sensor is used to verify the detection of contact forces that are obtained by the RFOb. Fig. 4-23(a) shows that the stability of the robust force control system changes significantly by the identification of motor inertia. It is improved by using $\widehat{J}_m < J_m$. Fig. 4-23(b) shows that imperfect identification of external disturbances degrades the performance of the explicit force control system when an RFOb is used. The

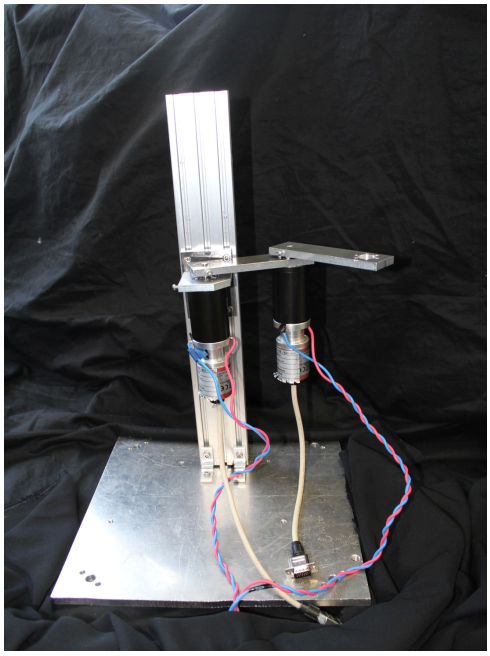

Fig. 4-24: Two link planar robot arm.

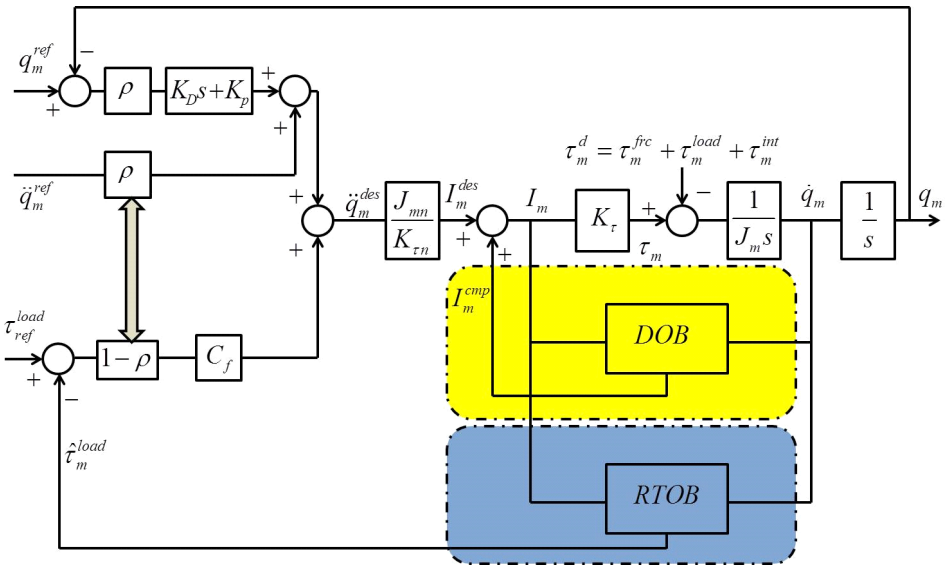

Fig. 4-25: Block diagram of an accelaration based hybrid motion control system.

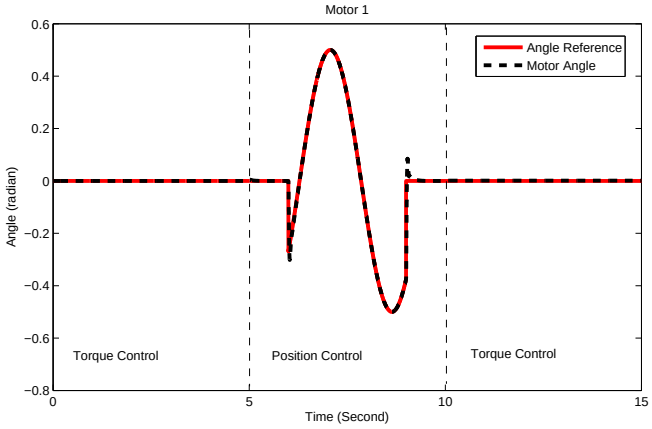

(a) First motor response.

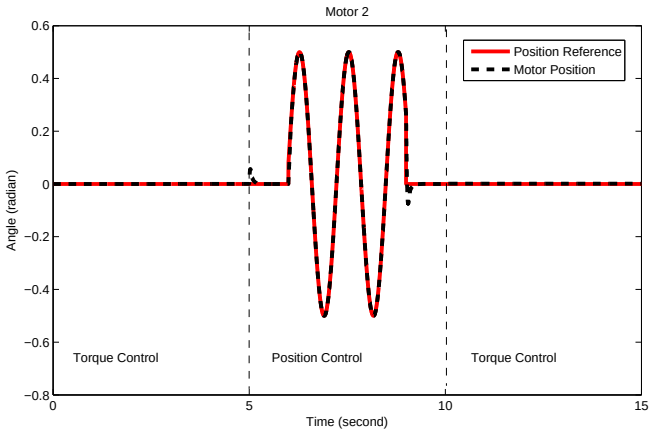

(b) Second motor response.

Fig. 4-26: Position control responses of the two link planar robot arm.

performance of the explicit force control system is influenced by the fictitious external disturbance even at low frequencies, since an RFOb cannot detect contact forces, accurately. Fig. 4-23(b) clearly shows the contact force estimation error of RFOb between 5 and 13 s. when $\psi \neq 1$.

Finally, two link planar robot arm, which is shown in Fig. 4-24, is controlled by using the proposed position and force control systems. Block diagram of the ABC hybrid motion control system is shown in Fig. 4-25. In this figure ρ denotes compliance selection constant. Torque control is conducted between 0 and 5, and 10 and 15 seconds; and position control is conducted between 5 and 10 seconds. Step torque

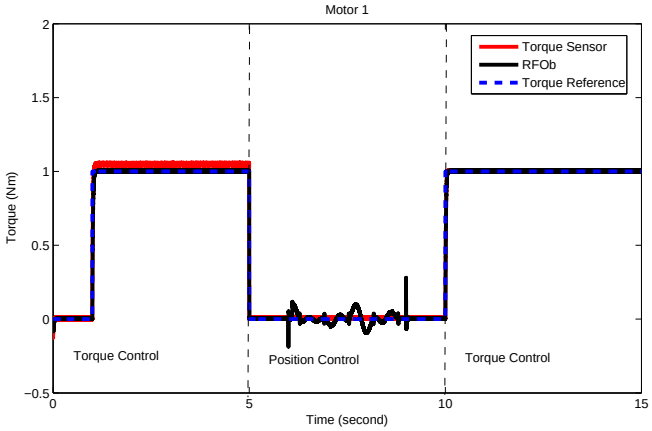

(a) First motor response.

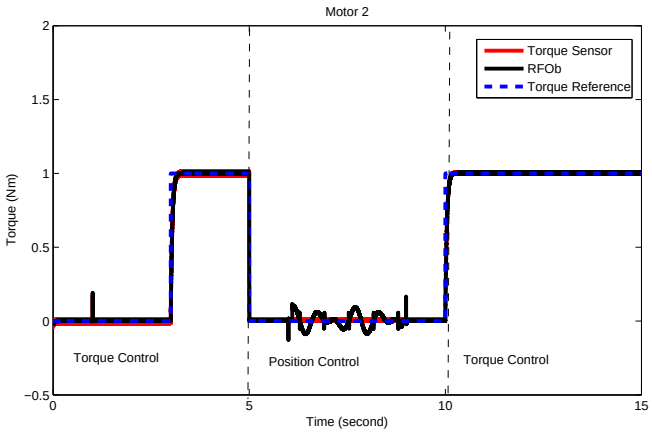

(b) Second motor response.

Fig. 4-27: Torque control responses of the two link planar robot arm.

reference inputs are applied to each joints at different times during the torque control, and the links interact with the environments initially; sinusoidal position reference inputs are applied to each joints. Fig. 4-26 and Fig. 4-27 show the position and torque control responses at each joints, respectively. As shown in the figures, the position and torque control goals can be achieved precisely when the proposed methods are used.

4.5 Adaptive Reaction Force Observer Design

In this section, a novel adaptive design method is proposed for RFOb based robust force control systems. In the design of the adaptive RFOb based robust force control system, practical constraints of DOb and RFOb are considered. Equation (4.22) clearly shows that the robust force control system depends on the environmental impedance, the dynamics of the plant, and the robustness and performance controllers. To achieve high performance force control systems, all dynamics of the robust force control system should be considered. Therefore, environmental impedance and plant uncertainties should be estimated. A new adaptive design method is proposed as follows:

a) Damping Environmet: K_{env} is zero.

Let us first consider environmental impedance as pure damping. If $\alpha = \beta$ and $g_{DOb} = g_{RFOb} = g$, then the open and closed loop transfer functions of the robust force control system are derived as follows:

$$L_{RFOb}(s) = C_f \frac{J_m \alpha g D_{env}}{J_m s^2 + (J_m \alpha g + D_{env}) s}, \tag{4.33}$$

$$\frac{\hat{\tau}_m^{load}}{\tau_{ref}^{load}} = C_f \frac{J_m \alpha g D_{env}}{J_m s^2 + (J_m \alpha g + D_{env}) s + J_m C_f \alpha g D_{env}}. \tag{4.34}$$

Let us consider a general second order transfer function by using,

$$T_{DES}(s) = \frac{w_n^2}{s^2 + 2\xi w_n s + w_n^2}. \tag{4.35}$$

The design parameters of the robust force control system are derived as follows:

$$\alpha g = 2\xi w_n - \frac{D_{env}}{J_m}, \tag{4.36}$$

$$C_f = \frac{w_n^2}{\alpha g D_{env}}. \tag{4.37}$$

If the bandwidth constraint of a DOb, which is given in eq. (4.7), is applied into eq. (4.36), then

$$\frac{D_{env}}{J_m} < 2\xi w_n < \frac{g_v}{2} + \frac{D_{env}}{J_m}. \tag{4.38}$$

Consequently, the adaptive robust force control system is designed as follows:

(1) ξ is chosen between $0.707 \leq \xi \leq 1$ to improve the stability.

(2) w_n is obtained by using $w_n = \frac{\gamma}{2\xi}\left(\frac{g_v}{2} + \frac{D_{env}}{J_m}\right)$ where $\frac{2D_{env}}{J_m g_v + 2D_{env}} < \gamma < 1$ to satisfy eq. (4.38).

(3) αg and C_f are obtained by using eq. (4.36) and eq. (4.37), respectively.

b) Stiff Environmet: D_{env} is zero.

Let us now consider environmental impedance as pure stiffness. If $\alpha = \beta$ and $g_{DOb} = g_{RFOb} = g$, then the open and closed loop transfer functions of the robust force control system are derived as follows:

$$L_{RFOb}(s) = C_f \frac{J_m \alpha g K_{env}}{s\left(J_m s^2 + J_m \alpha g s + K_{env}\right)}, \tag{4.39}$$

$$\frac{\hat{\tau}_m^{load}}{\tau_{ref}^{load}} = C_f \frac{J_m \alpha g K_{env}}{J_m s^3 + J_m \alpha g s^2 + K_{env} s + J_m C_f \alpha g K_{env}}. \tag{4.40}$$

Let us consider a desired characteristic polynomial by using

$$\begin{aligned} P_{DES}(s) &= (s+p)\left(s^2 + 2\xi w_n s + w_n^2\right) \\ &= s^3 + 2\left(\xi w_n + p\right)s^2 + \left(w_n^2 + 2\xi w_n p\right)s + w_n^2 p. \end{aligned} \tag{4.41}$$

The design parameters of the robust force control system are derived as follows:

$$p = \frac{K_{env} - J_m w_n^2}{2 J_m \xi w_n}, \tag{4.42}$$

$$\alpha g = 2\xi w_n + p, \tag{4.43}$$

$$C_f = \frac{w_n^2 p}{\alpha g K_{env}}. \tag{4.44}$$

If eq. (4.7) is applied into eq. (4.43), then

$$0 < 2\xi w_n + p \leq \frac{g_v}{2}. \tag{4.45}$$

Let us assume that $w_n = k\sqrt{\frac{K_{env}}{J_m}}$ where $k < 1$ to satisfy the stability. Then, eq. (4.42) and eq. (4.45) are re-written as follows:

$$p = \eta \xi w_n = \frac{1-k^2}{2\xi k^2} w_n, \tag{4.46}$$

$$w_n \leq \frac{2\xi k^2}{1 + (4\xi^2 - 1)k^2} \frac{g_v}{2}, \tag{4.47}$$

where $\eta = \frac{p}{\xi w_n}$. η is an important design parameter to adjust the performance of the system. If k is derived in terms of η by using eq. (4.46) and put into eq. (4.47), then

$$k = \frac{1}{\sqrt{1+2\eta\xi^2}}, \tag{4.48}$$

$$\eta^2 + (4-2R)\eta + 4 - \frac{R}{\xi^2} \leq 0, \tag{4.49}$$

where $R = \frac{J_m g_v^2}{4K_{env}}$. The real and positive values of η are derived from eq. (4.49) if the following conditions are held.

i If $\frac{J_m g_v^2}{K_{env}} \geq 16$, then ξ can take any value.

ii If $\frac{J_m g_v^2}{K_{env}} < 16$, then ξ should satisfy $\xi \leq \breve{\xi}$ where $\breve{\xi} = \frac{2\sqrt{K_{env}}}{\sqrt{16K_{env} - J_m g_v^2}}$ to obtain real η and $\breve{\xi} = 0.5\sqrt{\frac{J_m g_v^2}{4K_{env}}}$ to obtain $\eta > 0$.

Consequently, the adaptive robust force control system is designed as follows:

(1) η is determined by considering i and ii. If $\breve{\xi} < 1$, then η should be chosen small enough, e.g., $\eta = 0.1$, to suppress the effects of low damping poles; however, if $\breve{\xi} > 1$, then η can be chosen, freely.

(2) ξ is determined by using

(a) If $4(2+\eta)^2 K_{env} \leq 2J_m \eta g_v^2$, then ξ can take any value.

(b) If $4(2+\eta)^2 K_{env} > 2J_m \eta g_v^2$, then $\xi \leq \frac{J_m g_v^2}{4K_{env}(2+\eta)^2 - 2\eta J_m g_v^2}$.

(3) p and k are obtained by using eq. (4.46) and eq. (4.48).

(4) w_n is obtained by using $w_n = k\sqrt{\frac{K_{env}}{J_m}}$.

(5) αg and C_f are obtained by using eq. (4.43) and eq. (4.44).

c) Stiff and Damping Environmet: Finally, let us consider environmental impedance as damping and stiffness. If $\alpha = \beta$ and $g_{DOb} = g_{RFOb} = g$, then the closed-loop transfer function of the robust force control system is derived as follows:

$$\frac{\hat{\tau}_m^{load}}{\tau_{ref}^{load}} = C_f \frac{J_m \alpha g (D_{env} s + K_{env})}{J_m s^3 + (J_m \alpha g + D_{env}) s^2 + (C_f J_m \alpha g D_{env} + K_{env}) s + J_m C_f \alpha g K_{env}}. \tag{4.50}$$

If eq. (4.41) is considered, then the design parameters of the robust force control system are derived as follows:

$$p = \frac{K_{env}^2 - w_n^2 J_m K_{env}}{2\xi J_m w_n K_{env} - w_n^2 J_m D_{env}}, \tag{4.51}$$

$$\alpha g = 2\xi w_n + p - \frac{D_{env}}{J_m}, \tag{4.52}$$

$$C_f = \frac{w_n^2 p}{\alpha g K_{env}}. \tag{4.53}$$

If eq. (4.7) is applied into eq. (4.52), then

$$\frac{D_{env}}{J_m} < 2\xi w_n + p \leq \frac{g_v}{s} + \frac{D_{env}}{J_m}. \tag{4.54}$$

Let us assume that $w_n = k\sqrt{\frac{K_{env}}{J_m}} = \breve{k} 2\xi \frac{K_{env}}{D_{env}}$. Then, eq. (4.51) is re-written as follows:

$$p = \eta \xi w_n = \frac{1 - k^2}{2\xi^2 (1 - \psi k) k^2} \xi w_n, \tag{4.55}$$

where $\psi = \frac{\sqrt{\frac{K_{env}}{J_m}}}{2\xi \frac{K_{env}}{D_{env}}}$; and $\eta = \frac{p}{\xi w_n}$.

The stability of the robust force control system is achieved if

$$k < 1 \; and \; k < \frac{1}{\psi} \qquad or \qquad k > 1 \; and \; k > \frac{1}{\psi}, \tag{4.56}$$

and the bandwidth constraints of a DOb are satisfied if

$$\frac{D_{env}}{J_m} < (2 + \eta) \xi k \sqrt{\frac{K_{env}}{J_m}} \leq \frac{g_v}{2} + \frac{D_{env}}{J_m}. \tag{4.57}$$

However, it is not an easy task to design an adaptive RFOb when environmental impedance is modeled by using damping and stiffness. To overcome this challenging issue, a simple and effective design method is proposed as follows:

Let us consider the relation between k and η by using eq. (4.55)

$$\eta = \frac{1 - k^2}{2\xi^2 (1 - \psi k) k^2}. \tag{4.58}$$

Equation (4.58) shows that η is zero and infinite when k is equal to one and $\frac{1}{\psi}$, respectively. Therefore, k should be chosen close to one when η is desired to be small enough to suppress low damping poles' effects. Hence, the constraints on ξ are derived approximately as follows:

$$\xi^- < \xi \leq \xi^+, \tag{4.59}$$

where $\xi^- = \frac{\frac{D_{env}}{J_m}}{2\sqrt{\frac{K_{env}}{J_m}}}$; and $\xi^+ = \frac{\frac{g_v}{2}+\frac{D_{env}}{J_m}}{2\sqrt{\frac{K_{env}}{J_m}}}$.

If $\xi^+ < 1$, then the DOb constraints, i.e., $\xi^- < \xi \leq \xi^+$ and $\eta < 1$ should be satisfied. However, if $\xi^+ \geq 1$, then only the DOb constraints should be satisfied. Therefore, two different solutions should be considered to design an adaptive RFOb.

Consequently, the adaptive robust force control system is designed as follows:

(1) The constraints on ξ are determined by using eq. (4.59).

(a) If $\xi^+ < 1$, then

i. Chose ξ in the given interval, and $\eta < 1$

ii. Solve k by using eq. (4.59)

$$2\eta\xi^2\psi k^3 - (1 + 2\eta\xi^2)k^2 + 1 = 0, \tag{4.60}$$

iii. Chose the solution of k which is close to 1.

(b) If $\xi^+ \geq 1$, then

i. Chose $\xi = 1$

ii. Solve k by using eq. (4.59)

$$\begin{aligned} 4\xi^2\psi k^3 + (1 - 4\xi^2 - 2\xi\psi\varrho)k^2 + 2\xi\varrho k - 1 \geq 0, \\ 4\xi^2\psi k^3 + (1 - 4\xi^2 - 2\xi\psi\delta)k^2 + 2\xi\delta k - 1 < 0 \end{aligned} \tag{4.61}$$

where $\varrho = \frac{\frac{g_v}{2}+\frac{D_{env}}{J_m}}{\sqrt{\frac{K_{env}}{J_m}}}$; and $\delta = \frac{\frac{D_{env}}{J_m}}{\sqrt{\frac{K_{env}}{J_m}}}$.

iii. Chose the real and positive solution of k.

(2) w_n is obtained by using $w_n = k\sqrt{\frac{K_{env}}{J_m}}$.

(3) $p, \alpha g$, and C_f are obtained by using eq. (4.51),eq. (4.52) and eq. (4.53), respectively.

The solution of the cubic equations should satisfy positive and real k values. It can be shown by using the *Property* as follows:

Property: Let us consider a cubic polynomial and functions by using

$$\begin{aligned} & a_3x^3 + a_2x^2 + a_1x + a_0 = 0, \\ & \Delta = 18a_3a_2a_1a_0 - 4a_3^2a_0 + a_2^2a_1^2 - 4a_3a_1^3 - 27a_3^2a_0^2, \\ & \Delta_0 = a_2^2 - 3a_3a_1, \\ & \Delta_1 = 2a_2^3 - 9a_3a_2a_1 + 27a_3^2a_0, \end{aligned} \tag{4.62}$$

Then,

i If $\Delta \geq 0$, then the polynomial has three real roots.

ii If $\Delta < 0$, then the polynomial has imaginary roots.

The roots of the polynomial are as follows:

$$\begin{aligned} x_1 &= -\frac{1}{3a_3}\left(a_2 + \Gamma + \frac{\Delta_0}{\Gamma}\right), \\ x_{2,3} &= -\frac{1}{3a_3}\left(a_2 + \frac{-1 \pm i\sqrt{3}}{2}\Gamma + \frac{\Delta_0}{\frac{-1\pm i\sqrt{3}}{2}\Gamma}\right), \end{aligned} \tag{4.63}$$

where $\Gamma = \sqrt[3]{\frac{\Delta_1 + \sqrt{\Delta_1^2 - 4\Delta_0^3}}{2}}$.

Let us first assume that $\xi^+ < 1$. Equation (4.60) should be solved when $\eta < 1$. It can be easily checked that the polynomial has two positive real or imaginary and a negative real roots. To obtain a positive real k, all roots should be real. By using *Property*, it can be shown that all roots are real if the following inequality is satisfied.

$$8\xi^6\eta^3 - (27\psi^2 - 12)\xi^4\eta^2 + 6\xi^2\eta + 1 \geq 0, \tag{4.64}$$

By using *Property*, it can be easily shown that eq. (4.64) is satisfied if the following conditions hold.

$$
\begin{aligned}
&if \psi \leq 1, then\, \eta > 0, \\
&if \psi > 1, then\, 0 < \eta \leq \frac{\lambda_2}{\xi^2},\ or\, \eta \geq \frac{\lambda_3}{\xi^2},
\end{aligned} \tag{4.65}
$$

where $\lambda_1 < \lambda_2 < \lambda_3$ are the roots of the polynomial that is given in eq. (4.64). Consequently, the roots of the polynomial are obtained by using eq. (4.63).

Now, let us assume that $\xi^+ > 1$. η can be chosen freely, and only the bandwidth constraints of DOb should be considered. It can be easily checked that the polynomials given in eq. (4.61) have one positive real and two negative real or imaginary roots when the coefficients of k^2 are positive, and three positive roots when the coefficients of k^2 are negative. Therefore, the real positive solutions of the cubic polynomials can be obtained.

4.5.1 Online Parameter Identification

To design an adaptive RFOb, environmental impedance and plant uncertainties should be identified. An on-line parameter identification algorithm is proposed as follows:

The dynamic equation of a DOb based robust motion control system is written by using Fig. 4-1 as follows:

$$
\left(\frac{J_{mn}}{K_{\tau n}} \ddot{q}_m^{des} + \frac{\hat{\tau}_m^{dis}}{K_{\tau n}} K_\tau \right) = J_m \ddot{q}_m + \tau_m^{frc} + \tau_m^{load}, \tag{4.66}
$$

where $\tau_m^{load} = D_{env}(\dot{q}_m - \dot{q}_{env}) + K_{env}(q_m - q_{env})$. For the sake of simplicity, let us use the static model of the friction. However, more complex friction models, such as LuGre, can be used similarly [89]. The static model of friction is as follows:

$$
\tau_m^{frc} = k_{vsc}\dot{q}_m + k_{clmb}\varsigma(\dot{q}_m), \tag{4.67}
$$

where k_{vsc} and k_{clmb} denote viscous and coulomb friction coefficients, respectively; and $\varsigma(\dot{q}_m)$ denotes the approximation of the coulomb friction model [90].

J_m, k_{vsc}, k_{clmb}, D_{env}, and K_{env} should be estimated to design an adaptive RFOb. Because external load is estimated by using an RFOb, the plant parameters, i.e., J_m, k_{vsc} and k_{clmb}, and environmental impedance, i. e., D_{env}, and K_{env}, can be identified during non-contact and contact motions, separately.

Let us first consider non-contact motion to identify plant parameters and re-write eq. (4.66) in vector form as follows:

$$u_{nc} = \boldsymbol{\rho_{nc}}^T \boldsymbol{\delta_n c}, \tag{4.68}$$

where $u_{nc} = J_{mn}\ddot{q}_m^{des} + \hat{\tau}_m^{dis}$; $\boldsymbol{\rho}_{nc} = \begin{bmatrix} \ddot{q}_m & \dot{q}_m & \varsigma(\dot{q}_m) & 1 \end{bmatrix}^T$; and $\boldsymbol{\delta}_{nc} = \begin{bmatrix} J_m & k_{vsc} & k_{clmb} & \hat{\tau}_m^d \end{bmatrix}$.

Let us assume that unknown parameters are bounded by a convex set that is defined by $\forall \boldsymbol{\delta}_{nc}(i) \in \Xi_{nc} : \boldsymbol{\delta}_{nc}^{min}(i) \leq \boldsymbol{\delta}_{nc}(i) \leq \boldsymbol{\delta}_{nc}^{max}(i), i = 1, 2, 3, 4$.

A recursive least mean square error (RLMSE) algorithm is used to identify the plant parameters as follows:

$$\begin{aligned}
\boldsymbol{K}_{nc}(t) &= \boldsymbol{\Gamma}_{nc}(t-1)\boldsymbol{\rho}_{nc}(t)\left(\mu_{nc} + \boldsymbol{\rho}_{nc}^T(t)\boldsymbol{\Gamma}_{nc}(t-1)\boldsymbol{\rho}_{nc}(t)\right)^{-1}, \\
\boldsymbol{\delta}_{nc}(t) &= \boldsymbol{\delta}_{nc}(t-1) + Prj\left\{\boldsymbol{K}_{nc}(t)\left(u_{nc}(t) - \boldsymbol{\rho}_{nc}^T(t)\boldsymbol{\delta}_{nc}(t-1)\right)\right\}, \\
\boldsymbol{\Gamma}_{nc}(t) &= \frac{1}{\mu_{nc}}\left(\boldsymbol{I_4} - \boldsymbol{K}_{nc}(t)\boldsymbol{\rho}_{nc}^T(t)\right)\boldsymbol{\Gamma}_{nc}(t-1),
\end{aligned} \tag{4.69}$$

where μ_{nc} denotes forgetting factor; $\bullet_{nc}$ denotes the parameters in non-contact motion; and

$$Prj\left\{\bullet_{nc}(i)\right\} = \begin{cases} 0, & \boldsymbol{\delta}_{nc}(i) \leq \boldsymbol{\delta}_{nc}^{min}(i) \\ 0, & \boldsymbol{\delta}_{nc}(i) \geq \boldsymbol{\delta}_{nc}^{max}(i) \\ \bullet_{nc}(i) & otherwise \end{cases} \tag{4.70}$$

The projection function, $Prj\left\{\bullet_{nc}(i)\right\}, i = 1, 2, 3, 4$, provides that the plant parameters are updated only in non-contact motion and do not burst.

To estimate environmental impedance, eq. (4.66) is rewritten in vector form as follows:

$$u_c = \boldsymbol{\rho_c}^T \boldsymbol{\delta_c}, \tag{4.71}$$

where $u_c = \hat{\tau}_m^{load}$; $\boldsymbol{\rho}_c = \begin{bmatrix} \dot{q}_m & q_m & 1 \end{bmatrix}^T$; and $\boldsymbol{\delta}_c = \begin{bmatrix} D_{env} & K_{env} & \hat{\tau}_m^{load} \end{bmatrix}^T$.

The environmental impedance is identified by using an RLMSE algorithm as follows:

$$\begin{aligned}
\boldsymbol{K}_c(t) &= \boldsymbol{\Gamma}_c(t-1)\boldsymbol{\rho}_c(t)\left(\mu_c + \boldsymbol{\rho}_c^T(t)\boldsymbol{\Gamma}_c(t-1)\boldsymbol{\rho}_c(t)\right)^{-1}, \\
\boldsymbol{\delta}_c(t) &= \boldsymbol{\delta}_c(t-1) + Prj\left\{\boldsymbol{K}_c(t)\left(u_c(t) - \boldsymbol{\rho}_c^T(t)\boldsymbol{\delta}_c(t-1)\right)\right\}, \\
\boldsymbol{\Gamma}_c(t) &= \frac{1}{\mu_c}\left(\boldsymbol{I_3} - \boldsymbol{K}_c(t)\boldsymbol{\rho}_c^T(t)\right)\boldsymbol{\Gamma}_c(t-1),
\end{aligned} \tag{4.72}$$

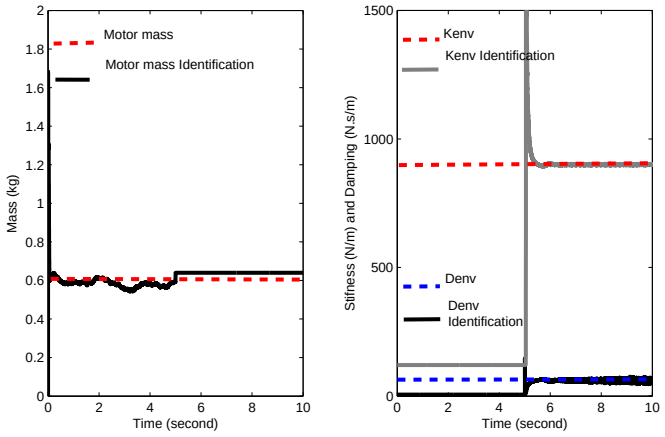

Fig. 4-28: Performance of the proposed identification algorithm.

where μ_c denotes forgetting factor; $\bullet_c$ denotes the parameters in contact motion; and

$$Prj\{\bullet_c(i)\} = \begin{cases} 0, & \boldsymbol{\delta}_c(i) \leq \boldsymbol{\delta}_c^{min}(i) \\ 0, & \boldsymbol{\delta}_c(i) \geq \boldsymbol{\delta}_c^{max}(i) \\ \bullet_c(i) & otherwise \end{cases} \tag{4.73}$$

It is obvious that the uncertainty range of environmental impedance is larger than the plant parameters' one. The projection function, $Prj\{\bullet_c(i)\}$, provides that the estimation of environmental impedance is conducted only in contact motion. In the proposed RLMSE algorithm, the projection functions work discontinuously, and the parameters are updated conditionally [91–93].

Fig. 4-28 shows the performance of the proposed RLMSE algorithm. During non-contact motion, the inertia of a linear motor is identified. To achieve contact motion, a known environmental impedance is designed by using zero position control of a linear DC motor, in which $K_P = 900$ and $K_D = 60$ are the parameters of the PD position controller. Fig. 4-28 indicates that the plant parameters and environmental impedance can be identified by using the proposed algorithm. It is obvious that the convergence rates of the parameters influence the performance of the adaptive RFOb based robust force control system. Besides, impact forces cause high identification errors initially in the environmental impedance identification. Therefore, the parameters of the adaptive RFOb should be updated by considering the drawbacks of the proposed on-line RLMSE algorithm, i.e., the parameters should be updated when they converge. Fig. 4-29 shows the block diagram of the proposed adaptive RFOb based robust force control system.

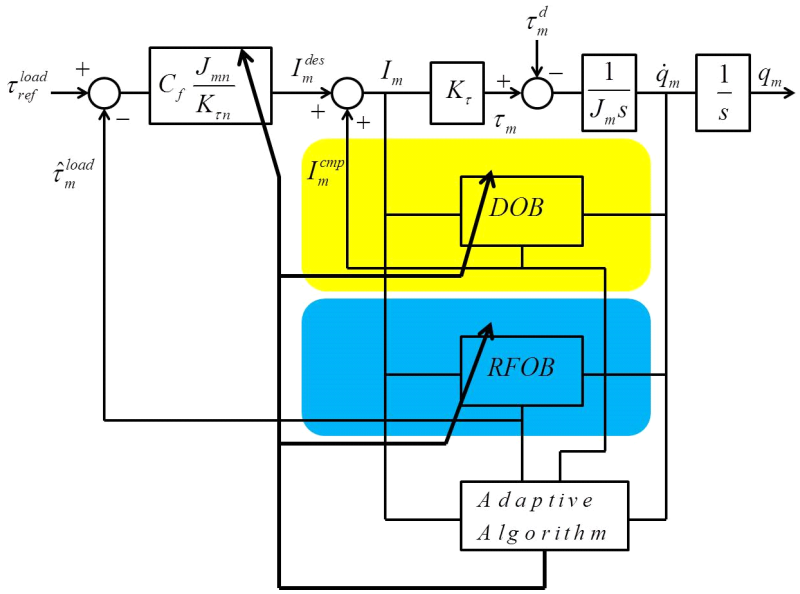

Fig. 4-29: Block diagram of the proposed adaptive RFOb based robust force control system.

Table 4.5: Simulation Parameters of the adaptive RFOb design.

Variables	Definition of variables	Value
J_{mn}	Nominal mass	0.025 kg
$K_{\tau n}$	Nominal torque coefficient	0.5 N/A
g_v	Cut-off frequency of velocity measurement	1000 rad/s.

4.5.2 Simulations and Experiment

In this section, simulation and experimental results are given for adaptive RFOb based explicit force control systems. Simulation parameters are shown in Table 4.5.

Fig. 4-30, Fig. 4-31, and Fig. 4-32 show the tunings of the design parameters by using the proposed adaptive algorithms. It is assumed that $\alpha = 1$, so the maximum achievable bandwidth of DOb is 500 rad/s. to satisfy a good robustness. As shown in the figures, the maximum bandwidth of DOb can be achieved if damping environment is considered. However, if stiff environment is considered, then the bandwidth of DOb should be limited to improve the stability and performance when the environmental stiffness is low. The performance and robustness of the force control system can be improved if the

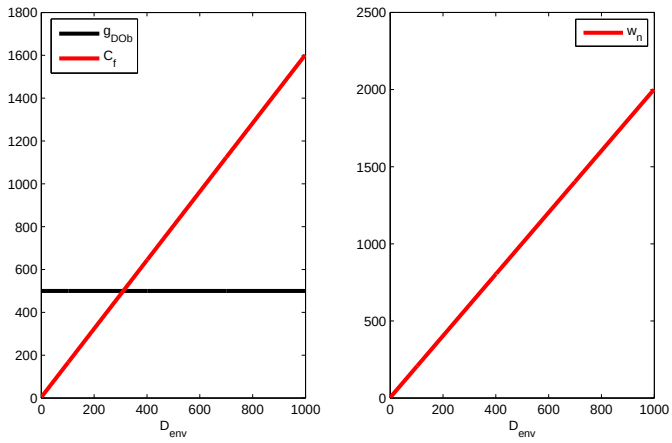

Fig. 4-30: Parameter tuning of adaptive RFOb when $K_{env} = 0$ and $D_{env} \neq 0$.

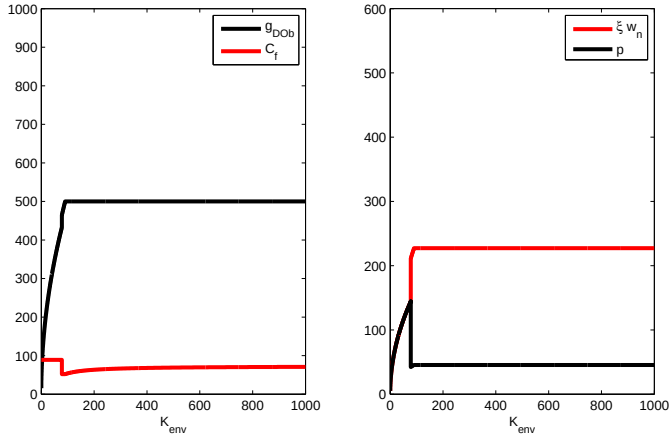

Fig. 4-31: Parameter tuning of adaptive RFOb when $K_{env} \neq 0$ and $D_{env} = 0$.

environmental stiffness is considered as damping and stiffness. In this case, the bandwidth of a DOb can be increased even if the environmental stiffness is low. Although there is a small pole near the origin, the performance of the force control system is not affected due to the zero near the pole.

An XZ-table mechanism, which is shown in Fig. 4-33, is carried out to show the validity of the proposals. The specifications of the experimental setup are shown in Table 4.6. The sampling time is 0.1 ms. KYOWA LUR-A-50NSA1 force sensor is used to verify the performance of RFOb.

Let us start by considering how identification of plant parameters improves the performance of the robust force control system. In the Z (vertical) direction of table mechanism, force control is implemented

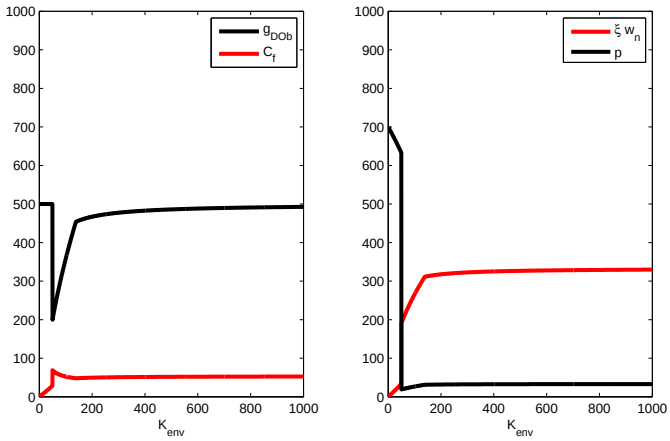

Fig. 4-32: Parameter tuning of adaptive RFOb when $K_{env} \neq 0$ and $D_{env} = 0.25$.

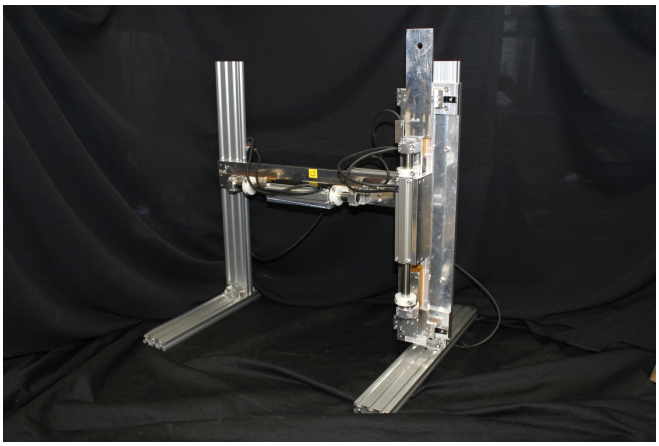

Fig. 4-33: An XZ table mechanism.

Table 4.6: Experiment Parameters of the adaptive RFOb design.

Variables	Definition of variables	Value
J_{m1}	Nominal mass	0.81 kg
J_{m2}	Nominal mass	3.2 kg
$K_{\tau n}$	Nominal torque coefficient	33.0 N/A
g_v	Cut-off frequency of velocity measurement	1000 rad/s.
K_P	Proportional gain of position control	1200
K_D	Derivative gain of position control	90

between 0 and 5, and 10 and 15 seconds; position control is implemented between 5 and 10 seconds, and the uncertain plant parameters, i.e., motor mass and friction, are identified by considering gravity. Fig. 4-34 shows that the position and force control goals are achieved. The performance of the RFOb is improved between 10 and 15 seconds by identifying the plant parameters during non-contact motion. A soft environment (sponge) is used during force control. The bandwidths of DOb and RFOb are set to 500 rad/s., and $C_f = 5$.

Let us now consider how identification of plant parameters improves the stability of the robust force control system. Force control is implemented in the X (horizontal) direction by using different nominal and identified mass values in the design of DOb and RFOb, respectively. The open loop gain is set to a fixed value by using $C_f\alpha = 2.5$. Fig. 4-35- Fig. 4-38 show the stability of the robust force control system. Fig. 4-35 and Fig. 4-36 show that as the nominal mass of the plant is increased in the design of DOb, the stability of the robust force control system is improved. However, as shown in eq. (4.7), the nominal mass cannot be increased freely due to the robustness constraint. Fig. 4-37 and Fig. 4-38 show that the value of the identified mass that is used in the design of RFOb changes the stability of the robust force control system, significantly. An RFOb should be designed by using $\widehat{J}_m \leq J_m$, i.e., $\alpha \leq \beta$ to improve the stability of the force control system. A hard environment (aluminum box) is used in the experiment. Since the transient between non-contact and contact motions is not treated, the wide impact forces are occurred in force control. It is obvious that the impact force can be suppressed by controlling the approaching velocity between non-contact and contact motions.

So far, identification of environmental impedance has not been considered. Finally, let us consider how identification of environmental impedance improves the robust force control system. The plant parameters are identified in free motion, and DOb and RFOb are designed by using $\alpha = 2$ and $\beta = 2$ to improve the stability. The force control response is shown in Fig. 4-36 when the adaptive algorithm is

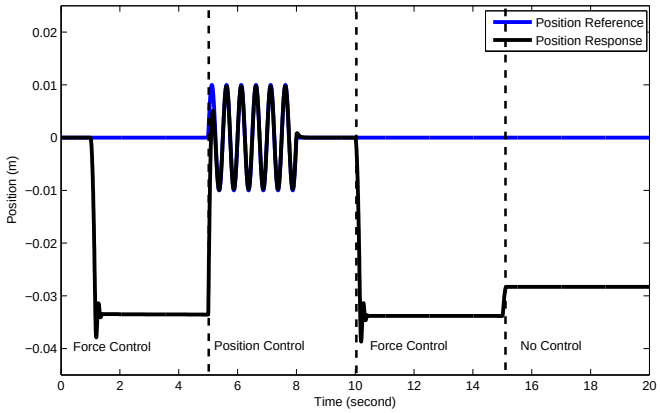

(a) Positin control response.

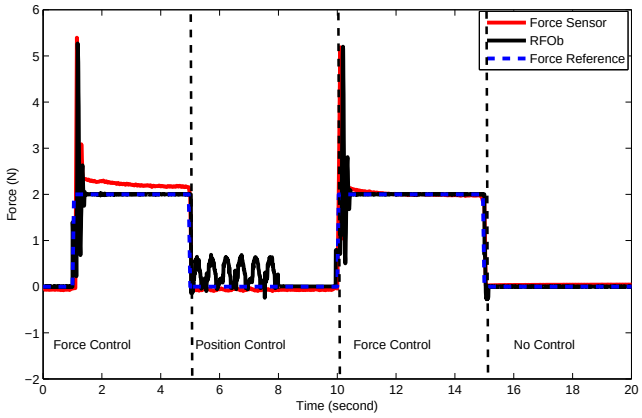

(b) Force control response.

Fig. 4-34: Position and force control responses in the Z-direction.

not implemented. The bandwidths of DOb and RFOb and the force control gain are tuned by using the adaptive algorithm with on-line and off-line parameter identification methods. Fig. 4-39 shows the force control responses when the adaptive algorithm is implemented. It is clear from Fig. 4-39(a) and Fig. 4-39(b) that the adaptive algorithm improves the force control response. However, as shown in Fig. 4-39(a), the adaptive algorithm with on-line identification is influenced by the dynamics of identification process during the transition between non-contact and contact motions, which is shown in Fig. 4-28. In the adaptive algorithm, the control parameters are not updated during the transition, so oscillations

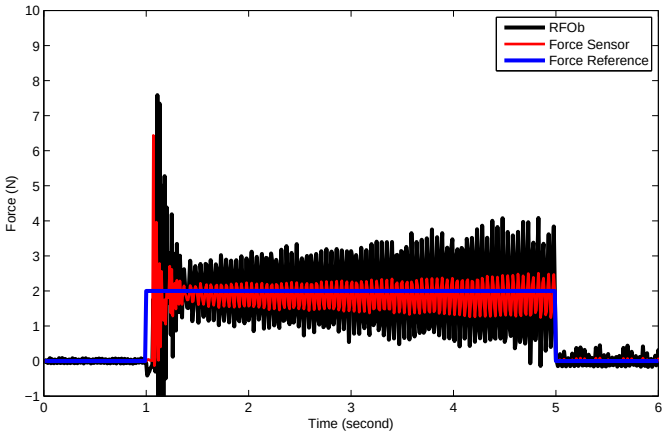

Fig. 4-35: Stability of the foce control system: $\alpha = \beta = 0.5$, $g_{DOb} = g_{RFOb} = 500$ rad/s., and $C_f = 5$.

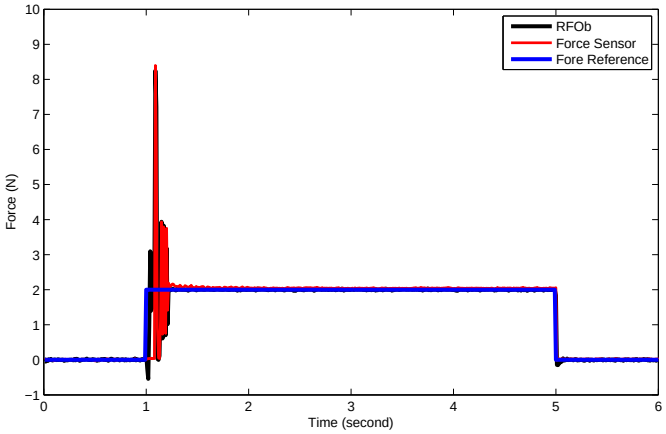

Fig. 4-36: Stability of the foce control system: $\alpha = \beta = 2$, $g_{DOb} = g_{RFOb} = 500$ rad/s., and $C_f = 1.25$.

cannot be suppressed precisely when on-line parameter identification is used. However, as shown in the Fig. 4-39(b), if environmental impedance is known a priori, which is impractical in many cases, then the oscillations can be suppressed precisely by using the proposed adaptive algorithm.

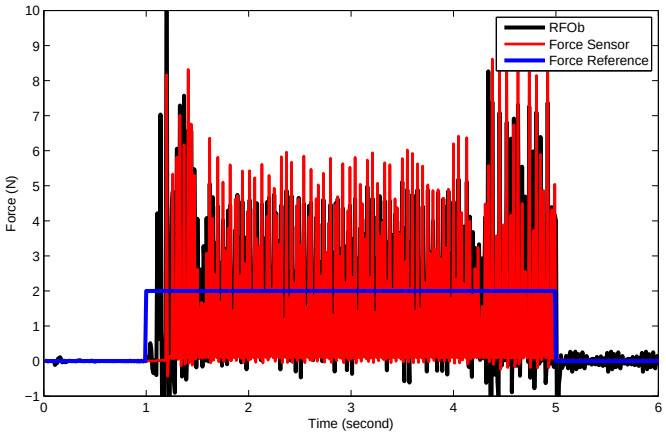

Fig. 4-37: Stability of the foce control system: $\alpha = 4$, $\beta = 2$, $g_{DOb} = g_{RFOb} = 500\,\text{rad/s.}$, and $C_f = 0.625$.

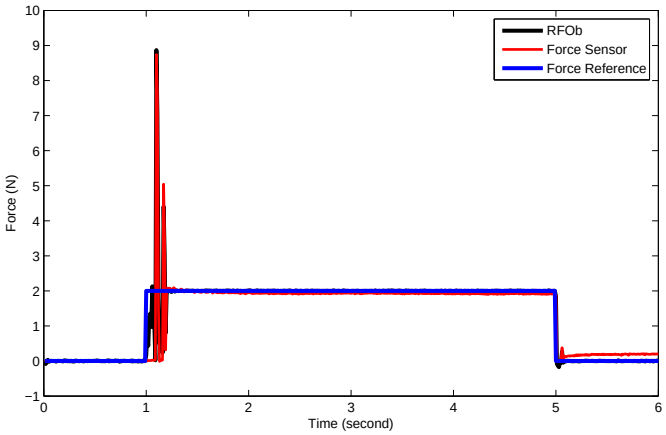

Fig. 4-38: Stability of the foce control system: $\alpha = 2$, $\beta = 4$, $g_{DOb} = 500\,\text{rad/s.}$, $g_{RFOb} = 1000\,\text{rad/s.}$, and $C_f = 1.25$.

4.6 Summary

In this chapter, novel analysis and design methods are proposed for DOb based motion control systems. Firstly, inner-loop, in which robustness of motion control systems is achieved, is considered, and a new robustness constraint is proposed. It is shown that the bandwidth of DOb and nominal inertia are bounded by the bandwidth of velocity measurement in the design of DOb. Secondly, the stability and performance analysis are proposed for the robust position and force control systems.

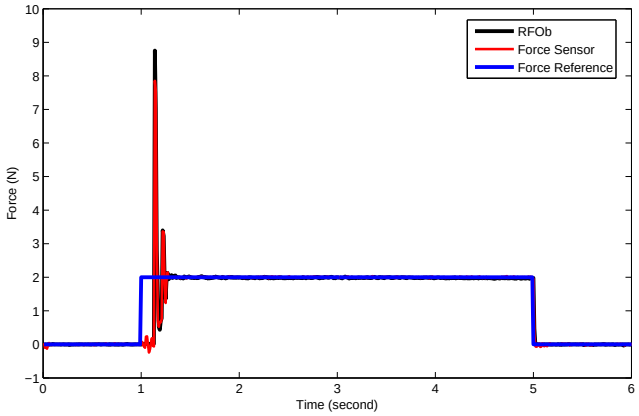

(a) Adaptive algorithm with on-line parameter estimation .

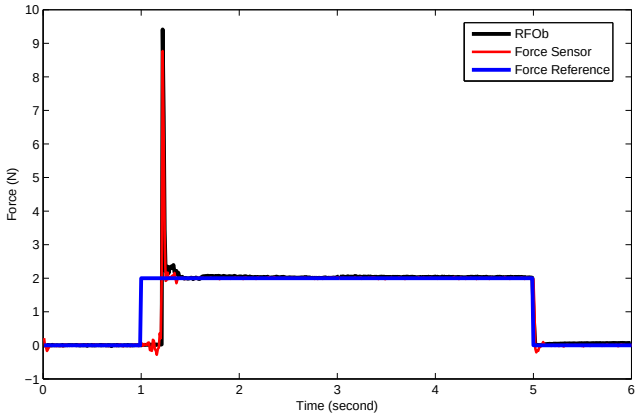

(b) Adaptive algorithm with off-line parameter estimation .

Fig. 4-39: Force control responses in X-direction when the adaptive algorithm is used.

In the analysis of DOb based robust position control systems, it is shown that the stability is improved as the nominal inertia is increased in the design of DOb. However, the nominal inertia is bounded by the robustness constraint of DOb. Therefore, there is a trade-off between the robustness and stability in the DOb based robust position control systems. Although, in general, it is assumed that the robustness and stability are adjusted in the inner and outer loops independently, it is not true. The robustness of the position control system is improved by the outer loop performance controller and good robustness may be achieved even if the proposed design constraint is not used in the position control system. However,

it should be kept in mind that the inner-loop suffers from noise and disturbances at high frequencies if the proposed design constraint is not satisfied.

Robust force control systems are analyzed and it is shown that not only the performance, but also the stability improves significantly if the robustness of force control systems is achieved, i.e., uncertainties and the natural reactive feed-back loop that occurs in contact motion is canceled. A DOb provides a very useful control tool to eliminate the natural feed-back loop in a limited bandwidth and improve the stability of contact motion. However, the design constraints of DOb should be considered in the analysis of the robust force control systems. Besides, environmental impedance estimation is crucial and changes the stability and performance of the explicit force control systems significantly. Two different environmental impedance estimation methods, namely force sensor and RFOb, are considered, and their advantages and disadvantages are discussed in detail. It is shown that the stability and performance of the explicit force control systems can be improved by using RFOb. Besides that force control application can be realized without using a sensor. Therefore, I believe that RFOb is a very useful motion control tool for several applications such as surgical robotics. However, as shown in Chapter 4, RFOb has a model based control structure, and not only the performance, but also the stability deteriorates significantly by the imperfect identification of design parameters. A novel stability analysis is proposed for RFOb based robust force control systems. To improve the stability of contact motion, the identified inertia should be decreased in the design of RFOb. If acceleration is negligible during force control, then high performance force control responses can be achieved. The proposed analysis and design methods are very practical and can be easily implemented into several sensorless force control problems. Although force sensors have several disadvantages, such as increasing cost, against RFOb, they are not sensitive to system uncertainties. The results are discussed in detail, and simulation and experimental results are given to show the validity in this chapter.

Chapter 5

Robust Control of Robot Manipulators via Disturbance Observer

---

5.1 Introduction

Conventionally, robot manipulators are controlled by using model based control methods such as feedback linearization [84, 88]. However, the conventional design methods are very sensitive to modeling errors; not only the performance, but also the stability of robot control systems may deteriorate due to the modeling errors in the design of the conventional controllers [94]. Model-free control methods have been proposed by using intelligent based control methods; however, real time synchronism deteriorates due to high computational amount [95, 96]. It is a well known fact that robust control of robot manipulators is crucial to achieve high performance robot control systems [97]. In the literature, several robust control methods have been proposed to improve the performance of robot manipulators [98].

This chapter analyzes the robust control problem of robot manipulators by using DOb. In Chapter 4, robust control problem of motion control systems is analyzed in the joint space, and novel analysis and design methods are proposed. In the conventional analysis of the DOb based robust motion control problem of robot manipulators, joint space analyses are extended into multi-degrees-of-freedom systems directly to simplify the problem [99–101]. However, robot manipulators have highly non-linear dynamic characteristics so oversimplified linear analyses cannot provide a deep insight into the stability of DOb based robust motion control problem of robot manipulators. A decade ago, a new nonlinear DOb is proposed for a two link planar robot manipulator by Chen et. al in [102]. Recently, a general solution is derived for non-linear DOb based robot manipulators in [103]. In these papers, the authors consider

only the observation of un-modeled / un-known disturbance estimation and provide a stability analysis for the non-linear disturbance observer. However, experiments of DOb based robust motion control systems show that the stability of a DOb based motion control system cannot be guaranteed even if the disturbance estimation is stable, i.e., disturbance canceling in the inner-loop may cause instability if the design parameters of DOb are not tuned adequately [70]. A decentralized adaptive robust controller is proposed by using DOb in [104]. It is assumed that DOb guarantees the robustness of robot manipulators within its bandwidth; however, the design parameters of DOb are not discussed in this paper. Bickel and Tomizuka showed that DOb based robust position controller is equal to the passivity based one and claimed that the stability of the DOb based robot control systems can be achieved by using the passivity theorem [105]. However, they also have not considered the design parameters of DOb in their analysis. Therefore, the stability of the DOb based robust position control problem of robot manipulators have not been clarified yet.

In this chapter, a new nonlinear stability analysis method is proposed for DOb based robust position control problem of robot manipulators by using the equivalence of DOb and passivity based controller design methods. The design parameters of DOb, i.e., the nominal inertia matrix and the bandwidth of DOb, are considered in detail, and a new practical non-linear stability analysis method is proposed. It is shown that a DOb based robust position control system is uniformly ultimately bounded when it is applied into trajectory tracking control problem. The error bound is determined by the bandwidth of DOb and nominal inertia matrix; as the bandwidth of DOb and/or nominal inertia matrix are increased, the bound of error decreases. If the robust position control method is applied into a regulator problem, i.e., point to point motion control problem, then asymptotic stability is achieved. It is shown that the stability of the robust position control system is improved by increasing the nominal inertia matrix in the design of DOb. Although the robust position control system is not sensitive to inertia matrix variations, using very small nominal inertia matrix destabilizes the robust position control systems. This dissertation proposes that a DOb based robust motion control system should be designed by using $\mathbf{M_n}(\mathbf{q}) \geq \mathbf{M}(\mathbf{q})$, in which $\mathbf{M_n}(\mathbf{q})$ and $\mathbf{M}(\mathbf{q})$, respectively, represent nominal and uncertain inertia matrices, to improve the stability.

The rest of the chapter is organized as follows. In section 5.2, some preliminaries are given for the dynamic properties of robot manipulators. In section 5.3, DOb and ABC system are explained for robot manipulators, briefly. In section 5.4, a new non-linear stability analysis method is proposed for DOb based robust position control systems. In section 5.5, simulation studies are given. This chapter ends

with summaries given in section 5.6.

5.2 Preliminaries

The dynamic model of a robot manipulator with n-degrees-of-freedom is derived by using Euler-Lagrange formulation and expressed in joint space as follows:

$$\mathbf{M}(\mathbf{q})\ddot{\mathbf{q}} + \mathbf{C}(\mathbf{q}, \dot{\mathbf{q}})\dot{\mathbf{q}} + \mathbf{g}(\mathbf{q}) = \tau - \tau^{\mathbf{frc}} - \tau^{\mathbf{load}}, \tag{5.1}$$

where $\mathbf{M}(\mathbf{q}) \in \mathrm{R}^{nxn}$ is the inertia matrix; $\mathbf{C}(\mathbf{q}, \dot{\mathbf{q}})\dot{\mathbf{q}} \in \mathrm{R}^n$ is the vector of Coriolis and centrifugal torques; $\mathbf{g}(\mathbf{q}) \in \mathrm{R}^n$ is the vector of the gravitational torques that is obtained as the gradient of the robot potential energy due to gravity; $\tau \in \mathrm{R}^n$ is the vector of generalized torques in joint space; $\tau^{\mathbf{frc}}$ and $\tau^{\mathbf{load}} \in \mathrm{R}^n$ are the vectors of friction and load torques, respectively; $\mathbf{q}$, $\dot{\mathbf{q}}$ and $\ddot{\mathbf{q}} \in \mathrm{R}^n$ are the vectors of angle, velocity, and acceleration of the robot manipulator in joint space, respectively.

It is assumed that the robot manipulator under consideration has only revolute joints and reference trajectories, $\mathbf{q}^{\mathbf{ref}}(t)$, $\dot{\mathbf{q}}^{\mathbf{ref}}(t)$, and $\ddot{\mathbf{q}}^{\mathbf{ref}}(t)$, are continuous and bounded. The equation of motion given in eq. (5.1) has the following important properties that will be used in the stability analysis and controller design [94, 106].

Property 1: $\mathbf{M}(\mathbf{q})$ is a positive definite and symmetric matrix that satisfies

$$\beta_{\mathbf{M}}^{min}\mathbf{I} \leq \underline{\sigma}(\mathbf{M}(\mathbf{q}))\mathbf{I} \leq \mathbf{M}(\mathbf{q}) \leq \overline{\sigma}(\mathbf{M}(\mathbf{q}))\mathbf{I} \leq \beta_{\mathbf{M}}^{max}\mathbf{I}, \tag{5.2}$$

where $\underline{\sigma}(\cdot)$ and $\overline{\sigma}(\cdot)$ represent minimum and maximum eigenvalues of $(\cdot)$, respectively; $\beta_{\mathbf{M}}^{min}$ and $\beta_{\mathbf{M}}^{max}$ represent positive real constants.

Property 2:

$$\|\mathbf{C}(\mathbf{q}, \dot{\mathbf{q}})\dot{\mathbf{q}}^*\| \leq \beta_{\mathbf{C}} \|\dot{\mathbf{q}}\| \|\dot{\mathbf{q}}^*\|, \tag{5.3}$$

where $\beta_{\mathbf{C}}$ represents a positive real constant.

Property 3:

$$\|\mathbf{g}(\mathbf{q})\| \leq \beta_{\mathbf{g}}, \tag{5.4}$$

where $\beta_{\mathbf{g}}$ represents a positive real constant.

Property 4:

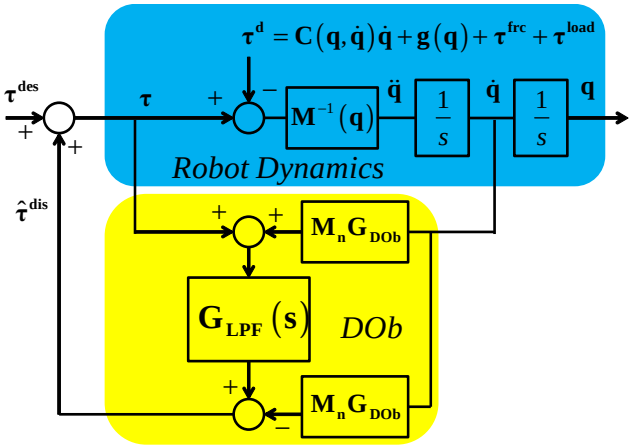

Fig. 5-1: Block diagram of a DOb when multi-degrees-of-freedom robot is used.

$$\mathbf{x}^T \left(\frac{d}{dt}\mathbf{M}(\mathbf{q}) - 2\mathbf{C}(\mathbf{q}, \dot{\mathbf{q}}) \right) \mathbf{x} = 0, \tag{5.5}$$

where $\mathbf{x} \in \mathrm{R}^n$ represents an n-dimensional vector, and $\frac{d}{dt}\mathbf{M}(\mathbf{q}) - 2\mathbf{C}(\mathbf{q}, \dot{\mathbf{q}})$ is a skew-symmetric matrix.

5.3 Acceleration Based Robust Position Control of Robot Manipulators

In this section DOb and acceleration based control systems will be explained for robot manipulators.

5.3.1 Disturbance observer design in multi-degrees-of-freedom systems

A block diagram of a DOb based robust motion control system is shown in Fig. 5-1 when the general dynamic model of robot manipulator given in eq. (5.1) is used. In this figure, $\mathbf{M}(\mathbf{q})$ and $\mathbf{M_n}(\mathbf{q}) \in \mathrm{R}^{nxn}$ represent uncertain and nominal inertia matrices, respectively; τ and $\tau^{\mathbf{des}}$ represent robot and desired joint torques, respectively; $\mathbf{G_{DOb}} = Diag\left(\left[g^1_{DOb}, g^2_{DOb}, ..., g^n_{DOb}\right]\right) \in \mathrm{R}^{nxn}$ in which $Diag\,(\bullet)$ is a diagonal matrix of vector $\bullet$ and g^i_{DOb} represents the bandwidth of DOb in the ith joint; $\mathbf{G_{LPF}}(s) = Diag\left(\left[\frac{g^1_{DOb}}{s+g^1_{DOb}}, \frac{g^2_{DOb}}{s+g^2_{DOb}}, ..., \frac{g^n_{DOb}}{s+g^n_{DOb}}\right]\right) \in \mathrm{R}^{nxn}$ represents the matrix of the LPF of DOb; $\tau^{\mathbf{d}} \in \mathrm{R}^n$ represents external disturbances; $\hat{\tau}^{\mathbf{dis}} \in \mathrm{R}^n$ represents the estimated disturbance; and $\mathbf{q}, \dot{\mathbf{q}}$, and $\ddot{\mathbf{q}} \in \mathrm{R}^n$ represent n-dimensional angle, velocity, and acceleration vectors, respectively.

The estimated disturbance,$\hat{\tau}^{\mathbf{dis}}$, includes not only external disturbances, but also the inertia variations. It is formalized as follows:

$$\hat{\tau}^{\mathbf{dis}} = \mathbf{G_{DOb}}(s)\tau^{\mathbf{dis}}, \tag{5.6}$$

where $\tau^{\mathbf{dis}} = (\mathbf{M_n} - \mathbf{M}(\mathbf{q}))\,\ddot{\mathbf{q}} + \tau^{\mathbf{d}}$; and $\tau^{\mathbf{d}} = \mathbf{C}(\mathbf{q}, \dot{\mathbf{q}})\dot{\mathbf{q}} + \mathbf{g}(\mathbf{q}) + \tau^{\mathbf{frc}} + \tau^{\mathbf{load}}$.

The dynamic equations of a DOb based robust motion control system are derived directly from Fig. 5-1 as follows:

$$\hat{\tau}^{\mathbf{dis}} = \mathbf{G_{DOb}}(s)(\hat{\tau}^{\mathbf{dis}} + \tau^{\mathbf{des}} - \mathbf{M_n}\ddot{\mathbf{q}}), \tag{5.7}$$

$$\hat{\tau}^{\mathbf{dis}} = \hat{\mathbf{G}}_{\mathbf{DOb}}(s)(\tau^{\mathbf{des}} - \mathbf{M_n}\ddot{\mathbf{q}}), \tag{5.8}$$

where $\hat{\mathbf{G}}_{\mathbf{DOb}}(s) = Diag\left(\left[\frac{g^1_{DOb}}{s}, \frac{g^2_{DOb}}{s}, ..., \frac{g^n_{DOb}}{s}\right]\right)$.

5.3.2 Acceleration based robust position control in multi-degrees-of-freedom systems

A block diagram of an acceleration based robust position control system is shown in Fig. 5-2 when the general dynamic model of robot manipulator given in eq. (5.1) is used. In this figure, $\mathbf{K_D}$ and $\mathbf{K_P} \in \mathrm{R}^{nxn}$ represent velocity and position gains of PD controller, respectively; $\ddot{\mathbf{q}}^{\mathbf{des}} \in \mathrm{R}^n$ represents desired acceleration; $\mathbf{q}^{\mathbf{ref}}$, $\dot{\mathbf{q}}^{\mathbf{ref}}$, and $\ddot{\mathbf{q}}^{\mathbf{ref}} \in \mathrm{R}^n$ represent reference vectors of angle, velocity, and acceleration, respectively. The other parameters are same as defined earlier.

As shown in Fig. 5-2, disturbances are estimated in the inner-loop by using a DOb, and the robustness of the position control system is achieved by feeding-back the estimated disturbances. The outer-loop acceleration controller is designed by considering the nominal inertia matrix, since DOb nominalizes the inner-loop.

There are four parameters, $\mathbf{G_{LPF}}(s)$, $\mathbf{M_n}, \mathbf{K_D}$, and $\mathbf{K_P}$, that should be tuned in the design of the robust acceleration based position control systems. It is a well-known fact that the higher the bandwidth of DOb is, the more the robustness improves. However, the bandwidth of DOb is limited by some practical constraints, such as noise and sampling time, as shown in Chapter 3 and Chapter 4. Therefore, in practice, the bandwidth of DOb is set as high as possible to improve the robustness of the position control systems. However, against the bandwidth of DOb, tuning the parameters of the nominal inertia matrix is not clear in the design of DOb. In the conventional design of DOb based motion control systems, a diagonal nominal inertia matrix is used and decentralized control structure is achieved by assuming that a DOb cancels disturbances precisely [99–101]. Thereby, the stability analysis is simplified and conducted

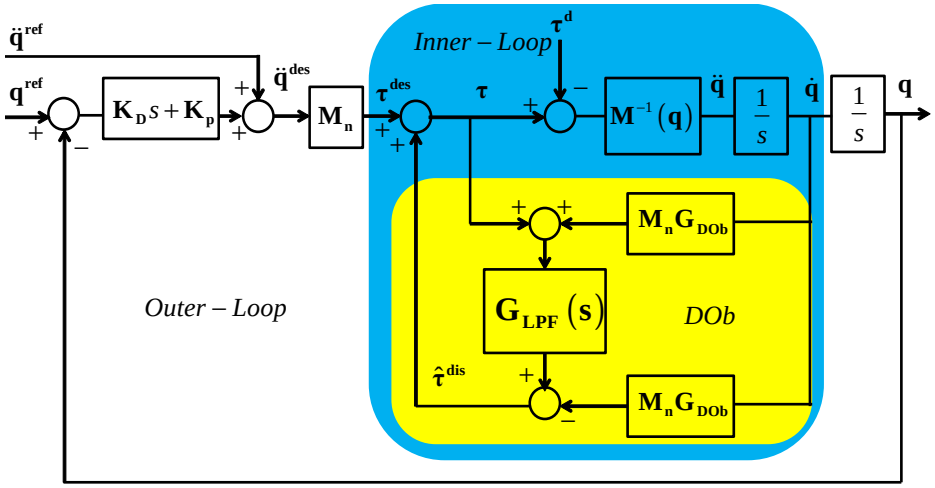

Fig. 5-2: Block diagram of a DOb based robust position control system when multi-degrees-of-freedom robot is used.

for each joint of robot manipulators by using linear models of servo systems. The oversimplified stability analysis shows that asymptotic stability can be achieved if nominal inertia is bounded by the design constraints given in [99]. However, in reality, it is not true, and oversimplified analyses are not sufficient to determine the stability of the robot manipulators. The parameters of the outer-loop controller, $\mathbf{K_D}$ and $\mathbf{K_P}$ are tuned directly by considering the nominal inertia matrix.

5.4 Stability Analysis of the Robust Position Control System

In this section, a new nonlinear stability analysis is proposed for the acceleration based robust position control problem of robot manipulators by using its passivity equivalence.

Let us assume that the bandwidths of DObs are same at each joints, i.e., $g_{DOb}^1 = g_{DOb}^2 = ... = g_{DOb}^n = g_{DOb}$. Let us also assume that the robot manipulator is not influenced by friction and external load torques, i.e., $\tau^{\mathbf{frc}} = \tau^{\mathbf{load}} = \mathbf{0}$. If the robot manipulator is controlled by using the robust ABC system, then the dynamic model of the robot manipulator is described as follows:

$$\mathbf{M}(\mathbf{q})\ddot{\mathbf{q}} + \mathbf{C}(\mathbf{q},\dot{\mathbf{q}})\dot{\mathbf{q}} + \mathbf{g}(\mathbf{q}) = \tau^{\mathbf{des}} + \hat{\tau}^{\mathbf{dis}}, \tag{5.9}$$

The vector of desired torque is derived from Fig. 5-2 as follows:

$$\tau^{\mathbf{des}} = \mathbf{M_n}\ddot{\mathbf{q}}^{\mathbf{des}}, \tag{5.10}$$

where $\ddot{\mathbf{q}}^{\mathbf{des}} = \ddot{\mathbf{q}}^{\mathbf{ref}} - \mathbf{K_D}(\dot{\mathbf{q}} - \dot{\mathbf{q}}^{\mathbf{ref}}) - \mathbf{K_P}(\mathbf{q} - \mathbf{q}^{\mathbf{ref}}) = \ddot{\mathbf{q}}^{\mathbf{ref}} - \mathbf{K_D}\dot{\mathbf{e}} - \mathbf{K_P}\mathbf{e}$, in which $\mathbf{e} = \mathbf{q} - \mathbf{q}^{\mathbf{ref}}$ represents the error of angle.

The vector of estimated disturbance is derived by using eq. (5.8) and eq. (5.10) as follows:

$$\hat{\tau}^{\mathbf{dis}} = g_{DOb}\mathbf{M_n}(\dot{\mathbf{q}}^{\mathbf{des}} - \mathbf{q}), \tag{5.11}$$

If eq. (5.10) and eq. (5.11) are applied into eq. (5.9), then

$$\mathbf{M}(\mathbf{q})\ddot{\mathbf{q}} + \mathbf{C}(\mathbf{q}, \dot{\mathbf{q}})\dot{\mathbf{q}} + \mathbf{g}(\mathbf{q}) = \mathbf{M_n}\ddot{\mathbf{q}}^{\mathbf{des}} + g_{DOb}\mathbf{M_n}(\dot{\mathbf{q}}^{\mathbf{des}} - \mathbf{q}), \tag{5.12}$$

Let us define an error dynamics by using $\mathbf{e_D} = \dot{\mathbf{q}} - \dot{\mathbf{q}}^{\mathbf{des}}$. Then, eq. (5.12) is re-written as follows:

$$\mathbf{M}(\mathbf{q})\dot{\mathbf{e}}_{\mathbf{D}} + \mathbf{C}(\mathbf{q}, \dot{\mathbf{q}})\mathbf{e_D} + g_{DOb}\mathbf{M_n}\mathbf{e_D} = -\mathbf{\Psi}, \tag{5.13}$$

where $\mathbf{\Psi} = \Delta\mathbf{M}(\mathbf{q})\ddot{\mathbf{q}}^{\mathbf{des}} + \mathbf{C}(\mathbf{q}, \dot{\mathbf{q}})\dot{\mathbf{q}}^{\mathbf{des}} + \mathbf{g}(\mathbf{q})$; $\mathbf{e_D} = \dot{\mathbf{e}} + \mathbf{K_D}\mathbf{e} + \mathbf{K_P}\int \mathbf{e}dt$ represents the error dynamics; $\mathbf{e} = \mathbf{q} - \mathbf{q}^{\mathbf{ref}}$ represents the error of angle; and $\Delta\mathbf{M}(\mathbf{q}) = \mathbf{M}(\mathbf{q}) - \mathbf{M_n}$.

Equation (5.13) shows that a DOb based robust position control system has same error dynamics as the passivity based control method. Therefore, the following general passivity theorem can be directly implemented into the DOb based robust position control systems.

Theorem 5.1: If the mapping $-\mathbf{e_D} \rightarrow \Psi$ is passive, i.e.,

$$\int_0^{t_f} \mathbf{e_D}(t)\mathbf{\Psi}(t)dt \geq -\phi, \tag{5.14}$$

for all t_f and for some $\phi \geq 0$, then $\mathbf{e_D} \in L_2^n \cap L_\infty^n, \dot{\mathbf{e}}_{\mathbf{D}} \in L_2^n, \mathbf{e_D}$ continuous and $\mathbf{e_D} \rightarrow \mathbf{0}$ as $t \rightarrow \infty$.

Proof: The inverse of the transfer function between $\mathbf{e_D}$ and $\mathbf{e}$, i.e.,

$$\mathbf{e_D} = \left(s + \mathbf{K_D} + \mathbf{K_P}\frac{1}{s}\right)\mathbf{e}, \tag{5.15}$$

is stable and strictly proper. Therefore, the robust motion control system is asymptotically stable if the mapping $-\mathbf{e_D} \rightarrow \Psi$ is passive [107].

Theorem 5.1 provides us a basic insight into the stability of DOb based robust position control systems. For instance, if it is assumed that $\mathbf{\Psi} = \mathbf{0}$, in which a DOb is designed by using perfect inertia identification, i.e., $\Delta\mathbf{M}(\mathbf{q}) = \mathbf{0}$, a planar robot application is considered and gravity is canceled, and Coriolis and centrifugal forces are neglected, then the asymptotic stability of the robust motion control

system is achieved directly by using *Theorem 5.1*. However, it is not an easy task to show the passivity mapping due to complex integration in eq. (5.14) when $\mathbf{\Psi} \neq \mathbf{0}$. Therefore, to show the stability of the DOb based robust position control systems, the main theorem of this chapter is proposed as follows:

Theorem 5.2: The origin of the system defined in eq. (5.13) is uniformly ultimately bounded with respect to the set $B_\Gamma \left\{ \|\mathbf{e_D}\|_2 > \Gamma \right\}$ where

$$\Gamma = \frac{\beta_{\Delta\mathbf{M}}^{max} \left\|\ddot{\mathbf{q}}^{\mathbf{des}}\right\|_2 + \beta_{\mathbf{C}} \|\dot{\mathbf{q}}\|_2 \left\|\dot{\mathbf{q}}^{\mathbf{des}}\right\|_2 + \beta_{\mathbf{g}}}{g_{DOb}\beta_{\Delta\mathbf{M}}^{min}}, \tag{5.16}$$

if DOb is designed by using $\mathbf{M_n} \geq \mathbf{M(q)}$, i.e., $\Delta\mathbf{M} \leq \mathbf{0}$.

Proof: Let us consider the Lyapunov function candidate by using

$$V = \frac{1}{2}\mathbf{e_D^T M(q) e_D}, \tag{5.17}$$

The time derivative of the Lyapunov function is derived as follows:

$$\begin{aligned} \dot{V} &= \frac{1}{2}\mathbf{e_D^T M(q)\dot{e}_D} + \frac{1}{2}\mathbf{e_D^T \dot{M}(q) e_D}, & (5.18)\\ &= \mathbf{e_D^T \Psi} - g_{DOb}\mathbf{e_D^T M_n e_D} + \frac{1}{2}\mathbf{e_D^T}\left(\mathbf{\dot{M}(q) - 2C(q,\dot{q})}\right)\mathbf{e_D}, & (5.19) \end{aligned}$$

If *Property 4* is applied into eq. (5.19), then

$$\begin{aligned} \dot{V} &= \mathbf{e_D^T \Psi} - g_{DOb}\mathbf{e_D^T M_n e_D}, & (5.20)\\ &= -g_{DOb}\mathbf{e_D^T M_n e_D} - \mathbf{e_D^T}\Delta\mathbf{M(q)}\ddot{\mathbf{q}}^{\mathbf{des}} - \mathbf{e_D^T}\left\{\mathbf{C(q,\dot{q})}\dot{\mathbf{q}}^{\mathbf{des}} + \mathbf{g(q)}\right\}, & (5.21) \end{aligned}$$

The time derivative of the Lyapunov function is smaller than zero if the following inequality is satisfied.

$$g_{DOb}\mathbf{M_n e_D} \geq -\Delta\mathbf{M(q)}\ddot{\mathbf{q}}^{\mathbf{des}} - \mathbf{C(q,\dot{q})}\dot{\mathbf{q}}^{\mathbf{des}} - \mathbf{g(q)}, \tag{5.22}$$

The conservative bound of the inequality given in eq. (5.22), i.e., the sufficient condition of the stability, is obtained by using *Property 1*, *Property 2* and *Property 3* as follows:

$$\dot{V} \leq g_{DOb}\beta_{\mathbf{M_n}}^{max} \|\mathbf{e_D}\|_2^2 + \beta_{\Delta\mathbf{M}}^{max} \left\|\ddot{\mathbf{q}}^{\mathbf{des}}\right\|_2 \|\mathbf{e_D}\|_2 + \beta_{\mathbf{C}} \|\dot{\mathbf{q}}\|_2 \left\|\dot{\mathbf{q}}^{\mathbf{des}}\right\|_2 \|\mathbf{e_D}\|_2 + \beta_{\mathbf{g}} \|\mathbf{e_D}\|_2 \leq 0, \tag{5.23}$$

Equation (5.23) shows that the time derivative of the Lyapunov function, $\dot{V}$, is negative outside of the compact set $B_\Gamma \{\|\mathbf{e_D}\|_2 > \Gamma\}$ where Γ is defined in eq. (5.16). Therefore, all solutions that start outside of B_Γ enter this set within a finite time, and remain inside the set for future time. As a result, the error dynamics, $\mathbf{e_D}$, is uniformly ultimately bounded with respect to B_Γ.

Remark 1: Equation (5.20) and eq. (5.21) show that as the bandwidth of DOb and / or nominal inertia matrix are increased, the Lyapunov function, i.e., the error dynamics, $\mathbf{e_D}$, decreases faster and the stability of the position control system is improved.

Remark 2: The radius of the compact set B_Γ can be controlled directly by using the bandwidth of DOb and nominal inertia matrix. Equation (5.16) shows that as the bandwidth of DOb and / or nominal inertia matrix are increased, the radius of the compact set B_Γ shrinks.

Remark 3: The stability of the robust position control system is improved by using $\mathbf{M_n} \geq \mathbf{M(q)}$, i.e., $\Delta\mathbf{M} \leq \mathbf{0}$.

Let us consider the first two terms of the right hand side of eq. (5.21).

$$\dot{V}^* = -g_{DOb}\mathbf{e_D^T M_n e_D} - \mathbf{e_D^T}\Delta\mathbf{M(q)}\ddot{\mathbf{q}}^{\mathbf{des}}, \tag{5.24}$$

It is obvious that if $\mathbf{M_n} = \mathbf{M(q)}$, then the second term of the right hand side of eq. (5.24) is canceled, so the robust position control system is not influenced by the desired acceleration fluctuations. However, it is not practical in many robotic applications.

Let us consider the practical case in which $\mathbf{M_n} \neq \mathbf{M(q)}$. The first term of the right hand side of eq. (5.24) is negative definite, so it is obvious that increasing the bandwidth of DOb and / or nominal inertia matrix improves the stability of the robust position control system. However, the second term of the right hand side of eq. (5.24) is not as clear as the first one.

Let us consider the error dynamics and desired acceleration by using

$$\mathbf{e_D} = \dot{\mathbf{e}} + \mathbf{K_D e} + \mathbf{K_P}\int \mathbf{e}dt, \tag{5.25}$$

$$\ddot{\mathbf{q}}^{\mathbf{des}} = \ddot{\mathbf{q}}^{\mathbf{ref}} - \mathbf{K_D}\dot{\mathbf{e}} - \mathbf{K_P e}, \tag{5.26}$$

It is assumed that the reference trajectory is continuous and bounded. Therefore, the error dynamics and desired acceleration are bounded if the robust position control system is stable. Equation (5.25) and eq. (5.26) show that the error dynamics and desired accelerations have different signs as the error of the position control system is increased, i.e., stability deteriorates.

Let us consider the second term of the right hand side of eq. (5.24) and apply *Property 1*.

$$\beta_{\Delta\mathbf{M}}^{min}\mathbf{I} \leq \underline{\sigma}(\Delta\mathbf{M}(\mathbf{q}))\mathbf{I} \leq \Delta\mathbf{M}(\mathbf{q}) \leq \overline{\sigma}(\Delta\mathbf{M}(\mathbf{q}))\mathbf{I} \leq \beta_{\Delta\mathbf{M}}^{max}\mathbf{I}, \tag{5.27}$$

If eq. (5.27) is applied into the second term of the right hand side of eq. (5.24), then

$$\beta_{\Delta\mathbf{M}}^{min}\mathbf{e_D^T}\ddot{\mathbf{q}}^{\mathbf{des}} \leq \mathbf{e_D^T}\Delta\mathbf{M}(\mathbf{q})\ddot{\mathbf{q}}^{\mathbf{des}} \leq \beta_{\Delta\mathbf{M}}^{max}\mathbf{e_D^T}\ddot{\mathbf{q}}^{\mathbf{des}}, \tag{5.28}$$

Equation (5.28) shows that as the error of the position control system tends to be increasing the second term of the right hand side of eq. (5.24) tends to be negative if $\Delta\mathbf{M}(\mathbf{q}) > \mathbf{0}$; however, it tends to be positive if $\Delta\mathbf{M}(\mathbf{q}) < \mathbf{0}$. Therefore, if a DOb is designed by using $\Delta\mathbf{M}(\mathbf{q}) < \mathbf{0}$, then the time derivative of the Lyapunov function is decreased by the second term of the right hand side of eq. (5.24) as the error of the position control system increases. However, if a DOb is designed by using $\Delta\mathbf{M}(\mathbf{q}) > \mathbf{0}$, then the time derivative of the Lyapunov function is increased by the second term of the right hand side of eq. (5.24) as the error of the position control system is increased. Consequently, the stability of the robust position control system is improved practically by using $\Delta\mathbf{M}(\mathbf{q}) \leq \mathbf{0}$ in the design of a DOb.

Although, in practice, the design of a DOb is not very sensitive to inertia variations, the stability may deteriorate significantly if the bandwidth of DOb cannot compensate the inertia variations when $\Delta\mathbf{M}(\mathbf{q}) > \mathbf{0}$. Therefore, a DOb should be designed by using $\Delta\mathbf{M}(\mathbf{q}) \leq \mathbf{0}$ to improve the stability of the robust position control system.

Remark 4: The proposed nonlinear stability analysis provides us a very practical design method for the DOb based robust position control problem of robot manipulators. The design constraints that are proposed in the previous chapters can be directly implemented into the robust position control problem of robot manipulators. Although the stability of the robust position control system is improved by increasing nominal inertia matrix, it is limited by the practical constraints and robustness as shown in Chapter 4.

Remark 5: Not only the robustness, but also the stability of the acceleration based position control systems is improved by increasing the bandwidth of DOb.

Let us now consider the regulator problem of robot manipulators, i.e., point to point motion control, in which $\ddot{\mathbf{q}}^{\mathbf{ref}}, \dot{\mathbf{q}}^{\mathbf{ref}} \rightarrow \mathbf{0}$, $\mathbf{q}^{\mathbf{ref}} \rightarrow \mathbf{q}^*$ and $\dot{\mathbf{q}}^* = \mathbf{0}$ as $t \rightarrow \infty$. The following theorem shows that asymptotic stability is achieved when the ABC system is implemented to the regulator problem of robot manipulators.

Theorem 3: If the final value of the desired trajectory is an equilibrium point, i.e., $\ddot{\mathbf{q}}^{\mathbf{ref}}, \dot{\mathbf{q}}^{\mathbf{ref}} \rightarrow \mathbf{0}$, and

$\mathbf{q^{ref}} \rightarrow \mathbf{q}^*$, in which $\mathbf{q}^*$ is a constant vector, as $t \rightarrow \infty$, and a DOb is designed by using $\Delta\mathbf{M}(\mathbf{q}) \leq \mathbf{0}$, then the robust position control system is asymptotically stable.

Proof: Theorem 1 shows that the stability of the robust position control system is achieved if eq. (5.22) is satisfied. If the equilibrium is a constant point, then the stable position control system should reach at a constant point as $t \rightarrow \infty$.

If *Theorem 1* holds for the constant equilibrium point and the robot reaches at a constant point as $t \rightarrow \infty$, then $\mathbf{e_D}$ becomes a constant vector. Then,

$$g_{DOb}\mathbf{e_D^T M_n e_D} = \varphi \geq \mathbf{e_D^T \Psi}, \tag{5.29}$$

where φ is a constant value. *Theorem 1* directly shows that the origin is asymptotically stable, since the mapping $-\mathbf{e_D} \rightarrow \mathbf{\Psi}$ is passive.

5.5 Simulation

In this section, simulation results will be presented. Two different robot arms, which are shown in Fig. 5-3, are considered in the simulations. The first one is a two-degrees-of freedom planar robot arm and the second one is a six-degrees-of freedom industrial robot manipulator. The virtual reality toolbox of Matlab is used to obtain animations and Simulink is used to design on-line robot control systems.

The robust position control responses of the two link planar robot manipulator are shown in Fig. 5-4. Fig. 5-4(a) shows the errors of the robust position control system when the two link planar robot manipulator follows a desired trajectory. It is clear from Fig. 5-4(a) that when trajectory tracking control problem is considered, the error of the robust position control system is bounded if the stability is achieved. The bound of the position control error can be decreased by increasing the bandwidth of DOb and nominal inertia matrix; however the error cannot be eliminated by using the conventional acceleration based robust motion control systems. Fig. 5-4(a) also shows that increasing the nominal inertia matrix improves not only the performance, but also the stability of the robust position control system. The stability can also be improved by increasing the bandwidth of DOb. Against the trajectory tracking problem, the asymptotic stability of the robust position control system can be achieved when regulator problem is considered as shown in Fig. 5-4(b). Fig. 5-4(b) also shows that the stability of the robust position control system is improved by increasing the nominal inertia matrix in the design of DOb.

Fig. 5-5(a) and Fig. 5-5(b), respectively, show the position control responses of a six-degrees-of-

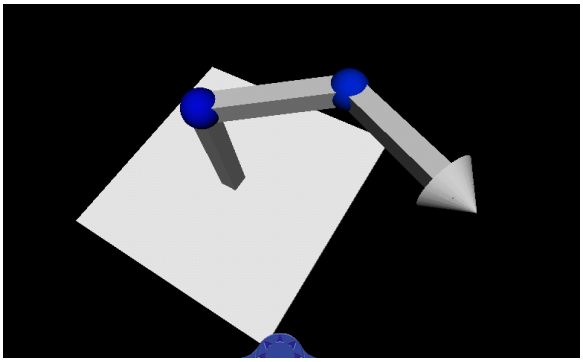

(a) Two link planar robot arm.

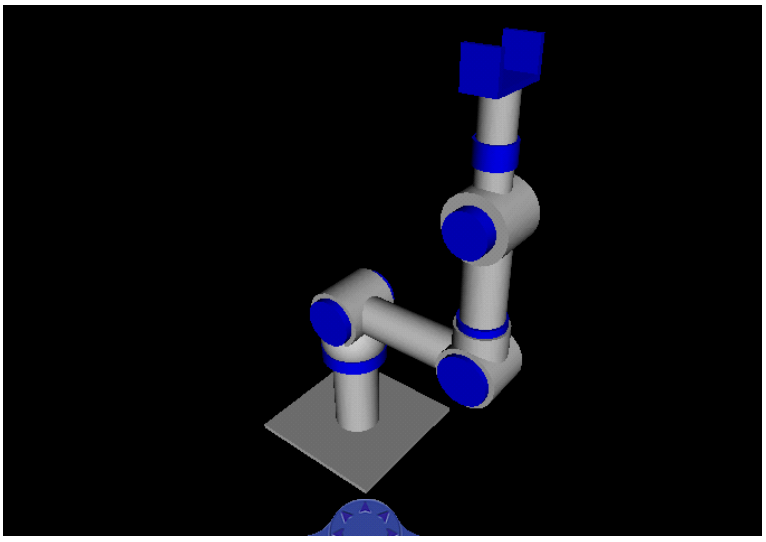

(b) Six-degrees-of-freedom robot manipulator.

Fig. 5-3: Two link planar arm and six-degrees-of-freedom robot manipulators.

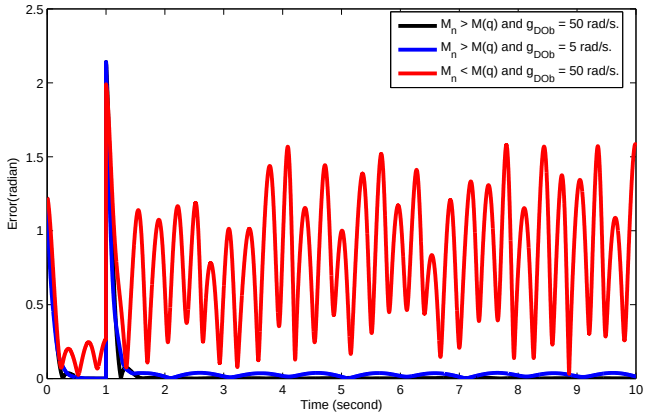

(a) Trajectory tracking control responses of two link planar robot arm.

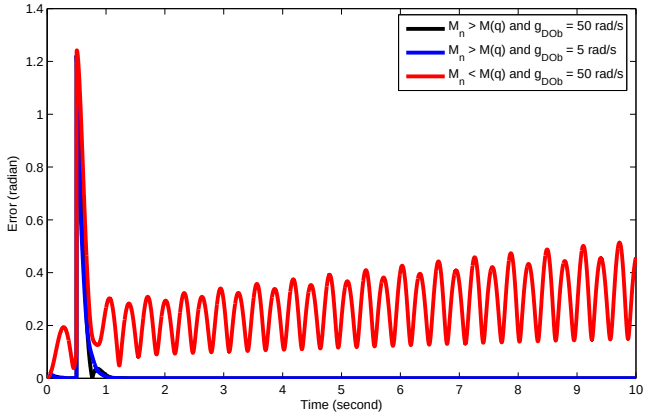

(b) Point to point control responses of two link planar robot arm.

Fig. 5-4: Robust position control responses of two link planar robot arm.

freedom robot manipulator when trajectory tracking and regulator problems are considered. Similar stability and performance results can be seen for the six-degrees-of-freedom robot manipulator in Fig. 5-5.

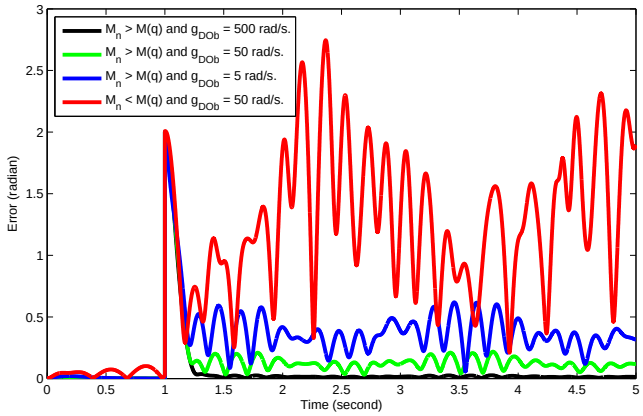

(a) Trajectory tracking control responses of six-degrees-of-freedom robot arm.

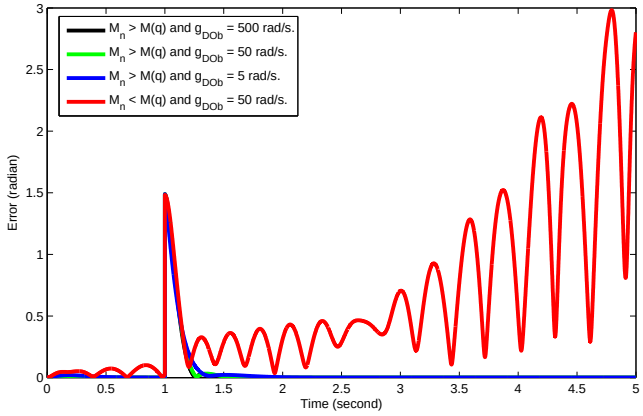

(b) Point to point control responses of six-degrees-of-freedom robot arm.

Fig. 5-5: Robust position control responses of six-degrees-of-freedom robot arm.

5.6 Summary

In this chapter, a novel practical nonlinear stability analysis method is proposed for the position control problem of robot manipulators when DOb is used to achieve robustness. A new design constraint, $\mathbf{M_n} \geq \mathbf{M(q)}$ in which $\mathbf{M_n}$ and $\mathbf{M(q)}$ denote nominal and uncertain inertia matrices, is presented to improve the stability of the robust position control systems. It is clear from Chapter 4 and Chapter 5 that the stability of the DOb based robust motion control systems is improved by increasing the nominal

inertia in the design of DOb. Although diagonal nominal inertia matrix is used in the conventional design of DOb based robust position control systems, the proposed analysis shows that non-diagonal terms can be also used to increase the nominal inertia matrix, i.e., to improve stability. As shown in Chapter 4, the nominal inertia in the design of DOb is limited by the practical constraints such as noise, sampling time, and robustness. Therefore, the stability of the robust position control system cannot be improved independently. As the nominal inertia is increased to improve the stability, the bandwidth of DOb should be decreased, which deteriorates the robustness and performance of the position control systems, to satisfy the practical constraints. Consequently, a DOb based robust position control system should be designed by considering the stability, performance, and robustness constraints given in Chapter 4 and Chapter 5. The author believes that optimal design methods, in which the bandwidth of DOb is maximized and nominal inertia matrix is minimized without degrading the stability of DOb, should be proposed to improve the performance of DOb based robust motion control systems. However, the optimal DOb design is out of the scope of this dissertation.

Chapter 6

Conclusions

Chapter 2 briefly describes the fundamentals of DOb based robust control systems, which is the basis of this dissertation. A DOb based robust control system is one of the most popular two-degrees-of-freedom control methods, in which robustness and performance are adjusted separately. There are two feed-back loops, namely inner and outer loops, in a DOb based robust robust control system. The robustness of control systems is achieved by using DOb in the inner-loop, and the performance goals are achieved by using a performance controller in the outer-loop. This control structure is explained in this chapter, briefly.

Chapter 3 analyzes the DOb based robust control systems by using advanced linear control methods. Firstly, the conventional analysis method, i.e., Small-Gain theorem, is considered in the robust stability and performance analysis of DOb based control systems. It is a well-known fact that Small-Gain theorem can be easily implemented into robust control problems; however, it suffers by conservatism, since only the amplitude response of Nyquist plot is considered. It is shown that the conservatism limits the bandwidth of DOb directly, and as the uncertainty of plant is increased the conservative constraints on the bandwidth of DOb become more severe. Although conservatism can be decreased by using SSV, it cannot be removed completely due to the discontinuity problem of real SSV. To remove the conservatism, it is assumed that uncertain plant includes only real parametric uncertainties. A new stability analysis is proposed for the first order DOb based robust control system by using Kharitonov and Edge Theorems. It is shown that if a minimum phase uncertain plant includes only real parametric uncertainties and the order of DOb is one, then the robust stability is achieved if the bandwidth of DOb is higher than its lower bound which is derived in Chapter 3. The robust stability margins of the DOb based robust

control systems are analyzed by using Tsypkin-Polyak theorem, and it is shown that the stability margin of the DOb based robust control system is increased as the bandwidth of DOb is increased. Although the proposed analysis method can be implemented into different plants, such as non-minimum phase plants, general design constraints cannot be achieved easily. To derive general design constraints of DOb based robust control systems, unstructured uncertainty based analysis re-considered by using Bode and Poisson integral theorems. It is shown that the bandwidth of a DOb is limited by the robustness constraint if an uncertain plant includes time delay and/or RHP zero(s); however, if an uncertain plant includes right half plane pole(s), then the bandwidth of a DOb has lower bound due to the robustness constraint. Besides, the performance of a DOb can be improved by increasing its order, yet the robustness deteriorates and the robustness constraint limits the bandwidth of DOb. The proposed method provides a deep insight into the robustness of DOb based control systems in a wide range of application area such as non-minimum phase and unstable plants; however, it suffers by the conservatism that is explained in Chapter 3. The author believes that the conservatism is not a severe problem, since the proposed method clarifies the robustness characteristics of a DOb based control system qualitatively. Besides, the conservatism can be lessened by using more realistic sensitivity function bounds, yet it increases the computational complexity.

Chapter 4 analyzes the DOb based robust motion control systems by using linear control methods. A new robustness constraint is proposed on the bandwidth of DOb and nominal inertia by considering practical velocity measurement that is obtained using a LPF. It is shown that the bandwidth of DOb and nominal inertia are limited by the bandwidth of velocity measurement. As the bandwidth of DOb is increased, the nominal inertia should be decreased and vice versa. Novel stability analysis are proposed for the DOb based robust position and force control systems. It is shown that the stability of the DOb based robust position control system is improved by increasing nominal inertia in the design of DOb; however, it is limited by the bandwidth of velocity measurement. Therefore, there is a trade-off between the robustness and stability in the DOb based robust position control systems. Although it is generally assumed that the robustness and performance are adjusted in the inner and outer loops separately, it is not true. It is shown that the robustness of the position control system is improved by increasing the performance controller gain. Robust force control systems are considered, and it is shown that not only the performance, but also the stability of the force control systems improves significantly by achieving robustness, i.e., canceling the natural feed-back loop. To estimate environmental impedance, force sensor and RFOb are used in this dissertation. An RFOb has several superiorities over force sensors, such as sensorless-force control, force control bandwidth improvement, stability improvement, cost decreasing,

and so on. The main disadvantage of RFOb is that the dynamic model of servo system should be known accurately to improve not only the performance but also the stability. In this chapter, a novel stability analysis is proposed for the RFOb based robust force control systems. As shown in this chapter, high performance force control systems can be obtained by using force sensors as well. The main advantage of force sensors is that force control goals can be achieved even if the dynamics of the servo system are not known accurately.

Chapter 5 analyzes the DOb based robust motion control systems by using non-linear control methods. Robot manipulators have generally highly non-linear dynamic models, so linear control based analysis methods do not provide deep insight into the stability of the multi-degrees-of-freedom systems. However, for the sake of simplicity, linear control methods are conventionally used in the DOb based robust control problem of robot manipulators. Although non-linear design methods have been considered to estimate disturbances, the stability of the robust control problem has not been discussed yet. In this approach, it is assumed that if disturbance estimation is stable, then the robust motion control system is stable. However, as shown in Chapter 4, the stability of the DOb based robust motion control systems is influenced by the design parameters of DOb. In this chapter, a novel stability analysis method is proposed by using the equivalence of DOb and passivity based controllers. A DOb based robust position controller is a special solution of the passivity based controller design method. It is shown that if a DOb is used in the robust trajectory tracking control problem of robot manipulators, then the error is uniformly ultimately bounded. The bound of position control error is adjusted by the bandwidth of DOb and nominal inertia matrix, i.e., the position control error is decreased by increasing the bandwidth of DOb and nominal inertia matrix. If a DOb is used in the regulator, i.e., point to point, motion control problem of robot manipulators, then asymptotic stability is achieved. To improve the stability of the robust position control systems, the nominal inertia matrix in the design of DOb should be higher than the uncertain one. Although diagonal nominal inertia matrix is used in the conventional design methods, this chapter shows that non-diagonal terms can also be used to increase the nominal inertia matrix, i.e., to improve the stability. As shown in Chapter 4, the nominal inertia matrix cannot be increased independently due to the practical and robustness constraints. Therefore, optimal solutions, in which the bandwidth of DOb is maximized and nominal inertia matrix is minimized without degrading the stability, should be considered to improve the performance in the DOb based robust position control systems.

As stated above, this dissertation proposes novel analysis and design methods for the DOb based robust control systems. DOb is one of the most efficient and practical robust control tools, in which the

robustness of control systems is adjusted intuitively in a predetermined bandwidth. Therefore, it is widely used in several control applications, specifically in motion control, in the literature. However, although DOb has long been used in several motion control applications in the literature, it suffers from insufficient analysis and design control methods; therefore, the applications of DOb based motion control systems generally depend on designers own experiences. This dissertation provides novel analysis and design methods for DOb based robust position and force control systems. Although it is generally assumed that the robustness is crucial in position control systems, it is clarified in this dissertation that the stability and performance of force control systems are improved significantly by the robustness. Therefore, the robust controllers are crucial not only for position, but also for force control systems. The validity of the proposals is verified by simulation and experimental results.

References

[1] K. Ogata, "Modern control engineering", Prentice-Hall, Upper Saddle River, New Jersey, 07458, 1997.

[2] B. Kuo, "Automatic control systems", Jhon Willey and Sons, New Jersey, 07030, 2002.

[3] K. Zhou and J. Doyle, "Essentials of robust control", Prentice Hall, Upper Saddle, NJ, 1997.

[4] S. Skogestad and I. Postlethwaite, "Multivariable feedback control: analysis and design, 2nd edition", Jhon Willey and Sons, New York, 2001.

[5] T. Kurabayashi and T. Murakami, "Operator assist control of overhead crane by emulating natural damping", In *Int. Conf. IEEE AMC*, March 2014.

[6] M. J. Dillsaver, C. E. S. Cesnik, and I. V. Kolmanovsky, "Gust load alleviation control for very flexible aircraft", In *Int. Conf. AIAA AFMC*, Aug. 2011.

[7] M. Athans, "On the LQG problem", *IEEE Trans. Autom. Control*, Vol. 16, No. 6, p. 528, Dec. 1971.

[8] F. Jabbari and R. W. Benson, "Robust stabilization and disturbance attenuation; high gain controllers", In *Int. Conf. IEEE ACC*, pp. 1411–1412, Jun. 1994.

[9] C. Cao, V. V. Patel, C. K. Reddy, and N. Hovakimyan, "Are phase and time-delay margins always adversely affected by high-gain?", In *Int. Conf. AIAA NCCE*, Aug. 2006.

[10] M. G. Safonov and M. K. H. Fan, "Special issue on multivariable stability analysis: Editorial", *Interat. J. Robust and Nonlinear Cont.*, Vol. 7, pp. 97–103, 1997.

[11] M. G. Safonov, "Origins of robust control: Early history and future speculations", *Annual Reviews in Control*, Vol. 36, No. 2, pp. 173–181, Dec. 2012.

[12] P. Dorato, "A historical review of robust control", *IEEE Trans. Cont. Syst. Magazine*, Vol. 7, No. 2, pp. 44–47, Apr. 1987.

[13] M. J. Grimble and M. A. Johnson, "H_∞ robust control design-a tutorial review", *Computing and Control Engineering Jounral*, Vol. 2, No. 6, pp. 275–282, Nov. 1991.

[14] J. Ackerman et al., "Robust control: the parameter space approach, 2nd edt.", Springer-Verlag, London, 2002.

[15] S.P. Bhattacharyya, H. Chapellat, and L. H. Keel, "Robust control: the parametric approach", Prentice Hall PTR, Upper Sadde NJ, 1995.

[16] V. L. Kharitonov, "Asymptotic stability of an equilibrium position of a family of systems of linear differential equations", *Differential Equations*, Vol. 14, pp. 1483–1485, 1979.

[17] B. R. Barmish, "A generalization of khatironov's four polynomial concept for robust stability problems with linearly dependent coefficient perturbation", *IEEE Trans. Automat. Cont.*, Vol. 34, No. 2, pp. 157–165, Feb. 1989.

[18] Y. C. Soh and Y. K. Foo, "Generalized edge theorem.", *Systems and Control Letter*, Vol. 12, pp. 219–224, 1989.

[19] Y. Z. Tsypkin and B. T. Polyak, "Frequency domain criterion for robust stability of polytope polynomials.", *In M. Mansour, S. Balemi, and W. Turol (Eds.), Control of uncertain dynamic systems*, pp. 113–124, 1992.

[20] F. Lin, "Robust control design: an optimal control approach", Jhon Willey and Sons, West Sussex, England, 07030, 2007.

[21] G. Zames, "Functional analysis applied to nonlinear feedback systems", *IEEE Trans. Circuit Theory*, Vol. CT-10, pp. 392–404, Sept. 1981.

[22] J. Doyle, B. Francis, and A. Tannenbaum, "Feedback control theory", McMillan, New York, 1990.

[23] G. Zames, "Feedback and optimal sensitivity: model reference transformations, multiplicative seminorms and approximate inverses", *IEEE Trans. Autom. Control*, Vol. 26, No. 2, pp. 301–320, 1981.

[24] A. Tannenbaum, "Feedback stabilization of linear dynamical plants with uncertainty in the gain factor", *Internat. J. Control*, Vol. 32, No. 1, pp. 1–16, 1980.

[25] A. A. Stoorvogel, "The H_∞ control problem: state space approach", Prentice Hall, Englewood Cliffs, 1992.

[26] G. Balas, R. Chiang, A. Packard, and M. Safonov, "Robust control toolbox", Mathworks, Mass, 2005.

[27] J. C. Doyle, "Analysis of feedback systems with structured uncertainties", *IEEE Proc. Cont. Theory and App.*, Vol. 129, No. 6, pp. 242–250, Nov. 1982.

[28] G. J. Balas, J. C. Doyle, and K. Glover, "μ analysis and synthesis toolbox", Mathworks, Mass, 2001.

[29] N. Lehtomaki, N. R. Sandell, and M. Athans, "Robustness results in linear-quadratic gaussian based multivariable control designs.", *IEEE Trans. Autom. Control*, Vol. 26, No. 1, pp. 75–93, Feb 1981.

[30] K. Zhou and Z. Ren, "A new controller architecture for high performance robust and fault-tolerant control", *IEEE Trans. Autom. Control*, Vol. 46, No. 10, pp. 1613–1818, Aug. 2001.

[31] E. Sariyildiz and K. Ohnishi, "Analysis the robustness of control systems based on disturbance observer", *Internat. J. Control*, Vol. 86, No. 10, pp. 1733–1743, 2013.

[32] K. Ohishi, K. Ohnishi, and K. Miyachi, "Torque-speed regulation of DC motor based on load torque estimation", In *Proc. Int. Conf. IEEJ IPEC*, pp. 1209–1216, 1983.

[33] K. Ohnishi, M. Shibata, and T. Murakami, "Motion control for advanced mechatronics", *IEEE/ASME Trans. Mechatron.*, Vol. 1, No. 1, pp. 56–67, Mar. 1996.

[34] G. Hostetter and J. S. Meditch, "Observing systems with un-measurable inputs.", *IEEE Trans. Autom. Control*, Vol. AC-18, pp. 307–308, June 1973.

[35] S. H. Wang, E. J. Davison, and P. Dorato, "Observing the states of systems with un-measurable disturbance", *IEEE Trans. Autom. Control*, Vol. 20, pp. 716–717, 1975.

[36] A. Sabanovic and K. Ohnishi, "Motion control systems", Jon Wiley and Son, Singapore, 2011.

[37] T. Umeno and Y. Hori, "Robust speed control of DC servomotors using modern two degrees-of-freedom controller design", *IEEE Trans. Ind. Electron.*, Vol. 38, No. 5, pp. 363–368, Oct. 1991.

[38] E. Schrijver and D. V. Johannes, "Disturbance observers for rigid mechanical systems: equivalance, stability and design", *ASME. Trans. J. Dyn. Sys., Meas., Control*, Vol. 124, No. 4, pp. 539–548, 2002.

[39] C. H. Wai and N. C. Cheung, "Disturbance and response time improvement of submicrometer precision linear motion system by using modified disturbance compensator and internal model reference control", *IEEE Trans. Ind. Electron.*, Vol. 60, No. 1, pp. 139–150, Jan. 2013.

[40] B. A. Guvenc, L. Guvenc, and S. Karaman, "Robust MIMO disturbance observer analysis and design with application to active car steering", *Internat. J. Robust Nonlinear Cont.*, Vol. 20, No. 8, pp. 873–891, May 2010.

[41] S. P. Chan, "A disturbance observer for robot manipulators with application to electronic components assembly", *IEEE Trans. Ind. Electron.*, Vol. 42, No. 5, pp. 487–493, Oct. 1995.

[42] T. Sato, S. Sakaino, and K. Ohnishi, "Walking trajectory planning on stairs using virtual slope for biped robots", *IEEE Trans. Ind. Electron.*, Vol. 58, No. 4, pp. 1385–1396, Apr. 2011.

[43] E. Sariyildiz and K. Ohnishi, "Bandwidth constraints of disturbance observer in the presence of real parametric uncertainties", *Eur. J. Control*, Vol. 19, No. 3, pp. 199–205, 2013.

[44] B. A. Guvenc and L. Guvenc, "Robustness of disturbance observer in the presence of structured real parametric uncertainty", In *Proc. Int. Conf. ACC*, pp. 4222–4227, June 2001.

[45] E. Sariyildiz and K. Ohnishi, "A guide to design disturbance observer", *ASME. Trans. J. Dyn. Sys., Meas., Control*, Vol. 136, No. 2, 2014.

[46] C. C. Wang and M. Tomizuka, "Design of robustly stable disturbance observer based on closed loop consideration using H_∞ optimization and its applications.", In *Proc. Int. Conf. ACC*, pp. 3764–3769, July 2004.

[47] E. Sariyildiz, D. Cattine, and K. Ohnishi, "Improving the performance of higher order disturbance observer: a position approach", In *Int. Conf. IEEE AMC*, pp. 1–6, March 2012.

[48] K. Yamada and S. Komada, "A study on higher-order disturbance observer and robust stability", *Elec. Eng. in Japan*, Vol. 128, No. 1, pp. 1776–1781, Dec. 1999.

[49] R. S. Chandra and R. D'Andra, "Necessity of the small gain theorem for multi-dimensional systems.", In *IEEE Int. Conf. CDC*, pp. 2859–2864, Dec. 2003.

[50] D. J. Hill, "A generalization of the small gain theorem for nonlinear feedback systems.", *Automatica*, Vol. 27, No. 6, pp. 1043–1045, Nov. 1991.

[51] H. K. Khalil, "Nonlinear systems", Prentice-Hall, 2002.

[52] M. A. Dahleh and M. H. Khammash, "Controller design for plants with structured uncertainty.", *Automatica*, Vol. 29, No. 1, pp. 37–56, 1993.

[53] J. Lee and F. Edgar, "Upper bounds of structured singular values for mixed uncertainties", In *Proc. IEEE Int. Conf. CDC*, Vol. 1, pp. 798–802, Dec. 2003.

[54] C. Marsh and H. Wei, "Robustness bound for systems with parametric uncertainty", *Automatica*, Vol. 32, No. 10, pp. 1447–1453, 1996.

[55] B. R. Barmish, "New tools for robustness of linear systems", Macmillan, New York, 1994.

[56] L. H. Keel and S. P. Bhattacharyya, "Robust parametric classical control design", *IEEE Trans. Aut. Control*, Vol. 39, No. 7, pp. 1524–1530, Jul. 1994.

[57] A. Rantzer, "Stability conditions for polytopes of polynomials", *IEEE Trans. Aut. Control*, Vol. 37, No. 1, pp. 79–89, Jan. 1992.

[58] H. Chapellat and S. P. Bhattacharyya, "An alternative proof of kharitonov theorem", *IEEE Trans. Aut. Control*, Vol. 34, No. 4, pp. 448–450, Apr. 1989.

[59] H. W. Bode, "Network analysis and feedback amplifier design", D. Van Nostrand Co., New York, 1945.

[60] J. S. Freudenberg and D. P. Looze, "A sensitivity trade-off for plants with time delay", *IEEE Trans. Aut. Control*, Vol. 32, No. 2, pp. 99–104, Feb. 1987.

[61] J. S. Freudenberg and D. P. Looze, "Right half plane poles and zeros design tradeoffs in feedback systems", *IEEE Trans. Aut. Control*, Vol. 30, No. 6, pp. 555–565, Jun. 1985.

[62] I. M. Horowitzh, "Synthesis of feedback systems", Academic Press, New York, 1963.

[63] M. M. Seron, J. H. Braslavsky, and G. C. Goodwin, "Fundemantal limitations in filtering and control", Springer-Verlag, London, 1997.

[64] R. H. Middleton and G. C. Goodwin, "Digital control and estimation: a unified approach", Prentice Hall in., Englewood Cliff NJ, 1990.

[65] E. Sariyildiz and K. Ohnishi, "A new solution for the robust control problem of non-minimum phase systems using disturbance observer", In *Int. Conf. IEEE ICM*, pp. 46–51, Mar. 2013.

[66] X. Chen, G. Zhai, and T. Fukuda, "An approximate inverse system for non-minimum phase systems and its application to disturbance observer", *Sys. and Cont. Letters*, Vol. 52, No. 3-4, pp. 193–207, Jul. 2004.

[67] D. E. Goldberg, "Genetic algorithms in search, optimization and machine learning", Addison-Wesley Longman Publishing Co., Inc., Boston, MA USA, 1989.

[68] C. R. Reeves and J. E. Rowe, "Genetic algorithms: principles and perspectives - a guide to GA theory", Kluwer Academic Publishers, Norwell, MA, USA, 2002.

[69] E. Sariyildiz and K. Ohnishi, “A guide to design disturbance observer based motion control systems.”, In *Int. Conf. IPEC*, May 2014.

[70] E. Sariyildiz and K. Ohnishi, “Stability and robustness of disturbance observer based motion control systems”, *IEEE Trans. Ind. Electron.*, 2014 to be published.

[71] A. Tesfaye, H. S. Lee, and M. Tomizuka, “A sensitivity optimization approach to design of a disturbance observer in digital motion control systems”, *IEEE/ASME Trans. Mechatron.*, Vol. 5, No. 1, pp. 32–38, Mar. 2000.

[72] S. Komada, N. Machii, and T. Hori, “Control of redundant manipulators considering order of disturbance observer”, *IEEE Trans. Ind. Electron.*, Vol. 42, No. 2, pp. 413–420, Apr. 2000.

[73] L. Yi and M. Tomizuka, “Two degree of freedom control with robust feed-back control for hard disk servo systems”, *IEEE/ASME Trans. Mechatron.*, Vol. 4, No. 1, pp. 17–24, Mar. 1999.

[74] P. Sang-Kyun and L. Sang-Hun, “Disturbance observer based robust control for industrial robots with flexible joints”, In *Int. Conf. IEEE ICCAS*, pp. 584–589, Oct. 2007.

[75] T. Satoh, H. Hara, N. Saito, J. Nagase, and N. Saga, “Disturbance observer based predictive functional critical control of a table drive system”, *Internat. J. of Mec., Aero., Ind. and Mechatron. Eng.*, Vol. 7, No. 12, pp. 1432–1437, 2013.

[76] S. Shimmyo, T. Sato, and K. Ohnishi, “Biped walking pattern generation by using preview control based on three-mass model”, *IEEE Trans. Ind. Electron.*, Vol. 60, No. 11, pp. 5137–5147, 2013.

[77] A. Suzuki and K. Ohnishi, “Frequency-domain damping design for time-delayed bilateral teleoperation system based on modal space analysis”, *IEEE Trans. Ind. Electron.*, Vol. 60, No. 1, pp. 177–190, Jan. 2013.

[78] T. Nozaki, T. Mizoguchi, Y. Saito, D. Yashiro, and K. Ohnishi, “Recognition of grasping motion based on modal space haptic information using DP pattern-matching algorithm”, *IEEE Trans. Ind. Informat.*, Vol. 9, No. 4, pp. 2043–2051, 2013.

[79] A. Hace, K. Jezernik, and A. Sabanovic, “SMC with disturbance observer for a linear belt drive”, *IEEE Trans. Ind. Electron.*, Vol. 54, No. 6, pp. 3402–3412, Dec. 2007.

[80] A. Sabanovic, “SMC framework in motion control systems”, *Int. J. Adapt. Control Signal Process.*, Vol. 21, No. 8, pp. 731–744, Oct. 2007.

[81] K. Watanabe, D. Suzuki, T. Mizoguchi, and K. Ohnishi, “Acceleration based reactive torque control”, In *Int. Conf. IEEE ISIE*, pp. 1–6, May. 2013.

[82] E. Sariyildiz and K. Ohnishi, “An adaptive reaction force observer design”, *IEEE/ASME Trans. Mechatron.*, 2014 to be published.

[83] I. S. Gradshteyn and I. M. Ryzhik, “Table of integrals, series and products. 7th edt.”, Academic Press, Sand Diego, CA, 2007.

[84] L. Vilani and J. D. Schutter, “Robotics handbook:force control”, Springer, 2008.

[85] S. Katsura, Y. Matsumoto, and K. Ohnishi, “Analysis and experimental validation of force bandwidth for force control”, *IEEE Trans. Ind. Electron.*, Vol. 53, No. 3, pp. 922–928, Jun. 2006.

[86] S. Katsura, Y. Matsumoto, and K. Ohnishi, “Modeling of force sensing and validation of disturbance observer for force control”, *IEEE Trans. Ind. Electron.*, Vol. 54, No. 1, pp. 530–538, Feb. 2007.

[87] E. Sariyildiz and K. Ohnishi, “A comparison study for force sensor and reaction force observer based force control systems.”, In *Int. Conf. IEEE ISIE*, June 2014.

[88] K. Khayati, P. Bigras, and L. A. Dessaint, “A robust feed-back linearization force control of a pneumatic actuator”, In *Int. Conf. IEEE Sys. Man and Cyb.*, pp. 6113–6119, Oct. 2004.

[89] C. Canudas de Wit, H. Olsson, K. J. Astrom, and P. Lischinsky, “New model for control of systems with friction”, *IEEE Trans. Aut. Cont.*, Vol. 40, No. 3, pp. 419–425, Mar. 1995.

[90] B. Yao, “Advance motion control: from classical PID to nonlinear adaptive robust control”, In *Int. Conf. IEEE AMC*, pp. 815–829, Mar. 2010.

[91] H. Fujimoto and B. Yao, “Multirate adaptive robust control for discrete time non-minimum phase systems and application to linear motors”, *IEEE/ASME Trans. Mechatron.*, Vol. 10, No. 4, pp. 371–377, Apr. 2005.

[92] L. Lu, B. Yao, Q. Wang, and Z. Chen, “Adaptive robust control of linear motors with dynamic friction compensation using modified Lugre model”, *Automatica*, Vol. 45, No. 12, pp. 2890–2896, Dec. 2009.

[93] B. Yao and A. Palmer, “Indirect adaptive robust control of SISO nonlinear systems in semi-strict feed-back forms”, In *Int. Cong. IFAC World*, pp. 2943–2948, 2002.

[94] M. W. Spong, S. Hutchinson, and M. Vidyasagar, “Robot modeling and control”, Willey, 2005.

[95] M. Leahy, M. A. Johnson, and S. K. Rogers, “Neural network payload estimation for adaptive control.”, *IEEE Trans. Neural Net.*, Vol. 2, No. 1, pp. 93–100, Jan. 1991.

[96] M. Saad, P. Bigras, L-A. Dessaint, and K. Al-Haddad, "Adaptive robot control using neural networks.", *IEEE Trans. Ind. Electron.*, Vol. 41, No. 2, pp. 173–181, Apr. 1994.

[97] A. G. A. Siqueira, M. H. Terra, and M. Bergerman, "Robust control of robot manipulators: Fault tolerant approaches", Springer, 2011.

[98] H. G. Sage, M. F. De Mathelin, and E. Ostertag, "Robust control of robot manipulators: A survey", *International Journal of Control*, Vol. 72, No. 16, pp. 1498–1522, Dec. 1999.

[99] T. Murakami, F. Yu, and K. Ohnishi, "Torque sensorless control in multi-degrees-of-freedom manipulator", *IEEE Trans. Ind. Electron.*, Vol. 40, No. 2, pp. 259–265, Apr. 1993.

[100] T. Murakami and K. Ohnishi, "A study of stability and workspace decoupling control based on robust control in multi-degrees-of-freedom robot", *IEEJ Trans. Ind. Appl.*, Vol. 113-D, No. 5, pp. 639–646, May 1993.

[101] T. Murakami, N. Oda, Y. Miyasaka, and K. Ohnishi, "A motion control strategy based on equivalent mass matrix in multi-degrees-of-freedom manipulator", *IEEE Trans. Ind. Electron.*, Vol. 42, No. 2, pp. 123–130, Apr. 1995.

[102] W. H. Chen, D. J. Ballance, and P. J. Gawthrop, "A nonlinear disurbance observer for robotic manipulators", *IEEE Trans. Ind. Electron.*, Vol. 47, No. 4, pp. 932–938, Aug. 2000.

[103] A. Mohammadi, M. Tvakoli, H. J. Marquez, and F. Hashemzadeh, "Nonlinear disurbance observer design for robotic manipulators", *Control Engineering Practice*, Vol. 21, No. 3, pp. 253–267, Mar. 2013.

[104] Z.J. Yang, Y. Fukushima, and P. Qin, "Decentralized adaptive robust control of robot manipulators using disturbance observer", *IEEE Trans. Cont. Syst. Technol.*, Vol. 20, No. 5, pp. 1357–1365, Sep 2014 to be published.

[105] R. Bickel and M. Tomizuka, "Passivity-based versus disturbance observer based robot control: equivalance and stability", *ASME Trans. J. Dyn. Sys. Meas., Control*, Vol. 121, No. 1, pp. 41–47, Mar. 1999.

[106] R. Kelly, V. Santibanez, and A. Loria, "Control of robot manipulators in joint space", Springer, Springer-Verlag, London, 2005.

[107] R. Ortega and M. Spong, "Adaptive motion control of robot manipulators: A tutorial", *Automatica*, Vol. 6, No. 3, pp. 877–888, Nov. 1989.

List of Achievements

Journals (First Author)

[1] Emre Sariyildiz and Kouhei Ohnishi, "Stability and robustness of disturbance observer based motion control systems," *IEEE Transactions on Industrial Electronics*, (Accepted for publication).

[2] Emre Sariyildiz and Kouhei Ohnishi, "An adaptive reaction force observer design," *IEEE/ASME Transactions on Mechatronics* , (Accepted for publication).

[3] Emre Sariyildiz and Kouhei Ohnishi, "A guide to design disturbance observer," *ASME Transactions Journal of Dynamic Systems, Measurement and Control*, vol.136, no. 2, pp. 1–10(021011), 2014.

[4] Emre Sariyildiz and Kouhei Ohnishi, "Analysis the robustness of control systems based on disturbance observer," *International Journal of Control*, vol.86, no. 10, pp. 1733–1743, 2013.

[5] Emre Sariyildiz and Kouhei Ohnishi, "Bandwidth constraints of disturbance observer in the presence of real parametric uncertainties," *European Journal of Control*, vol. 19, no. 3, pp. 199–205, 2013.

International Conferences (First Author)

[1] Emre Sariyildiz and Kouhei Ohnishi, "A comparison study for force sensor and reaction force observer based force control systems," in *International Symposium on Industrial Electronics , ISIE 2014, Istanbul, Turkey*, June 1–4, 2014.

[2] Emre Sariyildiz and Kouhei Ohnishi, "Adaptive reaction torque / force observer design II," in *International Symposium on Industrial Electronics , ISIE 2014, Istanbul, Turkey*, June 1–4, 2014.

[3] Emre Sariyildiz and Kouhei Ohnishi, "A guide to design disturbance observer based motion control systems," in *International Power Electronics Conference -ECCE ASIA-, IPEC 2014, Hiroshima, Japan*, May 18–21, 2014.

[4] Emre Sariyildiz and Kouhei Ohnishi, "Adaptive reaction torque / force observer design I," in *The 13th International Workshop on Advanced Motion Control, AMC 2014, Yokohama Japan*, March 14 – 16, 2014.

[5] Emre Sariyildiz and Kouhei Ohnishi, "On the robustness of disturbance observer," in *The 13th International Workshop on Advanced Motion Control, AMC 2014, Yokohama Japan*, March 14 – 16, 2014.

[6] Emre Sariyildiz and Kouhei Ohnishi, "Performance and robustness trade-off in disturbance observer design," in *The 39th Annual Conference of the IEEE Industrial Electronics Society, IECON 2013, Vienna, Austria*, Nov 11–13, 2013.

[7] Emre Sariyildiz and Kouhei Ohnishi, "Robust force control via disturbance observer," in *The 39th Annual Conference of the IEEE Industrial Electronics Society, IECON 2013, Vienna, Austria*, Nov 11–13, 2013.

[8] Emre Sariyildiz and Kouhei Ohnishi, "Robust control of systems with RHP zeros and poles via disturbance observer," in *IEEE International Conference on Mechatronics and Automation, ICMA2013, Kagawa, Japan*, August 4–7, 2013.

[9] Emre Sariyildiz and Kouhei Ohnishi, "Stability and robustness analysis of the position control systems with disturbance observer," in *IEEE International Conference on Mechatronics and Automation, ICMA2013, Kagawa, Japan*, August 4–7, 2013.

[10] Emre Sariyildiz, Kemal Ucak, Kouhei Ohnishi, Gulay Oke, and Hakan Temeltas, "Intelligent systems based solutions for the kinematics problem of the industrial robot arms," in *The 9th Asian Control Conference, ASCC2013, Istanbul, Turkey*, July 23–26, 2013.

[11] Emre Sariyildiz and Kouhei Ohnishi, "Robust stability analysis of the system with disturbance observer: the real parametric uncertainty approach II," in *Proceedings of the 38th Annual Conference of the IEEE Industrial Electronics Society, IECON2012, Montreal, Canada*, October 25–28, 2013.

[12] Emre Sariyildiz and Kouhei Ohnishi, "A new solution for the robust control of non-minimum phase systems using disturbance observer," in *Proceeding 4th IEEE International Conference on Mechatronics, ICM2013, Vicenza, Italy*, February 27 – March 1, 2013.

[13] Emre Sariyildiz and Kouhei Ohnishi, "Design constraints on the disturbance observer design in the presence of time delay," in *Proceeding 4th IEEE International Conference on Mechatronics, ICM2013, Vicenza, Italy*, February 27 – March 1, 2013.

[14] Emre Sariyildiz and Kouhei Ohnishi, "Robust stability analysis of the system with disturbance observer: the real parametric uncertainty approach I," in *IEEE International Conference on Mechatronics and Automation, ICMA2012, Chengdun, China*, August 5 – 8, 2012.

[15] Emre Sariyildiz, Kemal Ucak, Gulay Oke, Hakan Temeltas, and Kouhei Ohnishi, "Support vector regression based inverse kinematic modeling for a 7-DOF redundant robot arm," in *International Symposium on Innovations in Intelligent Systems and Applications, INISTA2012, Trabzon, Turkey*, July 2 – 4, 2012.

[16] Emre Sariyildiz and Kouhei Ohnishi, "Robust stability and performance analysis of the control systems with higher order disturbance observer: frequency approach," in *Proceeding of the 5th International Conference on Human System Interaction, HSI2012, Perth, Australia*, June 6 – 8, 2012.

[17] Emre Sariyildiz, Davide Cattine, and Kouhei Ohnishi, "Improving the performance of higher order disturbance observers: a position approach," in *Proceeding of the 12th IEEE International Workshop on Advanced Motion Control, AMC, Sarajevo, Bosnia and Herzegovina*, March 25 – 27, 2012.

International Conferences (Co-author)

[1] Davide Cattin, Emre Sariyildiz, and Kouhei Ohnishi, "A Null-space-based control for cable driven manipulators," in *Proceedings of the 38th Annual Conference of the IEEE Industrial Electronics Society, IECON2012, Montreal, Canada*, October 25–28, 2013.